Improving the stability and performance of n-type organic thin-film transistors

by

Samantha Brixi

A THESIS
SUBMITTED TO THE UNIVERSITY OF OTTAWA
IN PARTIAL FULFILMENT OF THE REQUIREMENTS
FOR THE DOCTORATE OF PHILOSOPHY
DEGREE IN CHEMICAL ENGINEERING

DEPARTMENT OF CHEMICAL AND BIOLOGICAL ENGINEERING

UNIVERSITY OF OTTAWA

Abstract

Organic electronics are electronic devices which contain an organic semiconductor (OSC) rather than a typical inorganic based semiconductor. Organic electronics have the potential to usher in a new generation of flexible, light-weight, and wearable electronic devices; whether it is ultra-thin high-quality images from organic light-emitting diode displays, or highly sensitive point-of-care sensors and wearable health-monitoring systems, organic electronics represent a new horizon of technological development. Behind all these emerging applications, high performance organic thin-film transistors (OTFTs) are required. OSCs for electron-transporting (n-type) OTFTs has lagged behind their hole-transporting (p-type) counterparts for many years in terms of both performance and stability. While research in n-type OTFT materials has been increasing in the past decade, these hurdles persist.

This thesis aims to address both the lower stability and performance of n-type OTFTs. Chapter 2 outlines a study that benchmarks the stability of various n-type OSCs, which can be used as a methodology for future studies. In Chapter 3, a study is presented that makes a first attempt to screen various chemical functionalities for OTFT performance stabilization. This chapter addresses a lack of organized approaches to the development of additives for organic electronic devices and highlights trends in potential chemical moieties to be used for improving device stability and performance. Particularly, pyridine was found to be a candidate material for enhancement of device stability. Chapter 4 directly applies the findings from Chapter 3, where poly(2-vinyl pyridine) (P2VP) was synthesized knowing the pyridine moiety had previously enhanced n-type OTFT stability. A variety of blend ratios with P2VP and our n-type OSC were studied, and the film properties examined to determine the optimal ratio for device stabilization. Finally, in Chapter 5 a study is presented incorporating not only an organic semiconducting layer, but also an organic poly(ionic liquid) gating layer. This represents a step towards fully-organic and less rigid device structures compared to previous studies. In this study, significant improvements in the OTFT operating voltages were found compared to previously fabricated devices, which would be feasible for real-world applications of these devices. All works beyond Chapter 2 have also used large numbers of replicate devices to address another issue endemic in the field: poorly represented statistics and few reported devices.

This thesis represents contributions to methodologies for studying OTFT stability, the development of practical and low-cost additives for n-type OTFT stability, and the fabrication of majority organic and low-voltage operation OTFTs.

Abstrait

L'électronique organique est un dispositif électronique qui contient un semi-conducteur organique (OSC) plutôt qu'un semi-conducteur inorganique typique. L'électronique organique a le potentiel de crée une nouvelle génération d'appareils électroniques flexibles, légers et portables ; qu'il s'agisse d'images ultra-minces de haute qualité provenant d'écrans à diodes électroluminescentes organiques, ou de capteurs très sensibles au point d'intervention et de systèmes portables de surveillance de la santé, l'électronique organique représente un nouvel horizon de développement technologique. Derrière toutes ces applications émergentes, des transistors à couches minces organiques (OTFT) hautes performances sont nécessaires. Les OSC pour les OTFT transporteurs d'électrons (type n) sont à la traîne par rapport à leurs homologues transporteurs de trous (type p) depuis de nombreuses années en termes de performances et de stabilité. Même si la recherche sur les matériaux OTFT de type n s'est intensifiée au cours de la dernière décennie, ces obstacles persistent.

Cette thèse vise à aborder à la fois la faible stabilité et les performances des OTFT de type n. Le chapitre 2 présente une étude qui évalue la stabilité de diverses OSC de type n, qui peut être utilisée comme méthodologie pour des études futures. Au chapitre 3, une étude est présentée qui constitue une première tentative de criblage de diverses fonctionnalités chimiques pour la stabilisation des performances de l'OTFT. Ce chapitre aborde le manque d'approches organisées pour le développement d'additifs pour les dispositifs électroniques organiques et met en évidence les tendances des fragments chimiques potentiels à utiliser pour améliorer la stabilité et les performances des dispositifs. En particulier, la pyridine s'est démontré comme être un matériau candidat pour améliorer la stabilité du dispositif. Le chapitre 4 applique directement les résultats du chapitre 3, où la poly(2-vinyl pyridine) (P2VP) a été synthétisée sachant que le fragment pyridine avait auparavant amélioré la stabilité de l'OTFT de type n. Une variété de rapports de mélange avec P2VP et notre OSC de type n ont été étudiés, ainsi que les propriétés du film examinées pour déterminer le rapport optimal pour la stabilisation du dispositif. Enfin, au chapitre 5, une étude est présentée intégrant non seulement une couche semi-conductrice organique, mais également une couche de diélectrique organique poly(ionique). Cela représente une étape vers des structures de dispositifs entièrement organiques et moins rigides par rapport aux études précédentes. Dans cette étude, des améliorations significatives des tensions de fonctionnement

OTFT ont été constatées par rapport aux dispositifs fabriqués précédemment, ce qui serait réalisable pour les applications réelles de ces dispositifs. Tous les travaux au-delà du chapitre 2 ont également utilisé un grand nombre de dispositifs répliqués pour adresser un autre problème endémique dans le domaine : le manque de statistiques pour la caractérisation de dispositifs.

Cette thèse représente des contributions aux méthodologies d'étude de la stabilité des OTFT, au développement d'additifs pratiques et peu coûteux pour la stabilité des OTFT de type n et à la fabrication d'OTFT à fonctionnement majoritairement organique et basse tension.

Acknowledgements

This thesis represents not only my work throughout graduate school, but the hard work, dedication, and persistence of a large number of people, only a handful of whom are included in the authors lists of my publications. First and foremost, I would like to thank my supervisor, Dr. Benoit Lessard, who has supported me through every success and struggle of this PhD. Thank you for encouraging my ideas, supporting my academic career, and for your patience through every challenge in publication and writing.

I would like to thank the members of the Lessard Research Group, who are by far the most accepting, easygoing, and fun coworkers I have had the pleasure to work alongside. In particular, thank you to Dr. Owen Melville, you gave me an incredible foundation to start from and our early talks about device theory shaped the entirety of my thesis. Thank you to Drs. Nicole Rice and Joseph Manion for your many efforts in cat-herding to keep our lab organized and running smoothly. There are too many others to name individually, but know each of you are wonderful people and researchers. Thank you to my friends in the Department of Chemical & Biological Engineering, especially my fellow Plant Design TAs. The hours we spent laughing and commiserating will be memories I hold for years to come.

I would like to thank my previous supervisors, Dr. Stephen Newman, Dr. Chaowu Xiao, and Dr. Max Hincke. The training each of you provided was instrumental in preparing me to succeed in graduate school, and I am so thankful for your faith in my abilities as a young researcher.

Thank you to our technical staff in the Department of Chemical & Biological Engineering and the Electronics Shop, who made it possible for me to accomplish much of the work in this thesis. From custom solutions that gave our group the ability to do high-throughput device fabrication and testing, to regular fixes of our most stubborn equipment, it would not have been possible to complete this thesis without your expertise.

Finally, I would like to thank my immediate and extended family. Your love and support as I decided to take on even more years of schooling is so appreciated, especially through the challenging times of the pandemic and everything that followed. To my parents, thank you for fostering my creativity and curiosity, and for providing me with everything I needed to succeed. To my partner Reid, you have been with me through so much in the past decade that has brought us to today, and I look forward to some more decades of joy, nonsense, and mayhem.

List of Peer-Reviewed Publications

1. **S. Brixi,** C. Dindault, B. King, H.R. Lamontagne, A. Shuhendler, S. Swaraj, B. Lessard (2023). "Poly(2-vinylpyridine) as an Additive for Enhancing N-Type Organic Thin-Film Transistor Stability" *Adv. Electron. Mater., ASAP, 2300660*
2. **S. Brixi,** H.R. Lamontagne, B. King, A. Shuhendler, B. Lessard (2023). "Solvent Additives for Enhanced N-type OTFT Stability." *Mater. Adv., 4, 4707-4711*
3. M. Cyr, **S. Brixi,** A. Ganguly, B. Lessard, J. Brusso (2022). "Synthesis of thieno[3,4-c] pyrrole-4,6-dione-based small molecules for application in organic thin-film transistors" *Dyes Pigm. 210, 110964*
4. **S. Brixi**, C. Radford, M. Tousignant, A. Peltekoff, J. Manion, T. Kelly, B. Lessard (2022). "Poly(ionic liquid) gating materials for high performance organic thin-film transistors: the role of block copolymer self-assembly at the semiconductor interface." *ACS Appl. Mater. Interfaces, 144, 36, 16456-16470*
5. N. Dallaire, **S. Brixi,** M. Claus, S. Blawid, B. Lessard (2022). "Benchmarking Contact Quality in N-type Organic Thin Film Transistors Through an Improved Virtual-Source Emission-Diffusion Model." *App. Phys. Rev. 9, 011418*
6. I. Park, **S. Brixi,** M. Martell, M. Ocheje, R. Pettipas, D. Harris, B. Gelfand, S. Rondeau-Gagné, B. Lessard, G. Welch (2021). "An air-stable n-type bay-and-headland substituted bis-cyano N-H functionalized perylene diimide for printed electronics." *J. Mater. Chem. C, 9, 13630-13634*
7. A. Peltekoff, **S. Brixi,** J. Niskanen, B. Lessard (2021). "Ionic Liquid Containing Block Copolymer Dielectrics: Designing for High-Frequency Capacitance, Low-Voltage Operation, and Fast Switching Speeds." *JACS Au, 1, 7, 1044-1056*
8. S. Rao, **S. Brixi,** D. Shaikh, M. Kobaisi, B. Lessard, S. Bhosale, S. Bhosale (2021). "The effect of TCNE and TCNQ Acceptor Units on Triphenylamine-Naphthalenediimide Push-Pull Chromophore Properties." *EurJOC, 18, 2615-2624*
9. S. Birajdar, **S. Brixi,** P. Rao, R. Bhosale, M. Kobaisi, A. Akhil Gupta, B. Lessard, S. Bhosale, S. Bhosale (2021). "Conjoint use of Naphthalene Diimide and Fullerene Derivatives to Generate Organic Semiconductors for n-type Organic Thin Film Transistors." *ChemistryOpen, 10, 1-8*

10. D. H. Harris, **S. Brixi,** B. Lessard, G. Welch (2020). "A N-H functionalized perylene diimide chromophore for alcohol processed organic electronics." *J. Mater. Chem. C,* 8, 9811-9815
11. **S. Brixi,** O.Melville, B. Mirka, Y. He, A. Hendsbee, H. Meng, Y. Li, B. Lessard (2020). "Air and temperature sensitivity of n-type polymer materials to meet and exceed the standard of N2200." *Sci. Rep., 10, 4014*
12. **S. Brixi,** O. Melville, N. Boileau, B. Lessard (2018). "The Influence of Oxygen and Temperature on the Performance of PBDB-T and P3HT in Organic Thin Film Transistors." *J. Mater. Chem.,* 6, 11972-11979

Table of Contents

List of Figures

List of Tables

1. Introduction

1.1. Organic Electronics

Organic electronics are simply electronic devices where the semiconductor, such as silicon, are replaced by carbon-based materials. These materials tend to be inherently flexible, and the devices can be made with low-cost manufacturing methods, enabling a new generation of inexpensive flexible and wearable electronics.

Organic semiconductors (OSCs) are highly conjugated molecules, which enables efficient charge transport their pi-electron systems.[1] OSCs are used as the active layers in a variety of electronics, such as organic photovoltaics (OPVs), organic thin film transistors (OTFTs), and organic light emitting diodes (OLEDs).

The majority of OSCs are intrinsic semiconductors, which are capable of transporting charge without addition of dopants.[2] Unipolar OSCs defined by their majority charge carrier. Those that transport positive charges (holes) are called p-type, and those which transport negative charges (electrons) are called n-type. Some materials are capable of effectively transporting both holes and electrons and are therefore ambipolar. Many OSCs are capable of transporting both charge carriers under appropriate conditions, but tend to be defined as unipolar when the majority charge carrier is orders of magnitude above the other.[3] Electrons are transported in the lowest unoccupied molecular orbital (LUMO) and holes are transported in the highest occupied molecular orbital (HOMO). These energy levels are analogous to the conduction band and valence band of inorganic materials, as seen in **Figure 1.1**.

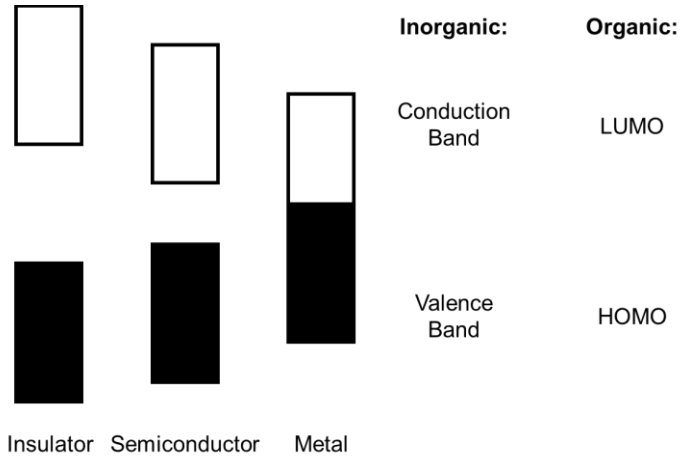

Figure 1.1. Energy band structures of insulators, semiconductors, and metals.

There are two broad classes of OSCs, small molecules and conjugated polymers. The focus of this thesis is on soluble OSCs, which enables them to be processed in solutions and inks for future applications in large-area printing. These materials can be used to fabricate devices with roll-to-roll processing, similar to the standard of the paper and print industry. Both small molecules and polymers can be processed this way, as long as the materials are soluble in the printing solvent. For the purpose of this thesis, the solution-processable polymeric semiconductor poly{[N,N′-bis(2-octyldodecyl)-naphthalene-1,4,5,8-bis(dicarboximide)-2,6-diyl]-alt-5,5′-(2,2′-bithiophene)} (P(NDI2OD-T2))[4] (**Figure 1.2a**) is used in all studies to provide a simple comparison between studies and to other studies in literature which use this material.

Increasing conjugation in these OSCs enhances the number of available energy states, effectively decreasing the gap between the HOMO and LUMO (see **Figure 1.2b**). This is what differentiates insulating organic materials from OSCs, and enables the ability to take advantage of these properties for electronics applications.

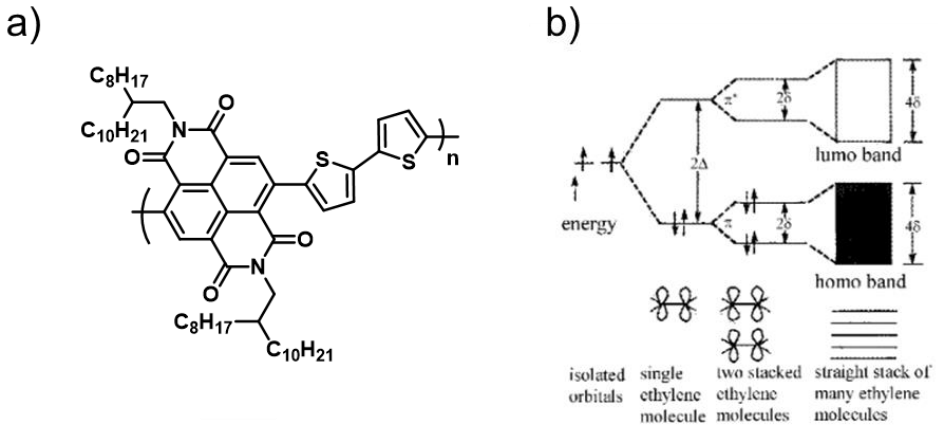

Figure 1.2. a) The structure of P(NDI2OD-T2). b) An example of the increasing energy states caused by increasing conjugation, given by the example of stacking ethylene molecules. Adapted from Cowie & Valeria Arrighi.[5]

To study these materials, it is essential to have a method to gauge their performance. OTFTs provide an excellent platform for studying the characteristics of materials used in organic electronic devices due to the various performance parameters that can be extracted from these devices.

1.2.Organic Thin-Film Transistors

OTFTs, also commonly referred to as organic field effect transistors (OFETs), function as an on/off switch, which is essential for numerous applications, from simply turning pixels on a screen on and off to complex logic circuits. A few examples of these applications include flexible displays[6–9], radio frequency identification tags (RFID)[10,11], and even new medical technologies such as bio-inspired artificial nerves[12].

The three main elements of an OTFT are the semiconductor layer, the dielectric layer, and the electrodes (gate and source). Polarization of the dielectric layer facilitates charge to be transferred in the semiconductor at the semiconductor-dielectric interface. The gate electrode and the source/drain electrodes are located at the opposite sides of the dielectric layer, and this enables the polarization of the dielectric layer by applying a voltage between the gate and contact. This placement of the three electrodes enables a variety of different OTFT configurations, as shown in **Figure 1.3**.

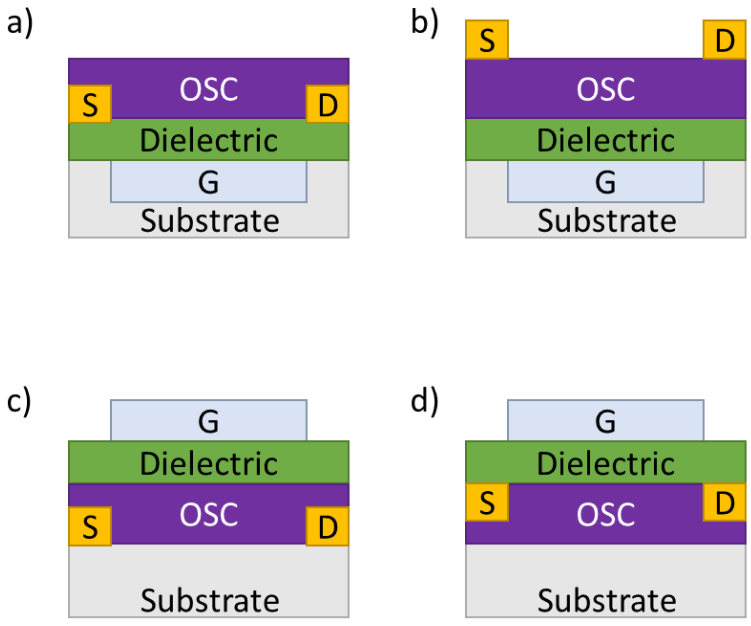

Figure 1.3. Structure of an OTFT. a) Bottom-gate bottom-contact (BGBC), b) Bottom-gate top-contact (BGTC), c) Top-gate bottom-contact (TGBC), d) Top-gate top-contact (TGTC).

Each OTFT structure displayed in **Figure 1.3** may be desirable for certain application or due to manufacturing restrictions. For example, a solution-processable semiconductor may require a

solvent which would solubilize the gate dielectric, but the gate dielectric could be cast from a solvent that does not impact the OSC layer.[13] For such situations, a top-gate structure would be advantageous. Top-contact devices may improve contact resistance compared to bottom-contact transistors in some systems, and thus a top-contact structure may be more desirable if contact resistance is found to be present in a bottom-contact device.[14]

The three main performance metrics used to characterize an OTFT are field-effect mobility (μ) of the majority charge carrier, the threshold voltage (V_T), and the on/off ratio. Each of these gives an important indication into the operation and effectiveness of a transistor. During operation, the voltage between the source and drain electrodes (V_{DS}) is constant, while the voltage between the gate and source (V_{GS}) is changed. The resulting current between the source and drain electrodes (I_{DS}) is measured. An example of the characteristic current-voltage curves generated to study the properties of OTFTs is given in **Figure 1.4**.

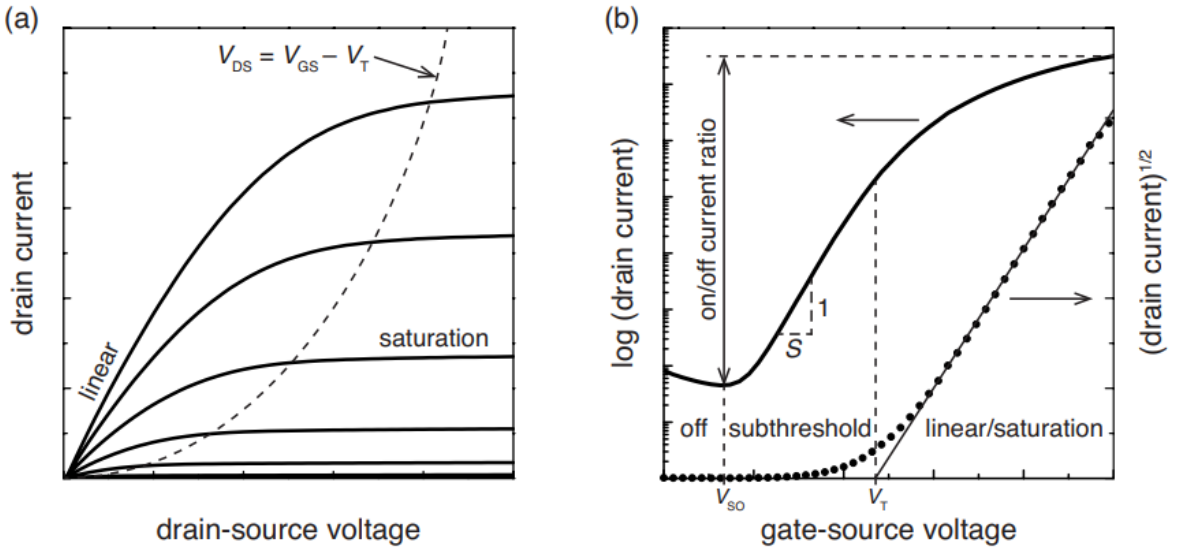

Figure 1.4. (a) A typical output curve with saturation and linear regions indicated. (b) A typical ideal transfer curve. Adapted from Herlogsson.[15]

The μ gives an indication of how effectively the semiconductor can move charge. This is the most common metric to compare devices and OSCs in the field. In general, the μ should be maximized, but to match amorphous silicon, the ideal μ of an OSC should be 0.1 - 1 cm^2/Vs for the most common commercial organic electronic devices such as OLEDs, as this competes with amorphous silicon.[16] The V_T of a transistor indicates how much voltage must be applied to mobilize

charges. A V_T close to zero is desired to enable low-energy operation. Finally, the on/off ratio (I_{on}/I_{off}) is a measure of the difference in the I_{DS} in the on and off states of the device. This allows for the device to effectively work as a switch, and it is essential for an effective transistor to have a high on/off ratio to be functional in practical applications.

The same theory for determination of charge transport characteristics that is applied to inorganic metal-organic semiconductor field effect transistors (MOSFETs) is often applied to OTFTs and provides a reasonable approximation for these performance characteristics.[17] A voltage is applied across the source and drain currents, but current cannot flow until a voltage is applied between the source and gate that is greater than the V_T. When $V_{GS} > V_T$, charge begins to accumulate in the channel between the gate and source, and the device can be operated. The transistor can then operate in one of two modes: linear or saturation, depending on the applied voltages. In the linear mode, low V_{DS} is applied, and $V_{DS} < (V_{GS} - V_T)$. When a higher V_{DS} is applied, such that $V_{DS} \geq (V_{GS} - V_T)$, the transistor operates in the saturation mode. This is illustrated in an output curve (**Figure 1.4**), which plots I_{DS} at V_{DS} for various applied V_{GS}. μ can be extracted from either the saturation or linear region of the device's operational range.

For the purposes of this thesis, and as commonly done in the literature, the saturation region is reported and will regularly be referred to simply as μ. The μ, I_{on}/I_{off}, and V_T can be determined in the saturation region based on the general expression relating current to μ and V_{GS} in the saturation mode (**Equation 1**), or linear mode (**Equation 2**):

$$(1)\ I_{DS} = \frac{\mu C_i W}{2L}(V_{GS} - V_T)^2$$

Where C_i is the capacitance of the dielectric material, W is the width of the channel and L is the length of the channel. By taking the square root of **Equation 1**, a linear relation can be obtained (as shown in **Equation 3**), so that the μ and V_T can be calculated directly from the slope and x-intercept of an $\sqrt{I_{DS}}$ *vs* V_{GS} curve, respectively.

$$(2)\ \sqrt{I_{DS}} = \sqrt{\frac{\mu C_i W}{2L}}(V_{GS} - V_T)$$

Finally, the on/off ratio is determined by **Equation 3**:

$$(3)\ On/Off\ Ratio\ = \frac{I_{on}}{I_{off}}$$

An example of the process of extracting these values from characteristic transfer curves is presented in **Figure 1.5**.

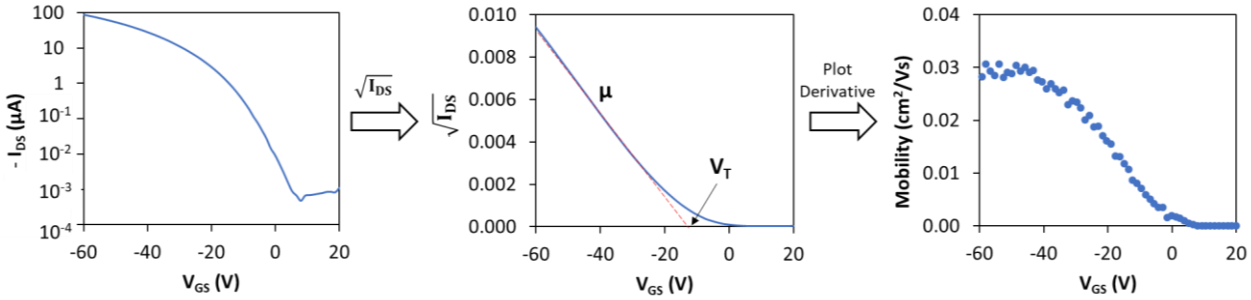

Figure 1.5. Typical transistor operation from a transfer curve and transformations used to find device performance parameters.

Due to non-ideality in the performance of some OTFTs, the linearization of the transfer curve is not always perfect, and thus the μ can be estimated inaccurately. Therefore, a μ vs V_{GS} curve is presented in some of this thesis to ensure transparency in the device measurements where high non-ideal device behaviour was observed. This non-ideality is discussed further in Chapter 2. In general, OTFTs often display higher contact resistance than MOSFETs, especially without proper optimization.[14,18] This often occurs due to poor energy level matching between the work function of the contacts and the frontier molecular orbital in which the majority charge carrier is transported; this can be overcome by choosing appropriate metals or interlayers for the source and drain contacts to reduce the gap in these energy levels.[19]

Another device characteristic of interest is the subthreshold slope. The subthreshold region of the transfer curve (which can be seen in Figure **1.4b**) is highly impacted by the presence of charge traps, as the trap states are rapidly being filled when the device is first subjected to bias.[20] The subthreshold slope can be calculated by **Equation 4**, taken in the subthreshold region:[21]

$$(4)\ S = \frac{dV_{GS}}{d(log\ I_{ds})}$$

By measuring this parameter from the OTFT output, the number of charge traps can be estimated. This can be useful for determining how much a device is impacted by traps caused by the device's surrounding environment[22] or to indicate whether device behaviour is non-ideal[23].

Electron mobilities observed in recently-developed n-type OSCs are in excess of 1 cm^2/Vs. **Table 1.1** summarizes recent high-performing examples of n-type OTFTs, both small molecules and polymers. These examples are limited to thin-film transistors, although it should be noted that single-crystal organic field-effect transistors can achieve exceptional mobility values in excess of 10 cm^2/Vs.[24]

Table 1.1. Recent developments in high-performance n-type OSCs.

OSC Material Abbreviation	Device Structure	Gate Dielectric	μ_e (cm^2/Vs)	V_T (V)	On/Off Ratio	Ref.
PNBS	TGBC	PMMA	7.8	57	10^3 - 10^4 *	25
PNDIF-T2	BGTC	SiO2/ODTS	3.93	14	10^5	26
2DQTT-*o*-B	BGBC	SiO2/ODTS	4.2	-13.9	10^5	27
NDI3HU-DTYM2	BGBC	SiO2/ODTS	3.03	-2.5	10^7	28
PDBPyBT	BGBC	SiO2/DDTS	4.54	25*	10^3	29
pSNT	BGTC	SiO2/NTMS	4.58	1	10^6 - 10^7	30
P(NDI2OD-T2)	TGBC	PMMA	4.1	0*	10^6	31
P4	BGTC	SiO2/OTMS	6.93	1-5	10^6 - 10^7	32

Average mobilities are reported where possible.
*Estimation based on available figures where no direct value was reported.

The electron mobilities of all materials listed in **Table 1.1** are competitive with, or even exceed the mobility that can be obtained with amorphous silicon, which has performance in the range of 0.1 – 1 cm^2/Vs.[16] Organic semiconductors therefore meet the mobility requirements for use in applications such as in transistor backplanes for displays.

While these mobility values promising, high threshold voltage can be observed in several examples. The V_T is controlled by a combination of the OSC's properties, the contacts used, and the dielectric material. Table 1.2 lists recent developments in OTFT dielectric materials leading to low-V_T operation.

Table 1.2. Dielectric materials for low-threshold voltage operation OTFTs.

Dielectric Material	Device Structure	OSC	μ (cm^2/Vs)	V_T (V)	On/Off Ratio	Ref.
HfO_2/ODTS	BGBC	P3HT	0.011	−1.4	10^4	33
ZrO_2/PAMS	BGTC	Pentacene	*N.R.*	-1.1	*N.R.*	34
TiO_2/PAMS	BGTC	Pentacene	0.8	-0.49	10^4	35
PVA/$BaTiO_3$	BGTC	Pentacene	0.35	-0.7	10^3 - 10^4 *	36
MXD6	BGTC	Pentacene	*N.R.*	-5	*N.R.*	37
PMMA	BGTC	Pentacene	0.1	-0.3	10^3 *	38
PS-PMMA-PS /[EMIM][TFSI]	TGBC	P3HT	*N.R.*	< 1	10^7	39
PS-PMMA-PS /[EMIM][TFSI]	TGBC	P3HT	0.5	0.3	*N.R.*	40

N.R. No reported value.
*Estimation based on available figures where no direct value was reported.

1.3.Stability in OTFTs

To enable functional circuits, especially those beyond the most basic applications, structures such as inverters are used. However, this requires balanced charge transport of both holes and electrons, and therefore requires effective p- and n-type OSCs based OTFTs to be used. While p-type materials have been widely explored and developed in the field, the development of materials for n-type OTFTs has lagged behind in terms of performance and stability.[41] The relatively low performance of n-type materials, in addition to the lack of stability of OSCs are some of the biggest hurdles to the adoption of organic electronics in commercial applications.[42] The instability of OSCs can be caused by a variety of factors. For n-type materials, a significant factor is the susceptibility of electrons in the lowest unoccupied molecular orbital (LUMO) to oxidation in air. However, it has been found that designing new n-type semiconductors with a LUMO level of approximately -4.0 eV or lower will enable operation in air.[43–45]

Material stability has been an ongoing challenge with organic electronics, and has recently been identified as the major barrier to the commercial adoption of this technology[42]. Stability can have a number of meanings, including operational stability of the devices, mechanical stability, thermal stability, and stability when exposed to air.[46–49] Air stability is an important factor to study and control, as it is the cause of long-term degradation of devices, ultimately decreasing their lifetime. N-type materials are particularly unstable in air due to the high-lying LUMO level making them susceptible to oxidation[50]. However, across the literature the term “air-stable” is often not

entirely accurate. A device or semiconductor material is often referred to as being air-stable when it is possible to operate the device in air briefly so that a researcher can determine its properties. But consistent use in air leads to loss of charge μ by orders of magnitude even if the LUMO level is below -4.0 eV.[51] This is not truly air stability, despite it being referred to this way. In order to enhance device lifetime and usefulness, air-stability is the major aspect of stability that needs to be improved[42], and with a particular focus on n-type materials.

The two main species identified as causing this instability in air are oxygen and water. These species participate in reactions that involve the extraction of electrons from the OSC exposed to air, which exhibits why n-type semiconductors are particularly susceptible to degradation by ambient conditions. **Figure 1.6** demonstrates the species involved in these reactions and how the LUMO level of -4.0 eV is determined via redox reactions, taking into account the overpotentials of these reactions[44].

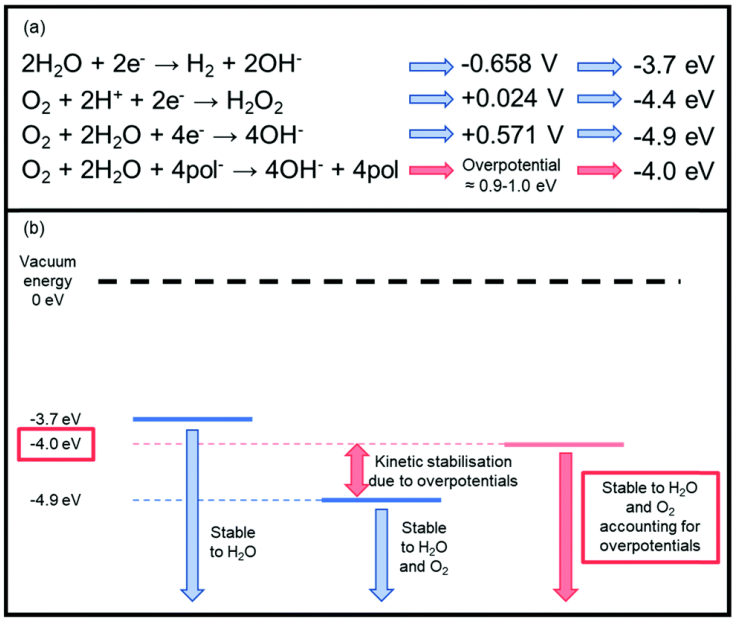

Figure 1.6. Energy levels at which charge carriers are susceptible to oxidation and water. Adapted from Griggs et al.[52]

A variety of approaches have been taken and are currently the standard for the improvement of air stability of organic semiconductors and devices. The main approach to improving n-type material stability is to design new materials to have a lower-lying LUMO energy level in order to avoid oxidation[43,44], which has been referred to as LUMO tuning. Devices can be also encapsulated

to prevent or slow the diffusion of air into the devices by including laminating layers that act as diffusion barriers[53]. The design of the device can also be manipulated, giving improved initial performance, and therefore the lifetime can be increased simply because it takes longer to degrade to the point where charge will no longer flow due to higher initial performance. Additionally, manipulation of device design can move the susceptible layers in such a way that they are less exposed to air, similar to device encapsulation[54].

The typical approaches to improve the stability of OTFTs are often slow, and significantly increase complexity of fabrication. LUMO tuning is a slow process that requires the development and design of entirely new materials, while perfectly good materials exist with excellent properties that could otherwise be used in OTFTs. The process of design, to small scale synthesis, to large scale synthesis can take years. Encapsulation can significantly slow the degradation in air, but air will still diffuse into the devices slowly over time, and adds another processing step which may not be compatible with certain device applications[55]. Changing the design of device architecture (for example, to bottom gate bottom contact, TGBC) will ultimately increase device lifetime by giving a higher initial level of performance, but ultimately devices will still degrade. This can also make the fabrication of these devices significantly more complicated. As the goal is to have inexpensive devices made with organic semiconductors, this is not a useful strategy to improve stability for commercialization[56]. We are left needing to look to other methods to improve OTFT stability.

1.4. Additives for OTFTs

Additives have been used in a variety of organic electronic devices, and in OTFTs they are typically used to improve device performance. An additive is any material which combined with the semiconductor layer to change its material properties in some way, and can be incorporated into the device through a variety of methods[57]. Additives can affect the semiconductor either through electronic or non-electronic processes[58]. Electronic processes are those wherein there is an interaction between the semiconductor and additive that affect the energy levels of the material, affecting its electronic properties. These materials are typically called dopants[58]. Processes described as non-electronic are any process by which the additive changes device performance without affecting the material's electronic properties. Both types of additives can affect almost any

criteria of device performance, including μ, I_{on}/I_{off}, and V_T. Therefore, additives are a promising avenue to improve both performance and stability of OTFTs[57].

Dopants function by donating electrons or holes, or changing the Fermi level of the material[59]. This has the effect of increasing charge μ[60] and bringing V_T closer to zero[61]. The I_{on}/I_{off} can be improved due to improved μ, but can also become worse due to the material conductivity increasing and leading to high off-currents[62]. There is often a delicate balance in the ratio of dopant to semiconductor to ensure improved μ and V_T, without sacrificing the I_{on}/I_{off} . Much like organic semiconductors, dopants can be p-type or n-type depending on whether they facilitate hole or electron transport. While the doping effect is essential to improve device performance, the modulation of other material properties by additives can also be highly beneficial.

There is no definitive term for an additive that does not affect the electronic properties of the material as they can have a variety of functions, and as such are simply called additives. Typically, additives are used to control the morphology of the thin film by influencing the solid-state packing of the semiconductor molecules[63]. However, some additives may interact with the environment the devices are exposed to, such as reacting with water in air[64]. Additives have also been known to fill physical voids in the materials, which slows or prevents the diffusion of oxygen into the organic semiconductor[65]. These interactions could result in increased stability due to the ability to prevent air from infiltrating the organic semiconductor, but there is little literature available currently available on the topic. When combined with the doping effect, additives give the possibility of a simultaneous improvement of charge transport and stability.

The n-doping effect occurs through the donation of electrons from the dopant molecules. Early studies showed that n-doping made organic semiconductors significantly less stable by raising the LUMO energy level[41]. However, relatively stable dopants have been discovered in the past decade, including derivatives of 1,3-dimethyl-2-phenyl-2,3-dihydro-1H-benzoimidazole (DMBI). This group of additives is one of the most-studied n-type dopants in recent years and has led to significant improvements in device performance, particularly due to the fact that electrons are highly stable and less likely to react with air[62,66]. These materials can require complex synthesis, making them a poor candidate for commercial applications due to high costs resulting from the difficult synthesis. Amines have shown promising results as dopants due to their electron donating effect[67], and have in some cases shown improved stability[64]. Other promising dopants include aminosilanes, which contain both the n-doping amine group and a silane group. Silanes

generally act as p-type dopants by removing electrons from the material, particularly if the silane is strongly electron-withdrawing[68]. However, the p-doping effect of the silane group is overcome by the electron-donation of the amine, and leads to n-doping, while still conveying other benefits from the silane[69]. The silane group tends to anchor the dopant to the semiconductor, making it highly effective at filling voids, which theoretically could prevent the diffusion of air into the semiconductor. The authors did not study the stability of this dopant. As this is not a well-studied part of the field, researchers still have not found widely applicable solution to improved performance and stability. The focus in the field has been largely on synthesizing more stable semiconductors, rather than improving stability-enhancing additives.

Additives are a promising and scalable method to improve device performance with low-cost that can be applied to any organic semiconductor to enable commercialization of technologies that are currently only in the research and development phase. Additives with air-stabilizing groups such as amines and silanes can enhance OTFT stability and are promising candidates for further study[64,67]. Particularly, aromatic amines have shown the dual effect of improving performance and stability[64]. While aminosilanes have been studied for device performance improvements, their air stability properties have not. The reported observation of the void-filling properties of the aminosilane dopants[69] should theoretically lead to stability enhancement. In addition to this, silanes have well-known reactivity with water, which could prevent water infiltration into the devices from humid air. Therefore, aminosilanes based on aromatic amines, rather than the simple alkyl aminosilanes that were previously studied, would be good candidates to improve OTFT stability. These additives would be applied to organic semiconductors and the device stability and performance would be studied to determine whether they could prove to be the next step in moving OTFTs towards commercialization.

1.5. Gate Insulation Layer

While the OSC is an essential component to consider for the performance of an OTFT, each layer has to be carefully chosen in the fabrication of an OTFT for each particular application. While all layers and interfaces can be subject to improvement, within the scope of this thesis, the layer insulating the gate electrode from the semiconductor (often called a dielectric, though this is not necessarily an accurate description for electrolyte-based systems) is the other main interface studied aside from the OSC.

The gate insulator functions by the formation of dipoles when subjected to an electric field between the gate and source electrodes, which then polarizes the semiconductor so that charge injected from the source electrode will travel through the semiconductor at the semiconductor-insulator interface.[70] This can be treated as a parallel-plate capacitor, so that the capacitance of the insulator can be found,[71] as shown in **Equation 5** and **Figure 1.7**:

$$(5)\ C_i = \frac{\epsilon A}{d}$$

Where C_i is the capacitance that would be used in **Equations 2** and **3**, A is the area, ϵ is the permittivity of the insulator, and d is the separation between the parallel plates (ie. the insulator layer thickness).

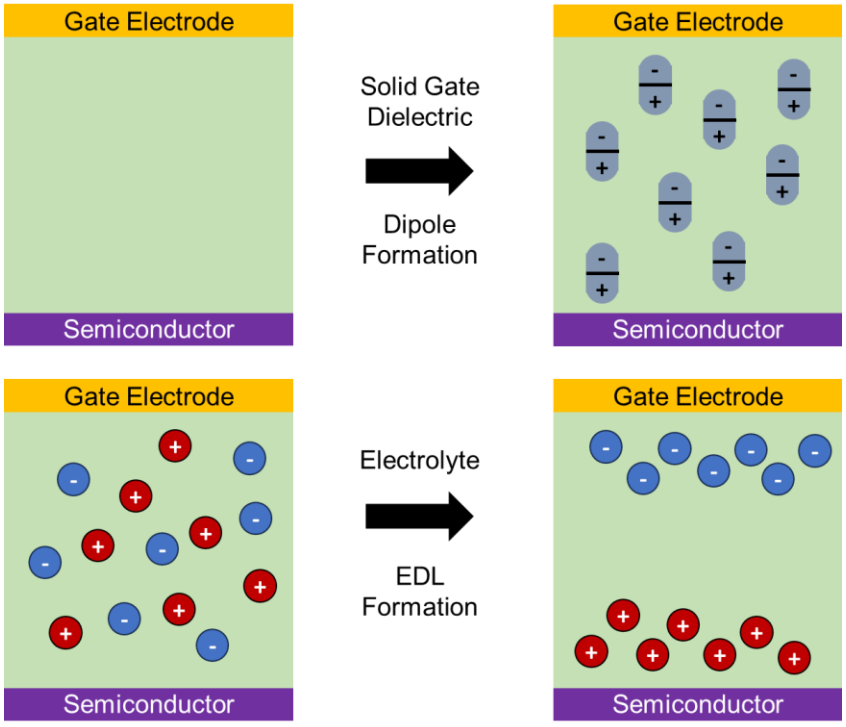

Figure 1.7. Formation of dipoles via polarization of solid gate dielectrics and formation of electrical double layer by electrolyte materials.

The gate insulator can impact all performance parameters discussed in Section 1.2. The interaction of the OSC with the insulator can impact how the OSC arranges in the solid state, which can have significant impact particularly on μ. The C_i of the dielectric will directly impact the V_T, as it affects how much current is needed to polarize the gate insulator.

Dielectrics with high dielectric constants can cause high energetic disorder at the semiconductor-insulator interface, which results in charge-trapping and ultimately lowers charge μ.[72] This is particularly problematic with dielectric materials having hydroxyl groups at the semiconductor-insulator interface, which also contribute to charge trapping.[73] Common dielectrics, such as SiO_2, suffer from this problem. A solution to this problem has been extensively investigated through the use of self-assembled monolayers, which react with the surface hydroxyls. This can reduce the number of charge traps, and thus improve device μ and enhance V_T.[1,74–76] SiO_2 is a consistent and well-known system, which can enable useful comparison across literature. Therefore, it has been used in a large portion of this thesis to provide a consistent baseline for comparison to devices in literature, and between the studies presented in these chapters.

Despite the use of self-assembled monolayers to improve device performance, solid dielectrics can suffer from additional limitations on performance, fabrication, and applications. Rigid solid dielectrics, such as SiO_2, are often impractical for applications that require flexible substrates, such as wearable electronics. There are numerous examples of flexible dielectrics, such as common polymers poly(styrene)[77–80] and poly(methyl methacrylate)[81–84]. Polymer dielectric materials can improve flexibility and some of these materials lack the issues relating to charge trapping mentioned above. However, if the dielectric is a rigid inorganic material or a flexible organic material, the corresponding performance is still a function of film thickness and therefore limits the choice of manufacturing. To enhance capacitance, thereby decreasing V_T, the dielectric must be made as thin as possible as indicated in **Equation 4**. This can impose practical constraints on fabrication, which may require specialized techniques[85] to achieve, or can lead to variation between batches or across large printed area.

If the insulating layer is able to form an electrical double layer (EDL) instead of forming these static dipoles found in solid dielectrics, then this thickness-independence can be overcome (**Figure 1.7**).[86] Therefore, electrolyte-based systems (**Figure 1.8**), electrolyte-gated transistors (EGTs), are an attractive option for a gate insulating layer, due to their ability to form an electrical double layer.[87–89] The inclusion of a liquid medium for the insulating layer in EGTs decreases their mechanical stability compared to all-solid devices, as any cracks or mechanisms for the electrolyte to escape will lead to a loss of device function. In addition to this, the electrolyte may diffuse into the semiconductor layer. This can cause doping in the semiconductor layer, which may or may not be desired. The diffusion into the semiconductor layer can cause high hysteresis and slower on/off

response times if the ionic conductivity of the semiconductor is not sufficiently high.[89] However, these EGTs can achieve very low V_T and low-voltage operation,[88] which makes this a desirable mode of operation.

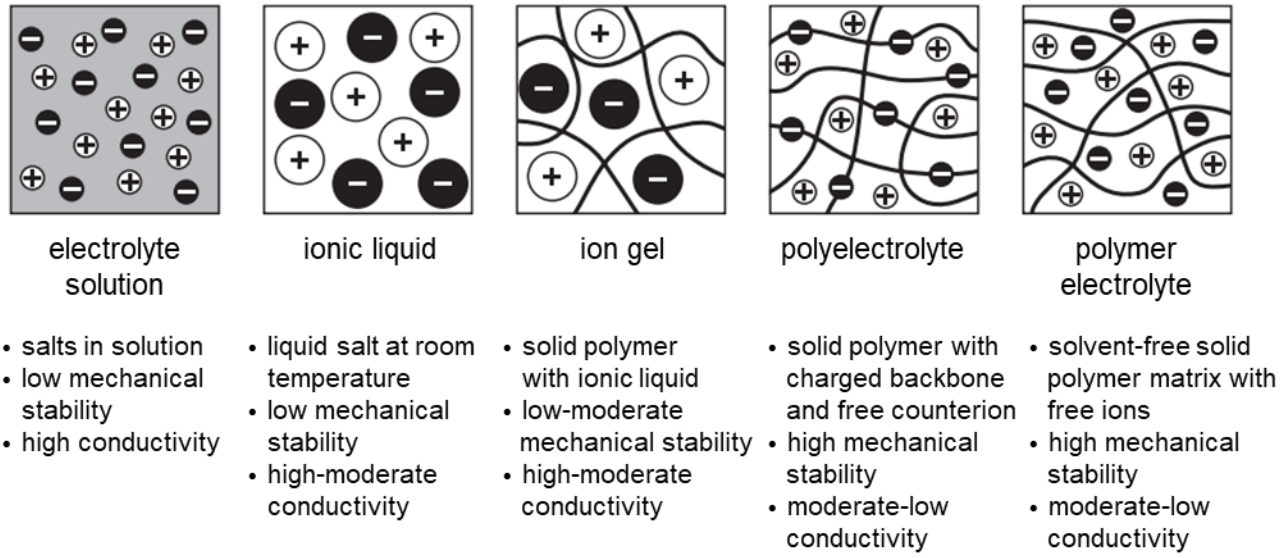

Figure 1.8. Comparison of different types of electrolyte solutions and electrolyte/polymer systems. Adapted from Herlogson.[15]

Ion gels bridge the gap between solids and electrolytes. Ion gels are a mixture of ionic liquid and polymer, which are also capable of forming an EDL as this ionic liquid diffuses through the network. In these systems, the polymer is ionically conductive, typically with polar groups such as hydroxides, oxides, and glycols.[90] These systems typically involve very low concentrations of polymer (eg. ~5 wt %), which results in high ionic conductivity.[91] However, this low composition of solid material in the ion gel also leads to low mechanical stability.

To this end, poly(ionic liquids) (PILs), also known as polyelectrolytes (**Figure 1.8**), have been devised as a solution to the issues with both mechanical stability and ion diffusion. These materials are polymers with a charged backbone and a mobile anion bearing the opposite charge to the backbone, which is freely mobile. This means that the charged backbone will remain stationary, while the mobile anion can migrate, facilitating the formation of an electrical double layer. If this configuration is used such that the mobile anion is negative and paired with an n-type OSC, or the mobile anion is positive and paired with a p-type OSC, then the mobile anion will migrate towards the gate electrode during ideal device operation, leaving the charged immobile backbone at the

semiconductor-insulator interface. This prevents the ion diffusing into the semiconductor, as discussed above, and simultaneously the electrical double layer is formed.

PIL gating materials can vary in complexity of design, from simple homopolymers[92,93], random copolymers[94,95], to di-[96–98] and even multi-block[99–101] copolymers. Homopolymer PILs tend to display low glass transition temperatures (T_g), often below room temperature, which leads to low rigidity and mechanical stability.[102] It has been shown that designing PIL gating copolymers can lead to improved mechanical properties when monomers with higher T_g are incorporated.[103] The type of copolymer chosen for PIL design will impact the properties of the gating material. For example, designing a random copolymer can lead to low capacitance, as the incorporation of a non-conducting monomer can reduce ionic conductivity with sufficient composition, and there will be no localized regions for ionic conductivity.[95,104,105] Block copolymers overcome this limitation with careful design of each block. A rigid block will provide mechanical stability, while a second conductive block will give rise to pathways for ionic conduction.[106] Block copolymer self-assembly is required to achieve this, as there must be localized areas of film that are highly conductive to facilitate ionic conductivity.

1.6 Block Copolymer Self-Assembly

Self-assembly is a process of phase separation between two incompatible materials. Using a di-block copolymer as an example, self-assembly occurs when block A and block B are immiscible and segregate into two separate phases: one rich in monomer A, and the other rich in monomer B.[107] This process is even more complex when the copolymer is fabricated in a thin film, such as in most organic electronics applications, as stretching/compression and surface interaction effects can impact how a block copolymer will self-assemble.[108]

During film formation, a block copolymer will experience numerous forces which will determine the film morphology. These forces include: interactions between the blocks, interactions between solvent and polymer, interactions between each block and the interface, and mechanical forces introduced by confinement in a thin film.[108–110] The first two forces are dominant while the block copolymer is in solution, and during film formation all of these forces can impact how the copolymer will phase separate in the solid thin film.

The phase separation of block A and B is caused by the immiscibility of the two blocks. It is more thermodynamically favourable for each block to “pool” with itself, and therefore a stable

state is formed when the two blocks have as little contact as possible.[111] Surface and solvent interactions will similarly impact how the blocks arrange themselves to reach the most thermodynamically favourable point. Shown in **Figure 1.9**, differing ratios of the size of the two blocks will determine the most favourable morphology for the copolymer to take on. The tendency to self-assemble is also affected by the distribution of the polymer's molecular weight, which is represented by the polydispersity index (PDI). The dotted line of **Figure 1.9a** represents a polymer with a perfect PDI of 1.0, while the solid line represents a polymer with a PDI of 2.0. As is demonstrated in the diagram, higher strength of segregation (low miscibility, high repulsion between blocks) will lead to formation of various morphologies. Those with high miscibility will be disordered and will not demonstrate any self-assembly.

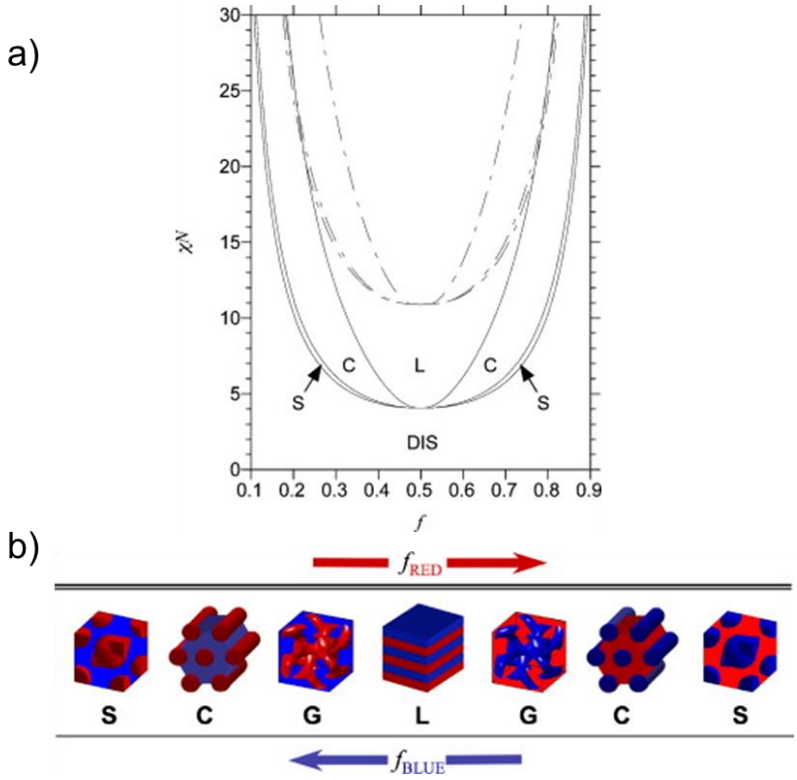

Figure 1.9. a) Thermodynamic stability diagram of a di-block copolymer melt. b) Morphology of block A (red) and block B (blue) with varying ratios of A and B present in the copolymer. χN = strength of segregation, f = volume fraction of a block, S = BCC spherical, C = hexagonally packed cylinders, G = gyroidal, L = lamellar, DIS = disordered. Adapted from Lynd *et al.*[112]

The most common modes of packing that are observed in block copolymers as a result of self-assembly are body-centered cubic (BCC) packed spheres, hexagonally packed cylinders, cubic

gyroid, and lamellae, shown in **Figure 1.9b**. In terms of organic electronics, the morphology that a block copolymer takes on will impact how effective the material will be in its desired application.[109] With respect to the design of PILs for gating materials, this means that ideal morphologies will allow for ionic conductivity throughout the thin film such that the formation of an EDL remains possible.

1.7 Thesis Scope

N-type OTFTs are essential components for emerging applications in the field of organic electronics, however, their stability and performance need improvement to be viable in a greater number of practical applications. These devices have numerous layers and interfaces which can be optimized to achieve desired performance for each application. Generally, the OSC and the gating material are two of the main components which impact device performance. In particular, the OSC is susceptible to instability in air. These layers are ideal candidates for study to improve the performance and stability of an OTFT.

This thesis addresses two major hurdles to the commercialization of n-type OTFTs: their stability and performance. In Chapter 2, the air-stability of various n-type OSCs was studied, and a methodology for examining air-stability was developed. Chapter 3 demonstrates the screening of various potential stabilizing additives for n-type OTFTs in air. Candidates were determined from literature review, and numerous device studies were conducted to determine whether any structure-property relationships could be determined between the additives and the improvement of device stability. Chapter 4 follows up on the results of Chapter 3, taking a candidate material from the screening study, performing more in-depth optimization of the ideal stabilizing additive. Optimal ratios of the OSC:additive were determined, and the properties of the films were studied to determine the impact of the additive on both device performance and film morphology. Finally, Chapter 5 examines another crucial component of the OTFT, the gating material. PILs were used as gating layers to enable practical operating voltage of the OTFTs. The film morphology was studied extensively to determine the ideal modes of self-assembly to achieve low-voltage device operation.

This thesis contributes methodologies for studying OTFT stability, demonstrates the practicality of broad screenings for candidate additives in devices, develops practical and low-cost additives

for the enhancement of n-type OTFT stability, and shows examples of novel PILs for low-voltage operation OTFTs with extensive examination of the PIL self-assembly.

1.8 References

(1) Coropceanu, V.; Cornil, J.; da Silva Filho, D.; Olivier, Y.; Silbey, R.; Brédas, J.-L. Charge Transport in Organic Semiconductors. *Chem. Rev.* 2007, *107*, 926–952.

(2) Klauk, H. *Organic Electronics*; Klauk, H., Ed.; Wiley, 2006.

(3) Baeg, K. J.; Caironi, M.; Noh, Y. Y. Toward Printed Integrated Circuits Based on Unipolar or Ambipolar Polymer Semiconductors. *Adv. Mater.* 2013, *25*, 4210–4244.

(4) Yan, H.; Chen, Z.; Zheng, Y.; Newman, C.; Quinn, J. R.; Dötz, F.; Kastler, M.; Facchetti, A. A High-Mobility Electron-Transporting Polymer for Printed Transistors. *Nature* 2009, *457*, 679–686.

(5) Cowie, J. M. G.; Arrighi, V. *Polymers : Chemistry and Physics of Modern Materials, Third Edition*, 3rd Editio.; CRC Press: Boca Raton, 2007.

(6) McCarthy, M. A.; Liu, B.; Donoghue, E. P.; Kravchenko, I.; Kim, D. Y.; So, F.; Rinzler, A. G. Low-Voltage, Low-Power, Organic Light-Emitting Transistors for Active Matrix Displays. *Science (80-.).* 2011, *332*, 570–573.

(7) Ohta, S.; Chuman, T.; Miyaguchi, S.; Satoh, H.; Tanabe, T.; Okuda, Y.; Tsuchida, M. Active Matrix Driving Organic Light-Emitting Diode Panel Using Organic Thin-Film Transistors. *Jpn. J. Appl. Phys.* 2005, *44*, 3678–3681.

(8) Klauk, H.; Gundlach, D. J.; Nichols, J. A.; Jackson, T. N. Pentacene Organic Thin-Film Transistors for Circuit and Display Applications. *IEEE Trans. Electron Devices* 1999, *46*, 1258–1263.

(9) Rogers, J. A.; Bao, Z.; Baldwin, K.; Dodabalapur, A.; Crone, B.; Raju, V. R.; Kuck, V.; Katz, H.; Amundson, K.; Ewing, J.; et al. Paper-like Electronic Displays: Large-Area Rubber-Stamped Plastic Sheets of Electronics and Microencapsulated Electrophoretic Inks. *Proc. Natl. Acad. Sci.* 2001, *98*, 4835–4840.

(10) Baude, P. F.; Ender, D. A.; Haase, M. A.; Kelley, T. W.; Muyres, D. V.; Theiss, S. D. Pentacene-Based Radio-Frequency Identification Circuitry. *Appl. Phys. Lett.* 2003, *82*, 3964–3966.

(11) Rotzoll, R.; Mohapatra, S.; Olariu, V.; Wenz, R.; Grigas, M.; Dimmler, K.; Shchekin, O.; Dodabalapur, A. Radio Frequency Rectifiers Based on Organic Thin-Film Transistors.

Appl. Phys. Lett. 2006, *88*, 123502.

(12) Kim, Y.; Chortos, A.; Xu, W.; Liu, Y.; Oh, J. Y.; Son, D.; Kang, J.; Foudeh, A. M.; Zhu, C.; Lee, Y.; et al. A Bioinspired Flexible Organic Artificial Afferent Nerve. *Science (80-.).* 2018, *360*, 998 LP – 1003.

(13) Zakhidov, A. A.; Lee, J. K.; Fong, H. H.; DeFranco, J. A.; Chatzichristidi, M.; Taylor, P. G.; Ober, C. K.; Malliaras, G. G. Hydrofluoroethers as Orthogonal Solvents for the Chemical Processing of Organic Electronic Materials. *Adv. Mater.* 2008, *20*, 3481–3484.

(14) Necliudov, P. V.; Shur, M. S.; Gundlach, D. J.; Jackson, T. N. Contact Resistance Extraction in Pentacene Thin Film Transistors. *Solid. State. Electron.* 2003, *47*, 259–262.

(15) Herlogsson, L. Electrolyte-Gated Organic Thin-Film Transistors, Linköping University, 2011.

(16) Paterson, A. F.; Anthopoulos, T. D. Enabling Thin-Film Transistor Technologies and the Device Metrics That Matter. *Nat. Commun. 2018 91* 2018, *9*, 1–4.

(17) Nisato, G.; Lupo, D.; Ganz, S. *Organic and Printed Electronics: Fundamentals and Applications*; Taylor & Francis: Boca Raton, 2016.

(18) Gundlach, D. J.; Zhou, L.; Nichols, J. A.; Jackson, T. N.; Necliudov, P. V.; Shur, M. S. An Experimental Study of Contact Effects in Organic Thin Film Transistors. *J. Appl. Phys.* 2006, *100*.

(19) Melville, O. A.; Grant, T. M.; Lochhead, K.; King, B.; Ambrose, R.; Rice, N. A.; Boileau, N. T.; Peltekoff, A. J.; Tousignant, M.; Hill, I. G.; et al. Contact Engineering Using Manganese, Chromium, and Bathocuproine in Group 14 Phthalocyanine Organic Thin-Film Transistors. *ACS Appl. Electron. Mater.* 2020, *2*, 1313–1322.

(20) Kalb, W. L.; Batlogg, B. Calculating the Trap Density of States in Organic Field-Effect Transistors from Experiment: A Comparison of Different Methods. *Phys. Rev. B - Condens. Matter Mater. Phys.* 2010, *81*, 035327.

(21) Klauk, H. Organic Thin-Film Transistors. *Chem. Soc. Rev.* 2010, *39*, 2643–2666.

(22) Harris, C. S.; Shuhendler, A. J.; Lessard, B. H.; Comeau, Z. J.; Rice, N. A.; Harris, C. S.; Shuhendler, A. J.; Lessard, B. H.; Comeau, Z. J.; Rice, N. A. Organic Thin-Film Transistors as Cannabinoid Sensors: Effect of Analytes on Phthalocyanine Film

Crystallization. *Adv. Funct. Mater.* 2022, *32*, 2107138.

(23) Phan, H.; Ford, M. J.; Lill, A. T.; Wang, M.; Bazan, G. C.; Nguyen, T. Q. Electrical Double-Slope Nonideality in Organic Field-Effect Transistors. *Adv. Funct. Mater.* 2018, *28*, 1707221.

(24) Dou, J.-H.; Zheng, Y.-Q.; Yao, Z.-F.; Lei, T.; Shen, X.; Luo, X.-Y.; Yu, Z.-A.; Zhang, S.-D.; Han, G.; Wang, Z.; et al. A Cofacially Stacked Electron-Deficient Small Molecule with a High Electron Mobility of over 10 Cm2 V−1 S−1 in Air. *Adv. Mater.* 2015, *27*, 8051–8055.

(25) Zhao, Z.; Yin, Z.; Chen, H.; Zheng, L.; Zhu, C.; Zhang, L.; Tan, S.; Wang, H.; Guo, Y.; Tang, Q.; et al. High-Performance, Air-Stable Field-Effect Transistors Based on Heteroatom-Substituted Naphthalenediimide-Benzothiadiazole Copolymers Exhibiting Ultrahigh Electron Mobility up to 8.5 Cm V−1 S−1. *Adv. Mater.* 2017, *29*, 1602410.

(26) Kang, B.; Kim, R.; Lee, S. B.; Kwon, S. K.; Kim, Y. H.; Cho, K. Side-Chain-Induced Rigid Backbone Organization of Polymer Semiconductors through Semifluoroalkyl Side Chains. *J. Am. Chem. Soc.* 2016, *138*, 3679–3686.

(27) Zhang, C.; Zang, Y.; Zhang, F.; Diao, Y.; McNeill, C. R.; Di, C.; Zhu, X.; Zhu Zhang, D. C.; Zang, Y.; Di, C.; et al. Pursuing High-Mobility n-Type Organic Semiconductors by Combination of “Molecule-Framework” and “Side-Chain” Engineering. *Adv. Mater.* 2016, *28*, 8456–8462.

(28) Zhang, F.; Hu, Y.; Schuettfort, T.; Di, C. A.; Gao, X.; McNeill, C. R.; Thomsen, L.; Mannsfeld, S. C. B.; Yuan, W.; Sirringhaus, H.; et al. Critical Role of Alkyl Chain Branching of Organic Semiconductors in Enabling Solution-Processed N-Channel Organic Thin-Film Transistors with Mobility of up to 3.50 Cm2 V-1 s-1. *J. Am. Chem. Soc.* 2013, *135*, 2338–2349.

(29) Sun, B.; Hong, W.; Yan, Z.; Aziz, H.; Li, Y.; Sun, B.; Hong, W.; Yan, Z.; Li, Y.; Aziz, H. Record High Electron Mobility of 6.3 Cm2V−1s−1 Achieved for Polymer Semiconductors Using a New Building Block. *Adv. Mater.* 2014, *26*, 2636–2642.

(30) Wang, Y.; Hasegawa, T.; Matsumoto, H.; Mori, T.; Michinobu, T.; Wang, Y.; Hasegawa, T.; Matsumoto, H.; Mori, T.; Michinobu, T. High-Performance n-Channel Organic Transistors Using High-Molecular-Weight Electron-Deficient Copolymers and Amine-

Tailed Self-Assembled Monolayers. *Adv. Mater.* 2018, *30*, 1707164.

(31) Bucella, S. G.; Luzio, A.; Gann, E.; Thomsen, L.; McNeill, C. R.; Pace, G.; Perinot, A.; Chen, Z.; Facchetti, A.; Caironi, M. Macroscopic and High-Throughput Printing of Aligned Nanostructured Polymer Semiconductors for MHz Large-Area Electronics. *Nat. Commun. 2015 61* 2015, *6*, 1–10.

(32) Wang, Y.; Hasegawa, T.; Matsumoto, H.; Michinobu, T. Significant Improvement of Unipolar N-Type Transistor Performances by Manipulating the Coplanar Backbone Conformation of Electron-Deficient Polymers via Hydrogen Bonding. *J. Am. Chem. Soc.* 2019, *141*, 3566–3575.

(33) Yoon, W. J.; Berger, P. R. Atomic Layer Deposited HfO2 Gate Dielectrics for Low-Voltage Operating, High-Performance Poly-(3-Hexythiophene) Organic Thin-Film Transistors. *Org. Electron.* 2010, *11*, 1719–1722.

(34) Zirkl, M.; Haase, A.; Fian, A.; Schön, H.; Sommer, C.; Jakopic, G.; Leising, G.; Stadlober, B.; Graz, I.; Gaar, N.; et al. Low-Voltage Organic Thin-Film Transistors with High-k Nanocomposite Gate Dielectrics for Flexible Electronics and Optothermal Sensors. *Adv. Mater.* 2007, *19*, 2241–2245.

(35) Tseng, G.; Ellenbogen, J.; N Mbindyo, J. K.; Reiss, B. D.; Martin, B. R.; Keating, C. D.; Natan, M. J.; Mallouk, T. E.; K Mbindyo, J. N.; Nicewarner, S. R.; et al. One Volt Organic Transistor. *Adv. Mater.* 2005, *17*, 192–196.

(36) Xia, Y.; Yang, P.; Sun, Y.; Wu, Y.; Mayers, B.; Gates, B.; Yin, Y.; Kim, F.; Yan, H.; Gogotsi, Y.; et al. High-Performance Organic Transistors Using Solution-Processed Nanoparticle-Filled High-k Polymer Gate Insulators. *Adv. Mater.* 2005, *17*, 1535–1539.

(37) Lewis, A.; Kheifetz, Y.; Shambrodt, E.; Radko, A.; Khatchatryan, E.; Demers, M.; Ginger, D. S.; Park, S. J.; Li, Z.; Chung, S. W.; et al. All-Organic Permanent Memory Transistor Using an Amorphous, Spin-Cast Ferroelectric-like Gate Insulator. *Adv. Mater.* 2004, *16*, 633–636.

(38) Ukah, N. B.; Granstrom, J.; Sanganna Gari, R. R.; King, G. M.; Guha, S. Low-Operating Voltage and Stable Organic Field-Effect Transistors with Poly (Methyl Methacrylate) Gate Dielectric Solution Deposited from a High Dipole Moment Solvent. *Appl. Phys. Lett.* 2011, *99*, 243302.

(39) Xia, Y.; Zhang, W.; Ha, M.; Cho, J. H.; Renn, M. J.; Kim, C. H.; Frisbie, C. D. Printed Sub-2 V Gel-Electrolyte-Gated Polymer Transistors and Circuits. *Adv. Funct. Mater.* 2010, *20*, 587–594.

(40) Braga, D.; Ha, M.; Xie, W.; Frisbie, C. D. Ultralow Contact Resistance in Electrolyte-Gated Organic Thin Film Transistors. *Appl. Phys. Lett.* 2010, *97*, 193311.

(41) Quinn, J. T. E.; Zhu, J.; Li, X.; Wang, J.; Li, Y. Recent Progress in the Development of N-Type Organic Semiconductors for Organic Field Effect Transistors. *J. Mater. Chem. C* 2017, *5*, 8654–8681.

(42) Brabec, C.; Egelhaaf, H.-J.; Salvador, M. The Path to Ubiquitous Organic Electronics Hinges on Its Stability. *J. Mater. Res.* 2018, *33*, 1839–1840.

(43) Zaumseil, J.; Sirringhaus, H. Electron and Ambipolar Transport in Organic Field-Effect Transistors. *Chem. Rev.* 2007, *107*, 1296–1323.

(44) de Leeuw, D. M.; Simenon, M. M. J.; Brown, A. R.; Einerhand, R. E. F. Stability of N-Type Doped Conducting Polymers and Consequences for Polymeric Microelectronic Devices. *Synth. Met.* 1997, *87*, 53–59.

(45) King, B.; Vebber, M. C.; Ewenike, R.; Dupuy, M.; French, C.; Brusso, J. L.; Lessard, B. H. Peripherally Fluorinated Silicon Phthalocyanines: How Many Fluorine Groups Are Necessary for Air-Stable Electron Transport in Organic Thin-Film Transistors? *Chem. Mater.* 2023, *35*, 8528.

(46) Lee, E. K.; Lee, M. Y.; Park, C. H.; Lee, H. R.; Oh, J. H. Toward Environmentally Robust Organic Electronics: Approaches and Applications. *Adv. Mater.* 2017, *29*, 1703638.

(47) Kim, J. H.; Lee, I.; Kim, T. S.; Rolston, N.; Watson, B. L.; Dauskardt, R. H. Understanding Mechanical Behavior and Reliability of Organic Electronic Materials. *MRS Bull.* 2017, *42*, 115–123.

(48) Logothetidis, S. Flexible Organic Electronic Devices: Materials, Process and Applications. *Mater. Sci. Eng. B* 2008, *152*, 96–104.

(49) Kuribara, K.; Wang, H.; Uchiyama, N.; Fukuda, K.; Yokota, T.; Zschieschang, U.; Jaye, C.; Fischer, D.; Klauk, H.; Yamamoto, T.; et al. Organic Transistors with High Thermal Stability for Medical Applications. *Nat. Commun.* 2012, *3*.

(50) Anthony, J. E. Organic Electronics: Addressing Challenges. *Nat. Mater.* 2014, *13*, 773–775.

(51) Brixi, S.; Melville, O. A.; Mirka, B.; He, Y.; Hendsbee, A. D.; Meng, H.; Li, Y.; Lessard, B. H. Air and Temperature Sensitivity of N-Type Polymer Materials to Meet and Exceed the Standard of N2200. *Sci. Rep.* 2020, *10*, 4014.

(52) Griggs, S.; Marks, A.; Bristow, H.; McCulloch, I. N-Type Organic Semiconducting Polymers: Stability Limitations, Design Considerations and Applications. *J. Mater. Chem. C* 2021, *9*, 8099–8128.

(53) Wang, F.; Dai, Y.; Wang, W.; Lu, H.; Qiu, L.; Ding, Y.; Zhang, G. Incorporation of Heteroatoms in Conjugated Polymers Backbone toward Air-Stable, High-Performance n-Channel Unencapsulated Polymer Transistors. *Chem. Mater.* 2018, *30*, 5451–5459.

(54) Hwang, D. K.; Fuentes-Hernandez, C.; Kim, J.; Potscavage Jr., W. J.; Kim, S.-J.; Kippelen, B. Top-Gate Organic Field-Effect Transistors with High Environmental and Operational Stability. *Adv. Mater.* 2011, *23*, 1293–1298.

(55) Su, W. Encapsulation Technology for Organic Electronic Devices. In *Printed Electronics*; Wiley Online Books; 2016; pp 287–315.

(56) Sheats, J. R. Manufacturing and Commercialization Issues in Organic Electronics. *J. Mater. Res.* 2004, *19*, 1974–1989.

(57) He, Z.; Zhang, Z.; Bi, S. Small-Molecule Additives for Organic Thin Film Transistors. *J. Mater. Sci. Mater. Electron.* 2019, *30*, 20899–20913.

(58) Lüssem, B.; Keum, C.-M.; Kasemann, D.; Naab, B.; Bao, Z.; Leo, K. Doped Organic Transistors. *Chem. Rev.* 2016, *116*, 13714–13751.

(59) Salzmann, I.; Heimel, G.; Oehzelt, M.; Winkler, S.; Koch, N. Molecular Electrical Doping of Organic Semiconductors: Fundamental Mechanisms and Emerging Dopant Design Rules. *Acc. Chem. Res.* 2016, *49*, 370–378.

(60) Zhang, F.; Dai, X.; Zhu, W.; Chung, H.; Diao, Y. Large Modulation of Charge Carrier Mobility in Doped Nanoporous Organic Transistors. *Adv. Mater.* 2017, *29*, 1700411.

(61) Zessin, J.; Xu, Z.; Shin, N.; Hambsch, M.; Mannsfeld, S. C. B. Threshold Voltage Control in Organic Field-Effect Transistors by Surface Doping with a Fluorinated Alkylsilane.

ACS Appl. Mater. Interfaces 2019, *11*, 2177–2188.

(62) Wei, P.; Oh, J. H.; Dong, G.; Bao, Z. Use of a 1 H -Benzoimidazole Derivative as an n -Type Dopant and to Enable Air-Stable Solution-Processed n -Channel Organic Thin-Film Transistors. *J. Am. Chem. Soc.* 2010, *132*, 8852–8853.

(63) Chou, W. Y.; Cheng, H. L. An Orientation-Controlled Pentacene Film Aligned by Photoaligned Polyimide for Organic Thin-Film Transistor Applications. *Adv. Funct. Mater.* 2004, *14*, 811–815.

(64) He, Y.; Quinn, J. T. E.; Lee, S.; Wang, G. Y.; Li, X.; Wang, J.; Li, Y. An Aromatic Amine-Containing Polymer as an Additive to Ambipolar Polymer Semiconductor Realizing Unipolar n-Type Charge Transport. *Org. Electron.* 2017, *49*, 406–414.

(65) Nikolka, M.; Nasrallah, I.; Rose, B.; Ravva, M. K.; Broch, K.; Sadhanala, A.; Harkin, D.; Charmet, J.; Hurhangee, M.; Brown, A.; et al. High Operational and Environmental Stability of High-Mobility Conjugated Polymer Field-Effect Transistors through the Use of Molecular Additives. *Nat. Mater.* 2017, *16*, 356–362.

(66) Naab, B. D.; Zhang, S.; Vandewal, K.; Salleo, A.; Barlow, S.; Marder, S. R.; Bao, Z. Effective Solution- and Vacuum-Processed n-Doping by Dimers of Benzimidazoline Radicals. *Adv. Mater.* 2014, *26*, 4268–4272.

(67) Sun, B.; Hong, W.; Thibau, E. S.; Aziz, H.; Lu, Z.-H.; Li, Y. Polyethylenimine (PEI) As an Effective Dopant To Conveniently Convert Ambipolar and p-Type Polymers into Unipolar n-Type Polymers. *ACS Appl. Mater. Interfaces* 2015, *7*, 18662–18671.

(68) Calhoun, M. F.; Sanchez, J.; Olaya, D.; Gershenson, M. E.; Podzorov, V. Electronic Functionalization of the Surface of Organic Semiconductors with Self-Assembled Monolayers. *Nat. Mater.* 2008, *7*, 84–89.

(69) Shin, N.; Zessin, J.; Lee, M. H.; Hambsch, M.; Mannsfeld, S. C. B. Enhancement of N-Type Organic Field-Effect Transistor Performances through Surface Doping with Aminosilanes. *Adv. Funct. Mater.* 2018, *28*, 1802265.

(70) Thomas, S. R.; Pattanasattayavong, P.; Anthopoulos, T. D. Solution-Processable Metal Oxide Semiconductors for Thin-Film Transistor Applications. *Chem. Soc. Rev.* 2013, *42*, 6910–6923.

(71) Wang, Z.; Nayak, P. K.; Caraveo-Frescas, J. A.; Alshareef, H. N.; Wang, Z.; Nayak, P. K.; Caraveo-Frescas, J. A.; Materials, A.; Engineering, S. &. Recent Developments in P-Type Oxide Semiconductor Materials and Devices. *Adv. Mater.* 2016, *28*, 3831–3892.

(72) Veres, J.; Ogier, S. D.; Leeming, S. W.; Cupertino, D. C.; Khaffaf, S. M. Low-k Insulators as the Choice of Dielectrics in Organic Field-Effect Transistors. *Adv. Funct. Mater.* 2003, *13*, 199–204.

(73) Chua, L. L.; Zaumseil, J.; Chang, J. F.; Ou, E. C. W.; Ho, P. K. H.; Sirringhaus, H.; Friend, R. H. General Observation of N-Type Field-Effect Behaviour in Organic Semiconductors. *Nat. 2005 4347030* 2005, *434*, 194–199.

(74) Zade, S. S.; Bendikov, M. From Oligomers to Polymer: Convergence in the HOMO-LUMO Gaps of Conjugated Oligomers. *Org. Lett.* 2006, *8*, 5243–5246.

(75) Wang, Y. Z.; Cao, L.; Qi, D. C.; Chen, W.; Wee, A. T. S.; Gao, X. Y. Tuning the Interfacial Hole Injection Barrier between P-Type Organic Materials and Co Using a MoO 3 Buffer Layer. *J. Appl. Phys.* 2012, *112*, 33704.

(76) Ma, H.; Acton, O.; Hutchins, D. O.; Cernetic, N.; Jen, A. K. Y. Multifunctional Phosphonic Acid Self-Assembled Monolayers on Metal Oxides as Dielectrics, Interface Modification Layers and Semiconductors for Low-Voltage High-Performance Organic Field-Effect Transistors. *Phys. Chem. Chem. Phys.* 2012, *14*, 14110–14126.

(77) Zhang, X. H.; Tiwari, S. P.; Kippelen, B. Pentacene Organic Field-Effect Transistors with Polymeric Dielectric Interfaces: Performance and Stability. *Org. Electron.* 2009, *10*, 1133–1140.

(78) Baeg, K. J.; Noh, Y. Y.; Kim, D. Y. Charge Transfer and Trapping Properties in Polymer Gate Dielectrics for Non-Volatile Organic Field-Effect Transistor Memory Applications. *Solid. State. Electron.* 2009, *53*, 1165–1168.

(79) Kim, S. H.; Yun, W. M.; Kwon, O. K.; Hong, K.; Yang, C.; Choi, W. S.; Park, C. E. Hysteresis Behaviour of Low-Voltage Organic Field-Effect Transistors Employing High Dielectric Constant Polymer Gate Dielectrics. *J. Phys. D. Appl. Phys.* 2010, *43*, 465102.

(80) Huang, W.; Fan, H.; Zhuang, X.; Yu, J. Effect of UV/Ozone Treatment on Polystyrene Dielectric and Its Application on Organic Field-Effect Transistors. *Nanoscale Res. Lett.*

2014, *9*, 1–8.

(81) Zhou, J.; Zhang, F.; Lan, L.; Wen, S.; Peng, J. Influence of Polymer Dielectrics on C60-Based Field-Effect Transistors. *Appl. Phys. Lett.* 2007, *91*, 253507.

(82) Deman, A. L.; Tardy, J. Stability of Pentacene Organic Field Effect Transistors with a Low-k Polymer/High-k Oxide Two-Layer Gate Dielectric. *Mater. Sci. Eng. C* 2006, *26*, 421–426.

(83) Ortiz, R. P.; Facchetti, A.; Marks, T. J. High-k Organic, Inorganic, and Hybrid Dielectrics for Low-Voltage Organic Field-Effect Transistors. *Chem. Rev.* 2010, *110*, 205–239.

(84) Pillai, P. K. C.; Khurana, P.; Tripathi, A. Dielectric Studies of Poly(Methyl Methacrylate)/Polystyrene Double Layer System. *J. Mater. Sci. Lett.* 1986, *5*, 629–632.

(85) Shekhar, P.; Shamim, S.; Hartinger, S.; Schlereth, R.; Hock, V.; Buhmann, H.; Kleinlein, J.; Molenkamp, L. W. Low-Temperature Atomic Layer Deposition of Hafnium Oxide for Gating Applications. *ACS Appl. Mater. Interfaces* 2022, *14*, 33967.

(86) Lee, K. H.; Zhang, S.; Lodge, T. P.; Frisbie, C. D. Electrical Impedance of Spin-Coatable Ion Gel Films. *J. Phys. Chem. B* 2011, *115*, 3315–3321.

(87) Tibaldi, A.; Fillaud, L.; Anquetin, G.; Woytasik, M.; Zrig, S.; Piro, B.; Mattana, G.; Noël, V. Electrolyte-Gated Organic Field-Effect Transistors (EGOFETs) as Complementary Tools to Electrochemistry for the Study of Surface Processes. *Electrochem. commun.* 2019, *98*, 43–46.

(88) Hyun Kim, S.; Hong, K.; Xie, W.; Hyung Lee, K.; Zhang, S.; Lodge, T. P.; Daniel Frisbie, C.; Kim, S. H.; Hong, K.; Xie, W.; et al. Electrolyte-Gated Transistors for Organic and Printed Electronics. *Adv. Mater.* 2013, *25*, 1822–1846.

(89) Torricelli, F.; Adrahtas, D. Z.; Bao, Z.; Berggren, M.; Biscarini, F.; Bonfiglio, A.; Bortolotti, C. A.; Frisbie, C. D.; Macchia, E.; Malliaras, G. G.; et al. Electrolyte-Gated Transistors for Enhanced Performance Bioelectronics. *Nat. Rev. Methods Prim. 2021 11* 2021, *1*, 1–24.

(90) Wang, D.; Zhao, S.; Yin, R.; Li, L.; Lou, Z.; Shen, G. Recent Advanced Applications of Ion-Gel in Ionic-Gated Transistor. *npj Flex. Electron. 2021 51* 2021, *5*, 1–16.

(91) Lee, J.; Kaake, L. G.; Cho, H. J.; Zhu, X. Y.; Lodge, T. P.; Frisbie, C. D. Ion Gel-Gated

Polymer Thin-Film Transistors: Operating Mechanism and Characterization of Gate Dielectric Capacitance, Switching Speed, and Stability. *J. Phys. Chem. C* 2009, *113*, 8972–8981.

(92) Vygodskii, Y. S.; Shaplov, A. S.; Lozinskaya, E. I.; Lyssenko, K. A.; Golovanov, D. G.; Malyshkina, I. A.; Gavrilova, N. D.; Buchmeiser, M. R. Conductive Polymer Electrolytes Derived from Poly(Norbornene)s with Pendant Ionic Imidazolium Moieties. *Macromol. Chem. Phys.* 2008, *209*, 40–51.

(93) Salas-De La Cruz, D.; Green, M. D.; Ye, Y.; Elabd, Y. A.; Long, T. E.; Winey, K. I. Correlating Backbone-to-Backbone Distance to Ionic Conductivity in Amorphous Polymerized Ionic Liquids. *J. Polym. Sci. Part B Polym. Phys.* 2012, *50*, 338–346.

(94) Chen, H.; Choi, J. H.; Cruz, D. S. D. La; Winey, K. I.; Elabd, Y. A. Polymerized Ionic Liquids: The Effect of Random Copolymer Composition on Ion Conduction. *Macromolecules* 2009, *42*, 4809–4816.

(95) Ye, Y.; Choi, J. H.; Winey, K. I.; Elabd, Y. A. Polymerized Ionic Liquid Block and Random Copolymers: Effect of Weak Microphase Separation on Ion Transport. *Macromolecules* 2012, *45*, 7027–7035.

(96) Yuan, J.; Schlaad, H.; Giordano, C.; Antonietti, M. Double Hydrophilic Diblock Copolymers Containing a Poly(Ionic Liquid) Segment: Controlled Synthesis, Solution Property, and Application as Carbon Precursor. *Eur. Polym. J.* 2011, *47*, 772–781.

(97) May, A. W.; Shi, Z.; Wijayasekara, D. B.; Gin, D. L.; Bailey, T. S. Self-Assembly of Highly Asymmetric, Poly(Ionic Liquid)-Rich Diblock Copolymers and the Effects of Simple Structural Modification on Phase Behaviour. *Polym. Chem.* 2019, *10*, 751–765.

(98) Park, J. B.; Isik, M.; Park, H. J.; Jung, I. H.; Mecerreyes, D.; Hwang, D. H. Polystyrene-Block-Poly(Ionic Liquid) Copolymers as Work Function Modifiers in Inverted Organic Photovoltaic Cells. *ACS Appl. Mater. Interfaces* 2018, *10*, 4887–4894.

(99) Meek, K. M.; Sun, R.; Willis, C.; Elabd, Y. A. Hydroxide Conducting Polymerized Ionic Liquid Pentablock Terpolymer Anion Exchange Membranes with Methylpyrrolidinium Cations. *Polymer (Guildf).* 2018, *134*, 221–226.

(100) Dai, Z.; Ansaloni, L.; Ryan, J. J.; Spontak, R. J.; Deng, L. Incorporation of an Ionic Liquid

into a Midblock-Sulfonated Multiblock Polymer for CO2 Capture. *J. Memb. Sci.* 2019, *588*, 117193.

(101) Srour, H.; Leocmach, M.; Maffeis, V.; Ghogia, A. C.; Denis-Quanquin, S.; Taberlet, N.; Manneville, S.; Andraud, C.; Bucher, C.; Monnereau, C. Poly(Ionic Liquid)s with Controlled Architectures and Their Use in the Making of Ionogels with High Conductivity and Tunable Rheological Properties. *Polym. Chem.* 2016, *7*, 6608–6616.

(102) Hu, H.; Yuan, W.; Lu, L.; Zhao, H.; Jia, Z.; Baker, G. L. Low Glass Transition Temperature Polymer Electrolyte Prepared from Ionic Liquid Grafted Polyethylene Oxide. *J. Polym. Sci. Part A Polym. Chem.* 2014, *52*, 2104–2110.

(103) Cho, J. H.; Lee, J.; Xia, Y.; Kim, B.; He, Y.; Renn, M. J.; Lodge, T. P.; Daniel Frisbie, C. Printable Ion-Gel Gate Dielectrics for Low-Voltage Polymer Thin-Film Transistors on Plastic. *Nat. Mater. 2008 711* 2008, *7*, 900–906.

(104) Choi, J. H.; Ye, Y.; Elabd, Y. A.; Winey, K. I. Network Structure and Strong Microphase Separation for High Ion Conductivity in Polymerized Ionic Liquid Block Copolymers. *Macromolecules* 2013, *46*, 5290–5300.

(105) Peltekoff, A. J.; Hiller, V. E.; Lopinski, G. P.; Melville, O. A.; Lessard, B. H. Unipolar Polymerized Ionic Liquid Copolymers as High-Capacitance Electrolyte Gates for n-Type Transistors. *ACS Appl. Polym. Mater.* 2019, *1*, 3210–3221.

(106) Choi, J. H.; Xie, W.; Gu, Y.; Frisbie, C. D.; Lodge, T. P. Single Ion Conducting, Polymerized Ionic Liquid Triblock Copolymer Films: High Capacitance Electrolyte Gates for N-Type Transistors. *ACS Appl. Mater. Interfaces* 2015, *7*, 7294–7302.

(107) Leibler, L. Theory of Microphase Separation in Block Copolymers. *Macromolecules* 1980, *13*, 1602–1617.

(108) Albert, J. N. L.; Epps, T. H. Self-Assembly of Block Copolymer Thin Films. *Mater. Today* 2010, *13*, 24–33.

(109) Segalman, R. A.; McCulloch, B.; Kirmayer, S.; Urban, J. J. Block Copolymers for Organic Optoelectronics. *Macromolecules* 2009, *42*, 9205–9216.

(110) Kim, H. C.; Park, S. M.; Hinsberg, W. D.; Division, I. R. Block Copolymer Based Nanostructures: Materials, Processes, and Applications to Electronics. *Chem. Rev.* 2010,

110, 146–177.

(111) Sik Yoo, W.; Kang, K.; Murai, G. The Standard Gaussian Model for Block Copolymer Melts. *J. Phys. Condens. Matter* 2001, *14*, R21.

(112) Lynd, N. A.; Meuler, A. J.; Hillmyer, M. A. Polydispersity and Block Copolymer Self-Assembly. *Prog. Polym. Sci.* 2008, *33*, 875–893.

2. Air and temperature sensitivity of n-type polymer materials to meet and exceed the standard of P(NDI2OD-T2)

Context and Significance of Work

At the time of this study, our group had not yet taken significant strides in systematic studies of device stability. P(NDI2OD-T2) had been reported as an air-stable n-type polymer with good electron mobility, but many examples were top-gate with a fluorinated dielectric. Simultaneously, our collaborators at the Li Lab at the University of Waterloo had synthesized some materials with similar molecular structure to P(NDI2OD-T2), which we wished to compare in terms of stability. In this context, we considered it would be of value to have a benchmark comparison point for the stability of devices, similar to using P3HT:PCBM as a standard reference for organic solar cells. We considered P(NDI2OD-T2) to be the ideal material for this purpose as it is known to have some air stability, is similar in structure to several of the materials our collaborators synthesized, and is commercialized, which would allow others the field to make similar comparisons. This would enable similar studies to be related across literature even when studies are not done at the same time or place.

Contributions of Authors

I designed the device studies, performed all device experiments and UV-vis, prepared all figures except AFM and CV, and wrote the manuscript. Owen Melville contributed ideas to the analysis and contributed to editing of the manuscript. Brendan Mirka performed AFM and prepared the relevant figure. Yinghui He, Arthur Hendsbee, and Han Meng synthesized the polymers and performed cyclic voltammetry for determination of the HOMO and LUMO levels.

This work is published in Scientific Reports. Brixi, S.; Melville, O.; Mirka , B. ; He, Y.; Hendsbee, A.; Meng , H.; Li, Y.; Lessard, B. H. Air and temperature sensitivity of n-type polymer materials to meet and exceed the standard of N2200. doi:10.1038/s41598-020-60812-x

2.1 Abstract

N-type organic semiconductors are notoriously unstable in air, requiring the design of new materials that focuses on lowering their LUMO energy levels and enhancing their air stability in organic electronic devices such as organic thin-film transistors (OTFTs). Since the discovery of the notably air stable and high electron mobility polymer poly{[N,N'-bis(2-octyldodecyl)-naphthalene-1,4,5,8-bis(dicarboximide)-2,6-diyl]-alt-5,5'-(2,29-bisthiophene)} (P(NDI2OD-T2)), it has become a popular n-type semiconductor, with numerous materials being designed to mimic its structure. Although P(NDI2OD-T2) itself is well-studied, many of these comparable materials have not been sufficiently characterized to compare their air stability to P(NDI2OD-T2). To further the development of air stable and high mobility n-type organic semiconductors, P(NDI2OD-T2) was studied in organic thin film transistors alongside three P(NDI2OD-T2)-based analogues as well as a recently developed polymer based on a (3E,7E)-3,7-bis(2-oxoindolin-3-ylidene)benzo[1,2-b:4,5-b′]difuran-2,6(3H,7H)-dione (IBDF) core. This IBDF polymer has demonstrated promising field-effect mobility and air stability in drop-cast OTFTs. While P(NDI2OD-T2) outperformed its analogues, the IBDF-based polymer displayed superior air and temperature stability compared to P(NDI2OD-T2). Overall, polymers with more heteroatoms displayed greater air stability. These findings will support the development of new air-stable materials, and further demonstrate the persistent need for the development of novel n-type semiconductors.

2.2 Introduction

Semiconducting polymers may hold the key to the future of scalable high-production volume flexible electronics, with their solution processable properties making them transferrable to roll-to-roll printing technologies. Newly developed materials must exhibit high charge mobilities and air stability to be viable for commercial success, and numerous recent materials have achieved these desired characteristics.[1–6] Exceptional performance of the charge transporting semiconductor layer is essential to the fabrication of effective devices. Performance must be sustained under a variety of environmental stressors that would be experienced under typical fabrication and operation conditions, including exposure to air or elevated temperature. Particularly, it is desirable for a material to be shelf-stable under ambient conditions. Electron-transporting n-type materials are especially susceptible to air-induced degradation under ambient conditions.[7] Recent developments in the design of air-stable n-type materials has led to the discovery of the material poly{[N,N9-bis(2-octyldodecyl)-naphthalene-1,4,5,8-bis(dicarboximide)-2,6-diyl]-alt-5,59-(2,29-bisthiophene)} (P(NDI2OD-T2)), which was found to have exceptional air-stability among comparable materials in a protected top-gate configuration, along with excellent electron mobility.[8] In the hopes of achieving and improving upon the highly desirable characteristics of P(NDI2OD-T2), numerous materials have been developed based on this NDI core.[2,9–12] While polymers of this class have received significant focus, newer classes of polymers have also been developed with promising results. One such example are IBDF-based polymers (also referred to as BDOPV), which have shown promising charge transport characteristics and air stability.[13–18] However, the air stability of many of these materials is not well characterized, and little to no information is known about their response to temperature.

Charge transport has been studied through theoretical and experimental studies for numerous organic semiconductors. For amorphous and polycrystalline films, which are typical morphologies for thin films of organic semiconductors, an increase in mobility is observed with increasing temperature. However, in particularly high-mobility and highly crystalline materials, band-like transport may be observed, wherein mobility decreases with temperature.[19] These studies are almost exclusively performed at temperatures below ambient to accurately determine modes of charge transport.[19–22] While these studies are important for enhancing understanding of charge transport in organic semiconductors, it is important to ensure that these findings hold true under conditions relevant to practical operation. This is particularly important for polymers due to the

dependence of their morphology on temperature, which can have a significant impact on charge transport. Studies reporting material stability rarely include a side-by-side comparison of results to other well-known materials as a reference point, despite the ambient conditions (such as relative humidity) being significant factors in material stability, which differ in each laboratory these materials are studied. Our study attempts to control for these factors by comparing relative stability of all materials in the same time frame to remove this confounding factor.

This study examines the materials P(NDI2OD-T2), a fluorinated derivative (F-N2200), a derivative lacking a thiophene (NDI-20-T), an alkoxy derivative (NDIO-20-T), and another material based on a (3E,7E)-3,7-bis(2-oxoindolin-3-ylidene)benzo[1,2-b:4,5-b′]difuran-2,6(3H,7H)-dione core (PIBDF). **Figure 2.1** compares the polymer structures as well as the reported lowest unoccupied molecular orbital (LUMO) and highest occupied molecular orbital (HOMO) energy levels. Towards the goal of implementing practical applications for these high performing n-type polymer materials, their response to the effect of air and temperature were studied. This information will assist in informing future materials design choices for organic electronics and will be useful towards the design of new molecules to have desired properties such as air stability.

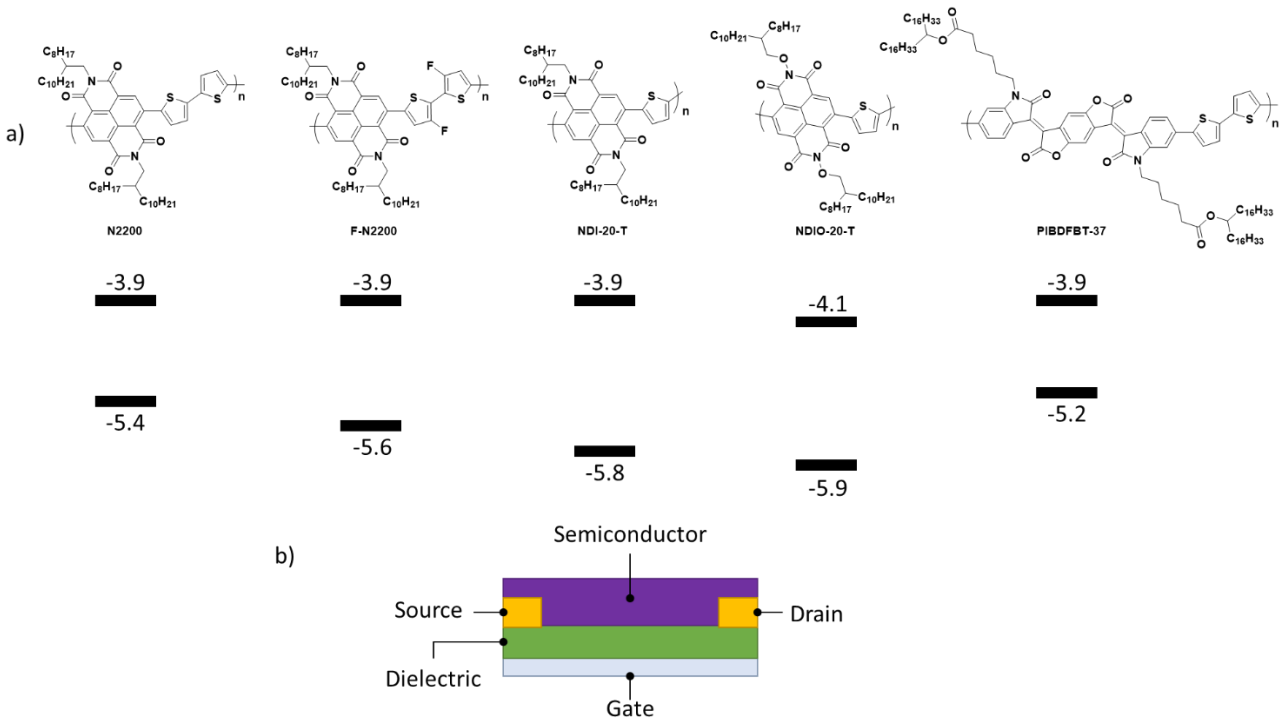

Figure 2.1. a) Polymers studied in this report and their respective frontier energy levels. **b)** Structure of a bottom gate bottom contact organic thin film transistor (OTFT). Corresponding lowest unoccupied molecular orbital (LUMO) and highest occupied molecular orbital (HOMO) energy levels for each polymer obtained through cyclic voltammetry (CV) and UV-visible spectra presented in Supplementary **Figure 2.8.** N2200 = P(NDI2OD-T2)

2.3 Results and Discussion

The Influence of Air

To investigate the effects of environment on the polymer semiconductors, organic thin film transistors (OTFTs) were fabricated with each material shown in **Figure 2.1** as the active semiconductor. Devices were fabricated by drop casting in the bottom-gate bottom-contact (BGBC) configuration to ensure the materials were adequately exposed to the environment. To characterize their electrical properties, the OTFTs were first characterized under vacuum ($P < 0.1$ Pa) followed by characterization in air. The resulting electrical properties are summarized in **Table 2.1**. The P(NDI2OD-T2) used in this study was prepared by two different methods; first, a sample prepared by Stille coupling (provided by 1-Material), and a second sample prepared by direct heteroarylation (provided by Brilliant Matters Organic Electronics). Both yielded identical results, thus the values for the 1-Material polymer are presented below.

Table 2.1. Properties of n-type polymers at 30 °C in air or vacuum environment.

	P(NDI2OD-T2)		F-N2200		NDI-20-T		NDIO-20-T		PIBDFBT-37	
	Vacuum	**Air**	**Vacuum**	**Air**	**Vacuum**	**Air**	**Vacuum**	**Air**	**Vacuum**	**Air**
μ_e (cm^2/Vs)	0.06	0.03	0.03	0.005	0.006	0.002	0.001	0.0006	0.1	0.02
$I_{on/off}$	10^3	10^2	10^4	10^3	10^4	10^3	10^3	10^3	10^4	10^3
V_T (V)	23.9	33.9	-0.31	10.6	11.4	18.4	15.5	32.9	32.1	41.5
HOMO (eV) [a)]	-5.4		-5.6		-5.8		-5.9		-5.2 (-5.7)[b)]	
LUMO (eV) [a)]	-3.9		-3.9		-3.9		-4.1		-3.9	

a) Lowest unoccupied molecular orbital (LUMO) and highest occupied molecular orbital (HOMO) energy levels (eV) were obtained by CV and band-gaps determined by UV-vis, presented in **Figure 2.8**.

b) Values presented in brackets were obtained directly from the onset of oxidation in CV experiments, while all other values are calculated by combining the band-gap from UV-visible spectroscopic studies with the LUMO value obtained by CV.

The highest electron mobilities (μ_e) were observed for P(NDI2OD-T2) and PIBDFBT-37 with values of 0.06 and 0.1 cm^2/Vs, respectively. F-N2200 also displayed relatively high mobility at 0.03 cm^2/Vs. Although the μ_e obtained for P(NDI2OD-T2) has been reported above 1 cm^2/Vs in top-gate configurations,[23] the values obtained in this study correspond with values found for unoptimized devices on Si/SiO_2 in bottom gate, bottom contact (BGBC) OTFT configuration.[24] The performance of these materials corresponds to values in literature.[8,12,13,25] Minor differences

can be attributed to differences in device architecture and processing method, as these material have previously been characterized with spin-coated devices.

Typically for n-type polymers, a deeper LUMO is less susceptible to charge trapping, thus requiring a lower bias to inject charge, resulting in a lower observed threshold voltage (V_T).[26] In this case, there is little difference in the frontier energy levels of each of these polymers, yet the threshold voltages range from 0 to 30 V. This implies that the difference in V_T cannot be entirely accounted for by this traditional explanation. The performance of numerous materials,[27–30] including P(NDI2OD-T2),[8] has been shown to vary with film morphology. Therefore, it is possible the difference in V_T between each polymer observed under vacuum is not due to relative LUMO energies, but instead the film morphology contributes to this difference. This variation in device performance with morphology is often attributed to charge traps formed at grain boundaries,[31,32] which can significantly affect V_T.[33] The charge traps at grain boundaries also has the added effect of decreasing the mobility, as a result of the mobile charges becoming localized to these trap states.[34] This may be a further explanation for the differences in observed μ_e compared to literature values, due to a different morphology obtained by drop-casting rather than the typical spin-coating.

The presence of air shifts the V_T in the positive direction and decreases μ_e, indicating p-type doping or electron trapping of the material by air. This is consistent with previous work with p-type polymers,[35] n- and p-type small molecules[36,37] and ambipolar carbon nanotubes.[38] It is known that electron traps formed at the semiconductor-dielectric interface require a more positive gate voltage to become filled and allow electron transport, thereby increasing V_T.[39] It is likely these traps act as p-type dopants and account for the observed effect for both p- and n-type polymers. This phenomenon is mainly observed in SiO_2 dielectrics.[40] The occurrence of interface traps can be observed in the shape of the subthreshold region in a transfer curve (representative transfer curves can be found in **Figure 2.9**), and calculation of the device subthreshold swing (S) allows for the number of interface traps (N_{it}) to be estimated.[41] The subthreshold swing and number of interface traps have been estimated for each of these devices in vacuum and in air, shown in **Table 2.2**. For all materials, a higher number of interface traps was found in air, confirming that air exposure increases number of interface traps.

Table 2.2. Subthreshold characteristics and interface traps of devices characterized in vacuum and in air at room temperature.

	S (V/dec)		N_{it} (cm^{-2} V^{-1})	
	Vacuum	**Air**	**Vacuum**	**Air**
P(NDI2OD-T2)	4.7	5.1	7.4×10^{12}	8.0×10^{12}
F-N2200	4.1	5.5	6.4×10^{12}	8.7×10^{12}
NDI-20-T	2.9	3.1	4.6×10^{12}	4.9×10^{12}
NDIO-20-T	3.7	5.5	5.7×10^{12}	8.7×10^{12}
PIBDF	6.4	6.9	1.0×10^{13}	1.1×10^{13}

The mechanism of the interaction of oxygen and water in air with P(NDI2OD-T2) has been studied rigorously to determine the individual effects by water and oxygen by Di Pietro *et al*.[42] The loss of mobility in air is reportedly due to an interaction between oxygen molecules and the fused benzene core of the naphthalene diimide unit. Each of the other NDI-containing polymers in this study could exhibit these same interactions. Similarly, the IBDF-based polymer contains fused π-conjugated rings at its core, and oxygen may exhibit similar interactions. Water was found to have the combined effect of creating electron traps as well as contributing to the degradation of the polymer film. This would explain why all materials see the same decrease in mobility in air by an order of magnitude under the combined effects of water and oxygen. It is interesting to note that P(NDI2OD-T2) had the least decrease in mobility compared to the other four polymers. Based on the results of Di Pietro's work, this could indicate that oxygen has a greater electronic interaction with the other polymers.

The effect of electron trapping is also observed in the decrease of the on/off ratio. Each material saw a decrease in $I_{on/off}$ of approximately one order of magnitude, with the exception of NDIO-20-T. The differences in on/off ratio were due to the decrease of the on current in air, however the off current decreased as well in all materials to a smaller degree.

The Influence of Temperature in Vacuum (P < 0.1 Pa)

The performance of these polymers at elevated temperature was also evaluated, giving insight into the mechanism of charge transport. The prepared devices were characterized under vacuum

from 30 °C to 150 °C and the corresponding electron mobility over the gate voltage (V_{GS}) range can be found in the μ_e curves presented in **Figure 2.2**, and corresponding transfer curves may be found in **Figure 2.10**. In the field of organic electronics, there is a push for more accurate and responsible representation of material mobility and device performance,[43–45] and as such, the figures presented examine the mobility of the materials over the given V_{GS} range. The characteristic shape of these μ_e curves is due to contact resistance, which is reported to have two significant effects: 1) the overestimation of μ_e at low V_{GS} resulting in a peak in the μ_e curve,[46] and 2) a decrease in the measured mobility at high V_{GS}, giving an overall downward trend of the μ_e curve.[47] These features result in what has been described as the electrical double slope,[45] which is the observation of two distinct slopes, or regions of linearity in the saturation curves. These features are observed in the presented μ_e curves, and by examining changes across the entire measured V_{GS} range, the changes in mobility can be accurately compared.

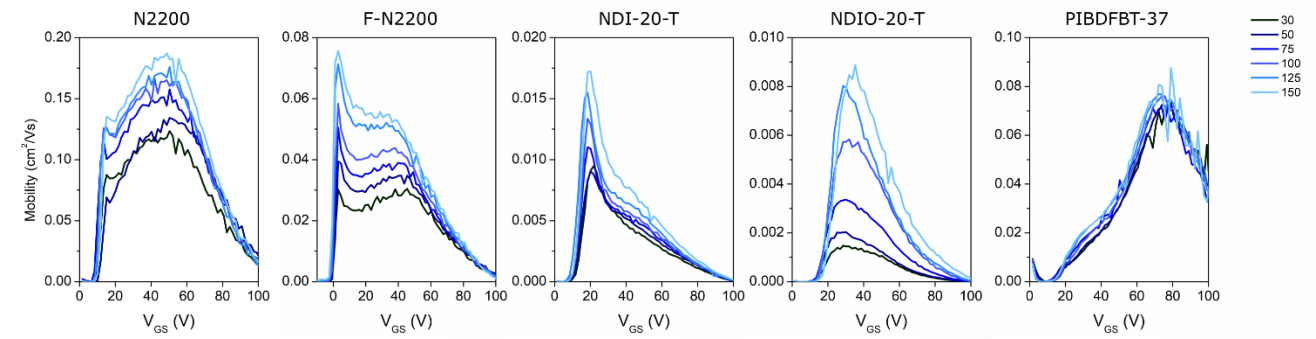

Figure 2.2. Effect of temperature under vacuum *(P < 0.1 Pa)* on electron mobility vs gate voltage (V_{GS}) of various n-type semiconducting polymers all in a bottom gate bottom contact (BGBC) organic thin film transistor (OTFT) device configuration. N2200 = P(NDI2OD-T2)

The mobility curve for all polymers increased with increasing temperature, but the degree of the effect varied significantly between polymers (**Figure 2.2**). While PIBDF saw only a 30 % increase in mobility at its maximum mobility, the mobility of NDIO-20-T increased by nearly 500 %. The V_T's of each material, which can be inferred from the μ_e-V_{GS} curves by the sharp increase in μ_e of each curve, did not substantially change with temperature. All materials exhibit the electrical double-sloping that results in a downwards trend of mobility at high V_{GS}, however only

F-N2200 and NDI-20-T exhibit the sharp peak in μ_e that is likely due to the contact resistance between the materials and electrodes.

The lack of change in V_T for these materials as temperature rises suggests that the density of electron charge traps is not changing, which could imply there is little change in the morphology or water content of the films as a result of changing temperature. These devices had all previously been exposed to air, so it is reasonable to assume that oxygen and water were adsorbed onto the films and dielectric interface, as was discussed previously. The devices were subjected to a vacuum atmosphere for 1 hour prior to testing to ensure any oxygen and water were desorbed. Due to the lack of significant shift in V_T in the tested temperature range, it appears this was sufficient to remove any oxygen and water that would cause charge trapping It is also likely there is little to no significant morphological change at the interface, as a change in size or number of grain boundaries would be expected to cause a change in V_T.[32] The devices were pre-annealed under vacuum to 200 °C in an attempt to minimize effects of changing morphology, so that the mainly the electronic effect of temperature could be isolated. Therefore, the results observed with respect to the variation of μ_e with temperature can be assumed to be mainly caused by the varying temperature, not due to the loss of charge traps caused by altered morphology or oxygen and/or water content.

The increase in μ_e with increasing temperature agrees with most modern charge transport mechanisms for both amorphous and polycrystalline materials, such as charge hopping or mobility edge, respectively. It has been previously suggested that P(NDI2OD-T2) exhibits electron hopping.[48] The very small effect of temperature on PIBDF may be an indication of low dependence on charge carrier concentration, as charge carrier concentration is temperature-dependent,[20] and μ_e is well-known to be dependent on charge carrier concentration.[49] This could also be indicative of a morphological change at increased temperature, which may interfere with organization at the dielectric interface, thus negating any positive effect of temperature on μ_e within the bulk of the film.[50] As it has previously been shown that organic semiconductors capable of hydrogen bonding have high thermal stability,[51] it is possible that the greater number of heteroatoms in the IBDF polymer that would allow for more hydrogen bonds compared to the other materials results in a greater electrical stability with respect to temperature. Further study may elucidate the nature of charge transport of the IBDF polymer.

The Influence of Temperature with Air Exposure

It is also important to examine the effect of air and temperature simultaneously. The presence of oxygen and moisture in the air may compound with the temperature effects previously observed. The same experiments carried out under vacuum were also performed in air, increasing the temperature at intervals from 30 °C to 100 °C, maintaining this temperature for 30 minutes prior to testing, and the corresponding electron mobility at varied V_{GS} can be found in **Figure 2.3**.

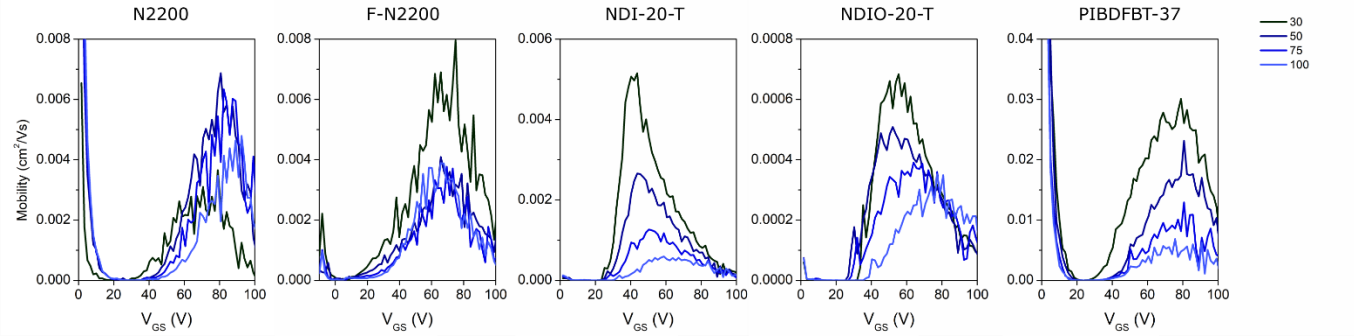

Figure 2.3. Effect of temperature in air on electron mobility vs gate voltage (V_{GS}) of various n-type semiconducting polymers all in a bottom gate bottom contact (BGBC) organic thin film transistor (OTFT) device configuration. N2200 = P(NDI2OD-T2)

The trends observed in vacuum are reversed when devices are heated while exposed to air. In the presence of air, the performance is decreased with increasing temperature. PIBDF is among the most strongly affected by this, despite being the least affected by temperature under vacuum. μ_e is decreased at high temperature for all materials, and V_T is increased as well. The increased V_T could indicate a difference in morphology or in chemical structure. Corresponding transfer curves can be found in **Figure 2.11**.

As previously noted, charge injection depends on the LUMO of the material. If the material becomes irreversibly oxidized, this change in structure will change the frontier energy levels and could potentially lead to an increase in the V_T as observed here. Morphological changes caused solely by the increasing temperature are unlikely, as it was observed that no V_T shift occurred under vacuum. However, a change in chemical structure may also induce morphological change, particularly at higher temperature. From **Table 2.3**, it is clear that heating samples in the presence

of air negatively affects the morphology, as all materials show increased roughness except for PIBDF, which showed a decreased roughness as determined using atomic force microscopy (**Figure 2.4**).

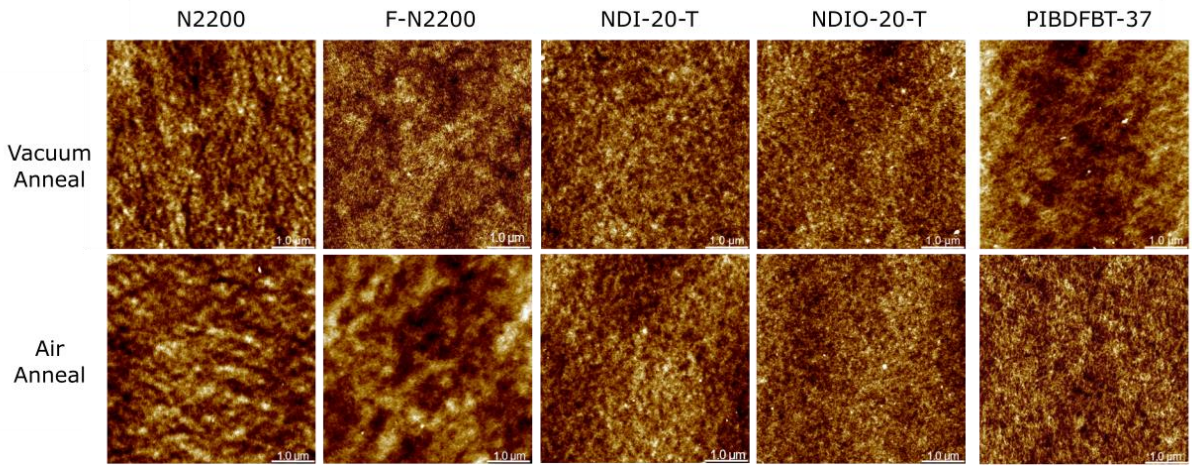

Figure 2.4. Atomic force microscopy (AFM) of 5µm x 5µm sections of each polymer film after annealing in vacuum and air. N2200 = P(NDI2OD-T2)

Table 2.3. Surface RMS roughness (nm) of drop-cast polymer samples following to heating in either air or vacuum at 100 °C determined using atomic force microscopy.

	P(NDI2OD-T2)	F-N2200	NDI-20-T	NDIO-20-T	PIBDFBT-37
Vacuum heated	1.13	1.23	0.884	0.786	2.16
Air heated	1.23	1.77	1.21	0.988	1.76

It has been proposed that due to the long aliphatic chains of P(NDI2OD-T2), the interaction with the core of the semiconductor at dielectric interface is minimized,[8] and the unaligned polymer will only take on a face-on orientation if annealed above 300°C.[52] As each of these polymers contain similarly sized aliphatic chains, this could be contributing to the instability at elevated temperatures under ambient conditions, as the core of the polymer does not interact directly with the dielectric, leading to the potential of diffusion of oxygen and moisture to this interface. The

different composition and branching point of the chain on the IBDF polymer may contribute to reducing this effect, leading to greater air stability.

Conserved Changes from Heating in Air

To examine whether the observed decreases in μ_e and increases in V_T due to heating in air were reversible, the performance of the materials at 30 °C under vacuum was examined prior to and immediately after heating the samples to 100 °C in air. **Figure 2.5** illustrates the difference observed using μ_e vs V_{GS} plots for each material.

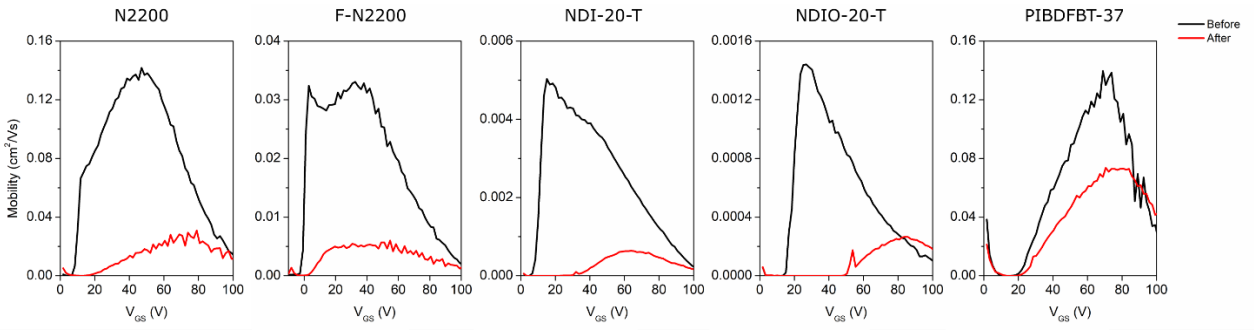

Figure 2.5. Electron mobility (μ_e) vs gate voltage (V_{GS}) of various n-type semiconducting polymers before and after heating films to 100 °C in air. All polymers characterized in a bottom gate bottom contact (BGBC) organic thin film transistor (OTFT) device configuration in a vacuum atmosphere. N2200 = P(NDI2OD-T2)

For all NDI-based materials, the positive V_T shift and loss of μ_e was conserved. The mobility of PIBDF-based OTFTs settled at approximately 50 % of their original value, where all other materials sustained at least 80 % decrease in mobility. These significant losses were not observed in P(NDI2OD-T2), F-N2200, or NDIO-20-T at elevated temperature (**Figure 2.3**). Yet, PIBDF saw a significant decrease in performance in air at high temperature, but this was not conserved when the device was re-exposed to vacuum. This may indicate that no significant chemical changes occurred to PIBDF when exposed to air at high temperature, while NDI-based materials were more susceptible to permanent damage. The loss of μ_e observed in **Figure 2.3** for PIBDF could be explained by an enhancement of the interaction with either water or oxygen resulting in a mostly reversible increase in the number of electron charge traps present.

Long-Term Stability

Finally, the stability of each material was examined over time (30 days) under ambient conditions in an OTFT, both in the presence of indoor light and in the dark (**Figure 2.6**).

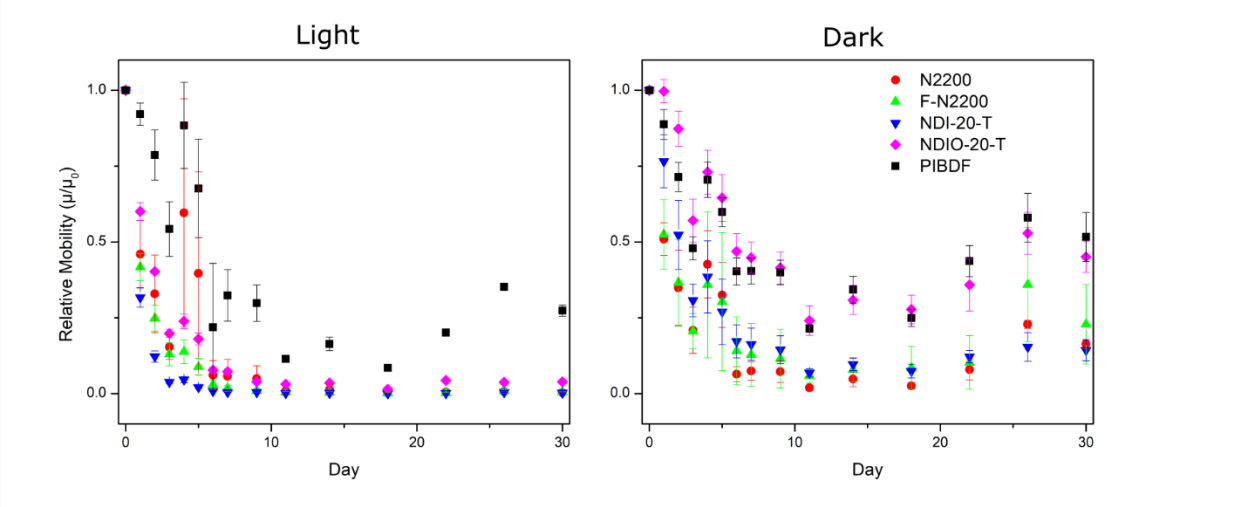

Figure 2.6. Average of normalized mobilities ($\mu/\mu_{day\ 0}$) for various n-type semiconducting polymers characterized daily over a period of one month. Each chip contains four 20 µm channel length devices which were characterized in air and averaged for each data point each day. N2200 = P(NDI2OD-T2)

When exposed to light, the μ_e of all devices decreased faster and to a greater extent. Triplet oxygen is expected to be the main culprit in the degradation of P(NDI2OD-T2).[42] As each of these materials is photoactive, this rapid decrease in μ_e compared to OTFTs stored in the dark could also be explained by electrons being photo-excited to the LUMO, and this excited state would readily react with oxygen. Di Pietro *et al.* also noted that other materials besides P(NDI2OD-T2) appear to undergo the same degradation, so this mechanism is likely to affect a wide range of materials.[42] However, PIBDF appears to be the most stable material when exposed to light, and matched by NDIO-20-T in the dark. Some fluctuation in results are likely due to variations in relative humidity (RH), but generally these are quite small. Devices were all measured on the same days and at the same time each day to make differences comparable within the dataset.

While all the materials see less decrease in μ_e while stored in the dark, PIBDF maintains the highest performance. Most materials experience over an order of magnitude decrease in μ_e (some even over 3 orders of magnitude when stored in light) except for PIBDF which largely retains its

high μ_e throughout the study (**Figure 2.6**). Despite PIBDF having the smallest band gap of the materials, absorbing in the NIR region, it has impressive stability in air under ambient conditions when exposed to light. The loss of μ_e over time could be caused on the short time scale by the formation of charge traps by adsorbed water and oxygen. This is reflected in the similar rate of μ_e decrease in the first 7 days of the study. Beyond this, the continued performance loss in the materials stored in light may be caused by slow chemical degradation by the UV- and visible-light activation of electrons in the semiconductors that are then reacted with oxygen and water in the air to degrade the film. NDIO-20-T appears to be the most strongly affected by the presence of light compared to the other materials. This may be due to the relative strength of the N-C and N-O bonds of the side chains, with bond energies of 305 kJ/mol and 201 kJ/mol, respectively. The weaker N-O bond may be more susceptible to cleavage in the presence of light.

UV-Visible spectroscopy

To further examine the effect of air on the material, UV-Visible spectroscopy was used to determine whether chemical changes occurred in the material. Degradation of a particular absorbance peak indicates the loss of a particular chromophore, while the growth of a new peak indicates the formation of a new chromophore and overall absorbance will decrease if the degree of conjugation is decreased.[53–56] Glass slides were spin-coated with the materials and their absorbances were measured. Following this, each slide was heated at 130 °C either in vacuum or in air to simulate the testing observed in the vacuum and air-temperature studies (**Figure 2.7**).

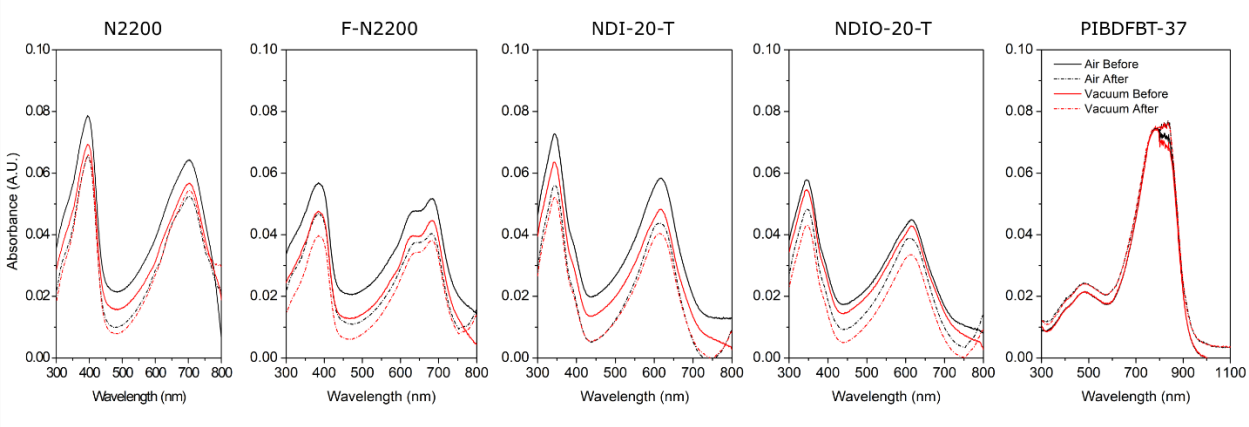

Figure 2.7. Normalized UV-vis comparison of thin films of n-type polymer materials before (solid lines) and after (dotted lines) heating to 130 °C in air (black) or vacuum (red). N2200 = P(NDI2OD-T2)

A clear trend emerges from the UV-visible spectra of these materials. For all materials except PIBDF and NDIO-20-T, there is a greater loss of absorbance intensity after exposure to heat in air than in vacuum. In NDIO-20-T, the magnitude of the change is greater following heating in vacuum. The only notable change in PIBDF is the shift of the absorption maximum at 750nm and 850nm, where before heating the peak is higher at 790 nm, and after heating higher at 850nm, which occurs in both air and vacuum. The magnitude of these changes are given in **Table 2.4**. This is consistent with the smaller relative loss of μ_e as a result of heating the PIBDF in air, as was shown in **Figure 5**. These results suggest the changes in μ_e and V_T observed in the NDI polymer based devices when heated in air, as these differences in the UV-visible spectra may indicate changing chemical structure, and irreversible changes to the material. These spectra further suggest that PIBDF is more stable than the other NDI-based polymers.

Table 2.4. Percent change in characteristic peak height intensity of UV-visible spectra.

	P(NDI2OD-T2)	F-N2200	NDI-20-T	NDIO-20-T	PIBDFBT-37
Peak (nm)	705	685	620	605	790
Air	-18.4%	-22.4%	-25.0%	-11.4%	-0.4%
Vacuum	-4.2%	-14.4%	-16.3%	-19.8%	+0.7%

Developing Structure-Property Relationships Towards More Stable Polymers

As previously discussed, these materials have similar LUMO levels and therefore it cannot be concluded that the relative stability of the polymers is related to molecular orbital energies in these examples. However, the differing structures of these materials enable a greater understanding of the effect structural changes have on air stability. It has previously been shown that heteroatoms increase chemical stability of semiconductors due to the stabilization of radicals.[57] Further supporting this, heteroatoms such as N, O, and S have been reported to significantly increase stability of radicals.[58] We can conclude that additional heteroatoms appear to lend enhanced stability in the example of the IBDF polymer being highly air-stable compared to the other examples presented in this work. This same factor may also lend greater air-stability to P(NDI2OD-T2), as it is possible the additional thiophene unit and subsequent incorporation of additional sulfur atom also enable additional radical stabilization, preventing degradation from air exposure. Moreover, P(NDI2OD-T2) is reported to have an optimized conformation interacting with oxygen that is stable.[42] This conformation involves the twisting of the thiophene units to form a "cradle" around the O_2 molecule. The addition of fluorine to the thiophene (Th) linkers in the form of F-N2200 or the removal of one Th linker in NDI-20-T could alter this interaction and lead to a less favourable conformation that would result in a more detrimental interaction of O_2 and polymer, and therefore lower observed air stability.

2.4 Conclusion

This study examined the environmental sensitivities of four polymers based on an NDI core, and one polymer based on an IBDF core. OTFTs were fabricated with each of these polymers and studied with varied temperature in air and vacuum environments. In vacuum, P(NDI2OD-T2) was not strongly affected by temperature compared to the similar NDI-based polymers, but PIBDF showed the lowest temperature response overall. In air, all polymers showed decreasing μ_e with increasing temperature, however P(NDI2OD-T2) was the least affected by elevated temperature in air. To expand on these results, the stability of these materials under ambient conditions was studied over a month-long period. PIBDF showed the highest stability when exposed to light, while both NDIO-20-T and PIBDF were the most stable materials when devices were stored in the dark under ambient conditions. The stability of PIBDF was further supported by the lack of change in its UV-visible spectrum when heated in air, compared to the decrease in overall absorbance of the

other materials, indicating that the PIBDF is not chemically altered by exposure to heated air while the other materials are. These studies support previous conclusions about the enhancement of air-stability in n-type materials through the inclusion of heteroatoms and suggest that the unique conformation of the NDI-2Th units in P(NDI2OD-T2) could lead to its comparative air stability next to other NDI-based polymers. These results are promising for the further development of materials for high-performance n-type air-stable polymers.

2.5 Experimental

Device Preparation

Prior to semiconductor deposition, pre-patterned Si/SiO_2 substrates with gold source-drain electrodes (W = 2000 µm, L = 20 µm; Fraunhofer IPMS) were first washed with acetone and dried with N_2, then plasma-treated for 15 minutes to clean. The surfaces of the substrates were functionalized with octyltrichlorosilane (OTS) by heating in a 1% (v/v) solution of OTS in toluene at 70 °C for 1 hour. Substrates were then dried for 1 hour under vacuum at 70 °C to remove residual toluene. Semiconducting polymers were dissolved in chloroform at 1 mg/mL and drop cast with 1 µL drops onto the cleaned substrates on the channels. Finally, devices were annealed at 200 °C for four hours under vacuum. P(NDI2OD-T2) was obtained from 1-Material and Brilliant Matters Organic Electronics. F-N2200 was obtained from 1-Material. NDI-20-T,[12] NDIO-20-T,[12] and PIBDFBT-37[13] were synthesized according to the literature.

Electrical Characterization

A custom Electrical probes station, oesProbe A10000-P290 (Element Instrumentation Inc. & Kreus Design Inc.) with Keithley 2614B were used to perform electrical measurements under controlled atmosphere. Device performance was measured in the saturation region, with control source-drain voltage (V_{DS}) maintained at a constant 60 V, while gate voltage (V_{GS}) was varied from -10 V to 100 V to obtain measurements of source-drain current (I_{DS}). **Equation 1**:

$$(1)\quad I_{DS} = \frac{\mu C_i W}{2L}(V_{GS} - V_T)^2$$

Where μ is the field-effect electron mobility of the material, C_i is the capacitance, W is the width of the channel, L is the length of the channel, and V_T is the threshold voltage. By taking the square root of **Equation 1**, a linear relation is obtained (as shown in **Equation 2**), so that the μ and V_T can be calculated directly from the slope and x-intercept of an $\sqrt{I_{DS}}\ vs\ V_{GS}$ curve, respectively.

$$(2)\ \sqrt{I_{DS}} = \sqrt{\frac{\mu C_i W}{2L}}(V_{GS} - V_T)$$

Finally, the on/off ratio is determined by the ratio of I_{on} and I_{off}, which are the highest and lowest currents, respectively, measured in the characterized gate voltage range.

2.6 Acknowledgments

The authors are grateful for financial support from the NSERC DG to B.H.L and Y. L. and the Ontario Graduate Scholarship (OGS) to S. B. and O.A.M. ADH is grateful for an NSERC Post-Doctoral Fellowship. Infrastructure used to complete this work was acquired using CFI-JELF and NSERC RTI. We thank Steven Xiao (1-Material) for the donation of N2200 and FN2200, as well as Jean-Rémi Pouliot (Brilliant Matters Organic Electronics) for the donation of N2200.

2.7 References

1. Katz, H. E. *et al.* A soluble and air-stable organic semiconductor with high electron mobility. *Nature* **404**, 478–481 (2000).

2. Han, Y. *et al.* Naphthalene Diimide-Based n-Type Polymers: Efficient Rear Interlayers for High-Performance Silicon-Organic Heterojunction Solar Cells. *ACS Nano* **11**, 7215–7222 (2017).

3. Wang, F. *et al.* Incorporation of Heteroatoms in Conjugated Polymers Backbone toward Air-Stable, High-Performance n-Channel Unencapsulated Polymer Transistors. *Chem. Mater.* **30**, 5451–5459 (2018).

4. Li, J. *et al.* A stable solution-processed polymer semiconductor with record high-mobility for printed transistors. *Sci. Rep.* **2**, 754 (2012).

5. Lei, T. *et al.* High-performance air-stable organic field-effect transistors: Isoindigo-based conjugated polymers. *J. Am. Chem. Soc.* **133**, 6099–6101 (2011).

6. Onwubiko, A. *et al.* Fused electron deficient semiconducting polymers for air stable electron transport. *Nat. Commun.* **9**, 416 (2018).

7. Zaumseil, J. & Sirringhaus, H. Electron and ambipolar transport in organic field-effect transistors. *Chem. Rev.* **107**, 1296–1323 (2007).

8. Yan, H. *et al.* A high-mobility electron-transporting polymer for printed transistors. *Nature* **457**, 679–686 (2009).

9. Kim, R. *et al.* High-mobility air-stable naphthalene diimide-based copolymer containing extended π-conjugation for n-channel organic field effect transistors. *Adv. Funct. Mater.* **23**, 5719–5727 (2013).

10. Guo, X., Kim, F. S., Seger, M. J., Jenekhe, S. A. & Watson, M. D. Naphthalene diimide-based polymer semiconductors: Synthesis, structure-property correlations, and n-channel and ambipolar field-effect transistors. *Chem. Mater.* **24**, 1434–1442 (2012).

11. Wu, Z. *et al.* N-Type Water/Alcohol-Soluble Naphthalene Diimide-Based Conjugated Polymers for High-Performance Polymer Solar Cells. *J. Am. Chem. Soc.* **138**, 2001–2013

(2016).

12. He, Y. *et al.* A new n-type polymer based on N,N0-dialkoxynaphthalenediimide (NDIO) for organic thin-film transistors and all-polymer solar cells. *J. Mater. Chem.* **6**, 1349–1352 (2017).

13. He, Y., Guo, C., Sun, B., Quinn, J. & Li, Y. Branched alkyl ester side chains rendering large polycyclic (3E,7E)-3,7-bis(2-oxoindolin-3-ylidene)benzo[1,2-b:4,5-b′]difuran-2,6(3H,7H)-dione (IBDF) based donor-acceptor polymers solution-processability for organic thin film transistors. *Polym. Chem.* **6**, 6689–6697 (2015).

14. He, Y., Quinn, J. T. E., Hou, D., Ngai, J. H. L. & Li, Y. A small bandgap (3E,7 E)-3,7-bis(2-oxoindolin-3-ylidene)benzo[1,2-b:4,5- b ′]difuran-2,6(3 H,7 H)-dione (IBDF) based polymer semiconductor for near-infrared organic phototransistors. *J. Mater. Chem. C* **5**, 12163–12171 (2017).

15. Yan, Z., Sun, B. & Li, Y. Novel stable (3E,7E)-3,7-bis(2-oxoindolin-3-ylidene)benzo[1,2-b:4,5- b′]difuran-2,6(3H,7H)-dione based donor-acceptor polymer semiconductors for n-type organic thin film transistors. *Chem. Commun.* 3790–3792 (2013) doi:10.1039/c3cc40531a.

16. Lei, T., Dou, J. H., Cao, X. Y., Wang, J. Y. & Pei, J. Electron-Deficient Poly(p-phenylene vinylene) Provides Electron Mobility over 1 cm2 V-1 s-1 under Ambient Conditions. *J. Am. Chem. Soc.* **135**, 12168–12171 (2013).

17. Lei, T., Xia, X., Wang, J. Y., Liu, C. J. & Pei, J. ‘Conformation Locked’ Strong Electron-Deficient Poly(p -Phenylene Vinylene) Derivatives for Ambient-Stable n-Type Field-Effect Transistors: Synthesis, Properties, and Effects of Fluorine Substitution Position. *J. Am. Chem. Soc.* **136**, 2135–2141 (2014).

18. Lei, T., Dou, J. H., Cao, X. Y., Wang, J. Y. & Pei, J. A BDOPV-based donor-acceptor polymer for high-performance n-type and oxygen-doped ambipolar field-effect transistors. *Adv. Mater.* **25**, 6589–6593 (2013).

19. Coropceanu, V. *et al.* Charge Transport in Organic Semiconductors. *Chem. Rev.* **107**, 926–952 (2007).

20. Liu, C. *et al.* A unified understanding of charge transport in organic semiconductors: The importance of attenuated delocalization for the carriers. *Mater. Horizons* **4**, 608–618 (2017).

21. Van Der Kaap, N. J. *et al.* Charge transport in disordered semiconducting polymers driven by nuclear tunneling. *Phys. Rev. B* **93**, 140206 (2016).

22. Jiang, Y., Peng, Q., Geng, H., Ma, H. & Shuai, Z. Negative isotope effect for charge transport in acenes and derivatives - A theoretical conclusion. *Phys. Chem. Chem. Phys.* **17**, 3273–3280 (2015).

23. Bucella, S. G. *et al.* Macroscopic and high-throughput printing of aligned nanostructured polymer semiconductors for MHz large-area electronics. *Nat. Commun.* **6**, 8394 (2015).

24. Chen, Z., Zheng, Y., Yan, H. & Facchetti, A. Naphthalenedicarboximide- vs perylenedicarboximide-based copolymers. synthesis and semiconducting properties in bottom-gate N-channel organic transistors. *J. Am. Chem. Soc.* **131**, 8–9 (2009).

25. Jung, J. W. *et al.* Fluoro-substituted n-type conjugated polymers for additive-free all-polymer bulk heterojunction solar cells with high power conversion efficiency of 6.71%. *Adv. Mater.* **27**, 3310–3317 (2015).

26. Jones, B. A., Facchetti, A., Wasielewski, M. R. & Marks, T. J. Tuning orbital energetics in arylene diimide semiconductors. Materials design for ambient stability of n-type charge transport. *J. Am. Chem. Soc.* **129**, 15259–15278 (2007).

27. Lee, S. S. *et al.* Controlling nucleation and crystallization in solution-processed organic semiconductors for thin-film transistors. *Adv. Mater.* **21**, 3605–3609 (2009).

28. Melville, O. A. *et al.* Ambipolarity and Air Stability of Silicon Phthalocyanine Organic Thin-Film Transistors. *Adv. Electron. Mater.* **5**, 1900087 (2019).

29. Li, R. *et al.* Direct structural mapping of organic field-effect transistors reveals bottlenecks to carrier transport. *Adv. Mater.* **24**, 5553–5558 (2012).

30. Rivnay, J. *et al.* Large modulation of carrier transport by grain-boundary molecular packing and microstructure in organic thin films. *Nat. Mater.* **8**, 952–958 (2009).

31. Kaake, L. G., Barbara, P. F. & Zhu, X. Y. Intrinsic charge trapping in organic and polymeric semiconductors: A physical chemistry perspective. *J. Phys. Chem. Lett.* **1**, 628–635 (2010).

32. Bolognesi, A. *et al.* Effects of grain boundaries, field-dependent mobility, and interface trap states on the electrical characteristics of pentacene TFT. *IEEE Trans. Electron Devices* **51**, 1997–2003 (2004).

33. Vladimirov, I., Kühn, M., Geßner, T., May, F. & Weitz, R. T. Energy barriers at grain boundaries dominate charge carrier transport in an electron-conductive organic semiconductor. *Sci. Rep.* **8**, 14868 (2018).

34. Bolognesi, A. *et al.* Effects of grain boundaries, field-dependent mobility, and interface trap states on the electrical characteristics of pentacene TFT. *IEEE Trans. Electron Devices* **51**, 1997–2003 (2004).

35. Brixi, S., Melville, O. A., Boileau, N. T. & Lessard, B. H. The influence of air and temperature on the performance of PBDB-T and P3HT in organic thin film transistors. *J. Mater. Chem. C* **6**, 11972–11979 (2018).

36. Rice, N., Magnan, F., Melville, O., Brusso, J. & Lessard, B. Organic Thin Film Transistors Incorporating Solution Processable Thieno[3,2-b]thiophene Thienoacenes. *Materials (Basel).* **11**, 8 (2017).

37. Boileau, N. T., Melville, O. A., Mirka, B., Cranston, R. & Lessard, B. H. P and N type copper phthalocyanines as effective semiconductors in organic thin-film transistor based DNA biosensors at elevated temperatures. *RSC Adv.* **9**, 2133–2142 (2019).

38. Aguirre, C. M. *et al.* The role of the oxygen/water redox couple in suppressing electron conduction in field-effect transistors. *Adv. Mater.* **21**, 3087–3091 (2009).

39. Sirringhaus, H. Reliability of organic field-effect transistors. *Adv. Mater.* **21**, 3859–3873 (2009).

40. Phan, H., Wang, M., Bazan, G. C. & Nguyen, T. Q. Electrical Instability Induced by Electron Trapping in Low-Bandgap Donor-Acceptor Polymer Field-Effect Transistors. *Adv. Mater.* **27**, 7004–7009 (2015).

41. Kalb, W. L. & Batlogg, B. Calculating the trap density of states in organic field-effect transistors from experiment: A comparison of different methods. *Phys. Rev. B - Condens. Matter Mater. Phys.* **81**, 035327 (2010).

42. Di Pietro, R., Fazzi, D., Kehoe, T. B. & Sirringhaus, H. Spectroscopic investigation of oxygen- and water-induced electron trapping and charge transport instabilities in n-type polymer semiconductors. *J. Am. Chem. Soc.* (2012) doi:10.1021/ja304198e.

43. Reese, C. & Bao, Z. Overestimation of the field-effect mobility via transconductance measurements and the origin of the output/transfer characteristic discrepancy in organic field-effect transistors. *J. Appl. Phys.* **105**, 024506 (2009).

44. Podzorov, V. Organic single crystals: Addressing the fundamentals of organic electronics. *MRS Bull.* **38**, 15–24 (2013).

45. Phan, H. *et al.* Electrical Double-Slope Nonideality in Organic Field-Effect Transistors. *Adv. Funct. Mater.* **28**, 1707221 (2018).

46. Bittle, E. G., Basham, J. I., Jackson, T. N., Jurchescu, O. D. & Gundlach, D. J. Mobility overestimation due to gated contacts in organic field-effect transistors. *Nat. Commun.* **7**, 10908 (2016).

47. Liu, C. *et al.* Device Physics of Contact Issues for the Overestimation and Underestimation of Carrier Mobility in Field-Effect Transistors. *Phys. Rev. Appl.* **8**, 034020 (2017).

48. Trefz, D. *et al.* Electrochemical Investigations of the N-Type Semiconducting Polymer P(NDI2OD-T2) and Its Monomer: New Insights in the Reduction Behavior. *J. Phys. Chem. C* **119**, 22760–22771 (2015).

49. Salleo, A. *et al.* Intrinsic hole mobility and trapping in a regioregular poly(thiophene). *Phys. Rev. B - Condens. Matter Mater. Phys.* **70**, 115311 (2004).

50. Vladimirov, I. *et al.* Dielectric–Semiconductor Interface Limits Charge Carrier Motion at Elevated Temperatures and Large Carrier Densities in a High-Mobility Organic Semiconductor. *Adv. Funct. Mater.* **29**, 1807867 (2019).

51. Głowacki, E. D. *et al.* Hydrogen-bonded diketopyrrolopyrrole (DPP) pigments as organic semiconductors. *Org. Electron.* **15**, 3521–3528 (2014).

52. Tremel, K. *et al.* Charge transport anisotropy in highly oriented thin films of the acceptor polymer P(NDI2OD-T2). *Adv. Energy Mater.* **4**, 1301659 (2014).

53. Hintz, H., Egelhaaf, H. J., Peisert, H. & Chassé, T. Photo-oxidation and ozonization of poly(3-hexylthiophene) thin films as studied by UV/VIS and photoelectron spectroscopy. *Polym. Degrad. Stab.* **95**, 818–825 (2010).

54. Rivaton, A. *et al.* Light-induced degradation of the active layer of polymer-based solar cells. *Polym. Degrad. Stab.* **95**, 278–284 (2010).

55. Manceau, M., Rivaton, A., Gardette, J. L., Guillerez, S. & Lemaître, N. The mechanism of photo- and thermooxidation of poly(3-hexylthiophene) (P3HT) reconsidered. *Polym. Degrad. Stab.* **94**, 898–907 (2009).

56. Manceau, M. *et al.* Effects of long-term UVvisible light irradiation in the absence of oxygen on P3HT and P3HT: PCBM blend. *Sol. Energy Mater. Sol. Cells* **94**, 1572–1577 (2010).

57. Enengl, C. *et al.* The Role of Heteroatoms Leading to Hydrogen Bonds in View of Extended Chemical Stability of Organic Semiconductors. *Adv. Funct. Mater.* **25**, 6679–6688 (2015).

58. Henry, D. J., Parkinson, C. J., Mayer, P. M. & Radom, L. Bond dissociation energies and radical stabilization energies associated with substituted methyl radicals. *J. Phys. Chem. A* **105**, 6750–6756 (2001).

2.8 Supplemental Information

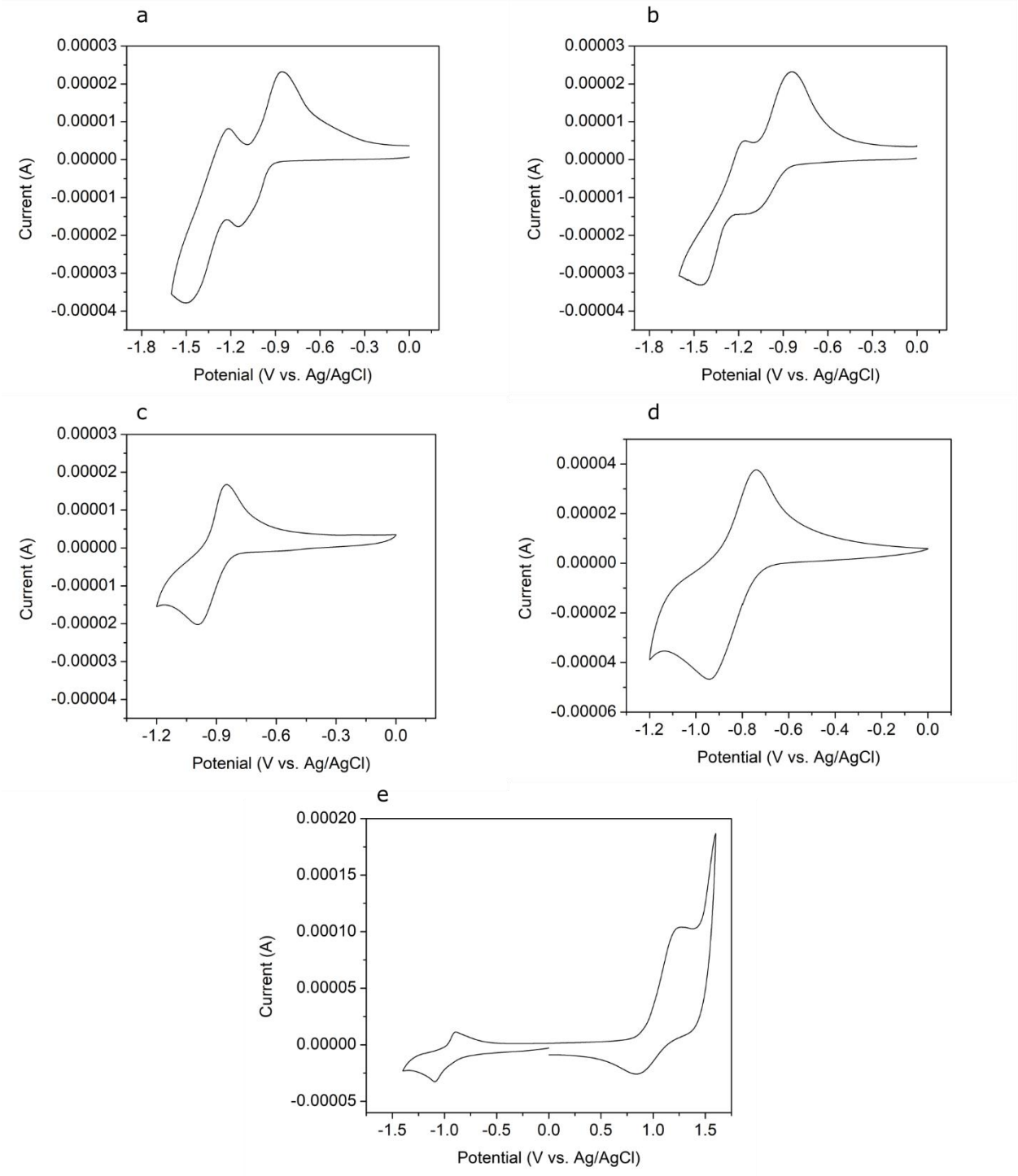

Figure 2.8. Cyclic voltammograms of each polymer. a. P(NDI2OD-T2) b. F-N2200 c. NDI-20-T d. NDIO-20-T f. PIBDFBT-37

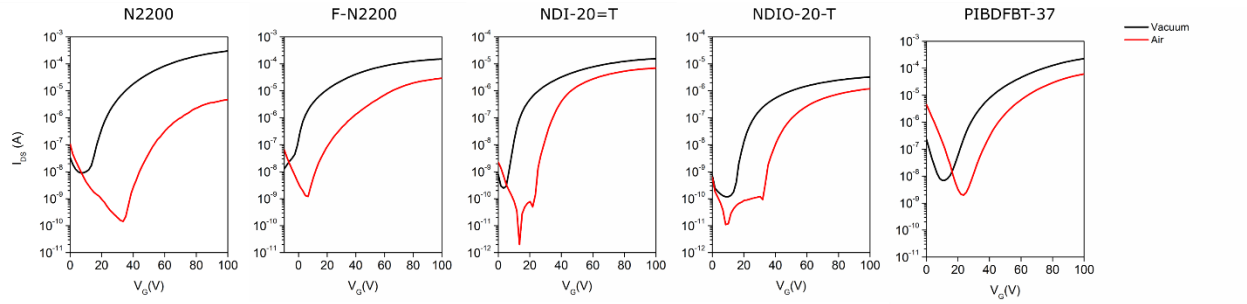

Figure 2.9. Transfer curves of each polymer at 30°C in air and vacuum. N2200 = P(NDI2OD-T2)

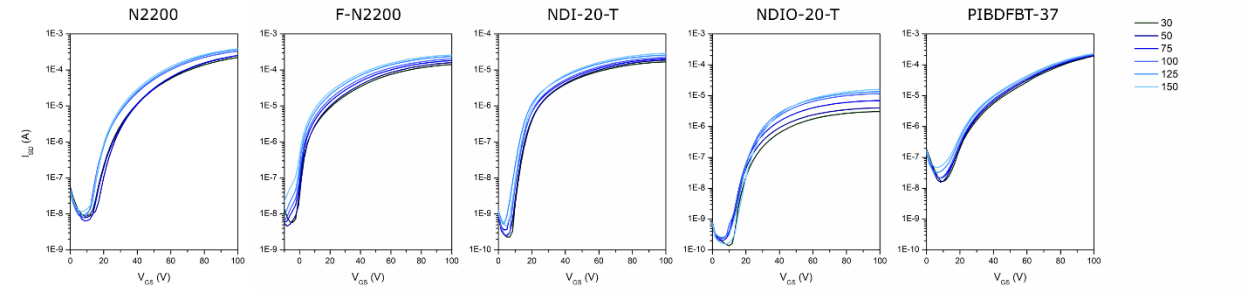

Figure 2.10. Transfer curves of each polymer from 30°C to 150°C in vacuum. N2200 = P(NDI2OD-T2)

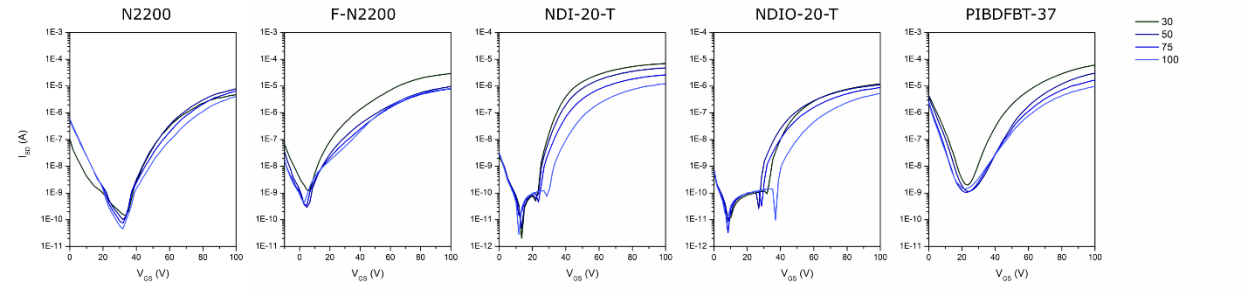

Figure 2.11. Transfer curves of each polymer from 30°C to 100°C in air. N2200 = P(NDI2OD-T2)

3. Exposure to Solvent Vapours for Enhanced N-type OTFT Stability

Context and Significance of Work

In the stability studies we observed in Chapter 2, we saw that even the polymer P(NDI2OD-T2) that was touted to be air stable was still not highly stable in air. Therefore, we wanted to study avenues of improving OTFT air stability that could apply to a broad range of materials and device structures. The idea of using additives was enticing, as it could be included in the inks used to print these devices. Additives have been studied, such as numerous dopants, but many of these materials are inherently stable. Additionally, many can be highly expensive due to synthetic complexity. Therefore, we wished to complete a more fundamental study of moieties of interest that may improve stability, or even performance, of n-type OTFTs, which could then later inform the design of stability-enhancing additives. We focussed on the use of inexpensive commodity chemicals to align with the goal of keeping the complexity and price of the additives low. These types of fundamental studies for device additives are not often seen in literature. In this study, we successfully identified ideal moieties, for which a follow-up study could be completed on the design of stability enhancers.

Contributions of Authors

I designed the study, completed all device work and the cyclic voltammetry, performed all data analysis, and wrote the manuscript. The GIWAXS studies were performed by Benjamin King and Halynne Lamontagne, and the corresponding experimental section was written by Benjamin and Halynne.

This work is published in Materials Advances: Brixi, S.; Lamontagne, H.; King, B.; Shuhendler, A. J.; Lessard, B. H. Exposure to Solvent Vapours for Enhanced N-type OTFT Stability. doi:10.1039/D3MA00402C

3.1 Abstract

To achieve commercialization of organic electronics, the field must see an improvement in both performance and material stability while maintaining a low cost of fabrication. To achieve this, low-cost additives provide a viable solution. A variety of additives containing amine and silane functional groups were tested to determine their impact on the performance and air-stability of n-type semiconductor poly{[*N*,*N*′-bis(2-octyldodecyl)-naphthalene-1,4,5,8-bis(dicarboximide)-2,6-diyl]-*alt*-5,5′-(2,2′-bithiophene)} (P(NDI2OD-T2)) in organic thin film transistors. Aniline and pyridine were found to both have a minimal impact on P(NDI2OD-T2) performance in an inert environment, but to improve stability of electron mobility and threshold voltage in air. Therefore, these compounds, or other compounds based on their structure, would be ideal candidates as additives for the improvement of n-type transistors.

3.2 Introduction

The stability of organic semiconducting materials used in n-type electronic devices must see improvement before widespread commercial adoption. While new complex materials are being developed and incremental improvements in performance are made, improving device performance using already commercially viable semiconductors is another promising strategy.[1,2] For example, the use of additives in ink formulations, thin film treatment or the use of encapsulation can improve the overall performance and stability without the need of synthesizing a new semiconductor. These techniques can be used in combination to enable enhanced stability.

Numerous additives have been shown to improve organic thin-film transistors (OTFTs) by altering film morphology or acting as dopants.[3–8] It has previously been reported that the presence of various solvent molecules within a film can enhance performance and stability of p-type materials.[8] Films of n-type semiconductors exposed to vapours of aminosilane molecules displayed enhanced performance,[9] but their stability was not studied. Aminosilanes contain two separate functional groups: an electron-donating amine and an electron-withdrawing silane. Amine molecules have been used as n-type dopants[7,10], while silanes have been used as p-type dopants[11]. The two functionalities could potentially have disparate effects. The silane group would be likely to have high reactivity with water and may enhance stability of the device by preferentially reacting with water and preventing interaction with the semiconductor. Isolating the effect of each functional group and developing structure property relationships between additives and the resulting n-type stability will lead to the design of high performance and stable n-type devices.

In this study we explore the use of commercially available solvents such as aminosilanes, amines, and silane molecules having similar size and structure. Bottom gate top contact (BGTC) OTFTs were fabricated using commercially available P(NDI2OD-T2) (poly{[*N*,*N*′-bis(2-octyldodecyl)-naphthalene-1,4,5,8-bis(dicarboximide)-2,6-diyl]-*alt*-5,5′-(2,2′-bithiophene)}), then treated with various aminosilanes, amines, and silanes to determine the impact of these compounds on device performance (**Figure 3.1**).

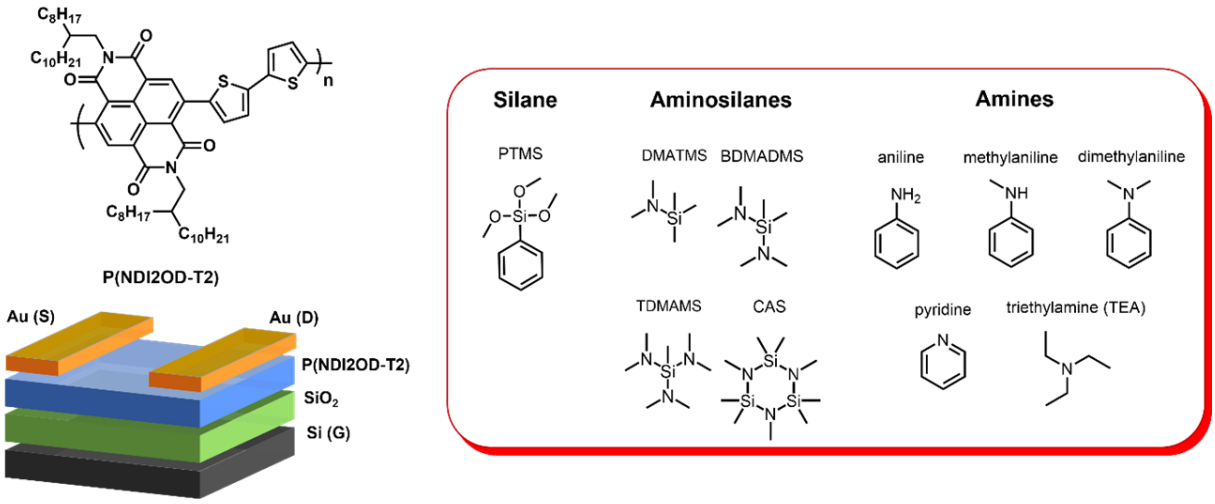

Figure 3.1. (a) Structure of P(NDI2OD-T2) and OTFT configuration. (b) Aminosilane, amine, and silane additives used in this study.

3.3 Discussion

Typical BGTC P(NDI2OD-T2) OTFTs were fabricated according to literature.[12] After fabrication, devices were characterized under inert conditions in a N_2 glovebox. The control sample, which was not exposed to any vapour, was then exposed to air and characterized again (**Figure 3.2**). The remaining devices were all exposed to the respective solvent vapour for 30 minutes, then characterized in the same glovebox environment (remaining in the glovebox for the duration of the experiment) immediately after vapour exposure was completed to compare performance before and after exposure. Directly following testing under inert conditions, these vapour-exposed devices were then moved to air and characterized again, which would allow the impact on air stability to be assessed. Immediate testing after air exposure ensured that the effects of each additive could be assessed directly without concern from any difference in relative volatility or preferential film adsorption, which will allow for the identification of ideal functional groups in the future design of additives.

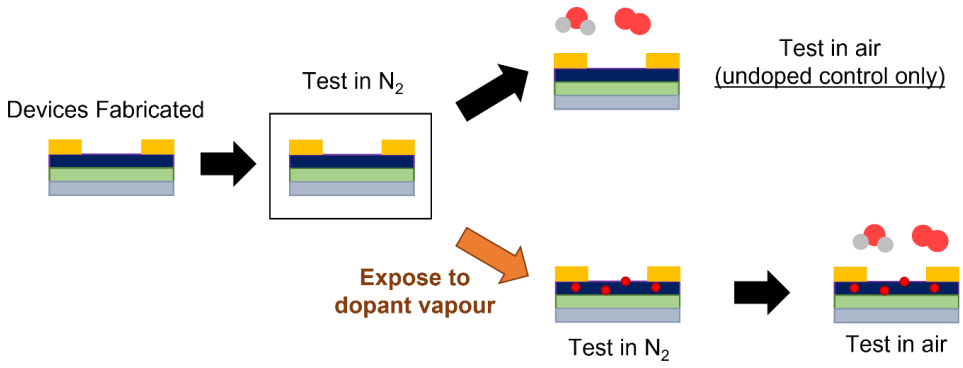

Figure 3.2. Visual schematic of methodology of characterizing P(NDI2OD-T2) OTFT air stability with the use of solvent doping.

Figure 3.3 shows the saturation electron mobility (μ_e) and threshold voltage (V_T) of OTFTs fabricated with P(NDI2OD-T2) and treated with various solvent additives. For each of the following comparisons, the comparison is made with the initial performance of the same device before exposure to the additive and exposure to air. These are then compared to the untreated devices (left-hand side of the figure) for comparison of the impact of air exposure. Typically, a modest increase in V_T and a drop in μ_e is observed for P(NDI2OD-T2) based OTFTs[13] when operated in air, which was observed for the untreated samples. The (dimethylamino)trimethylsilane (DMATMS) and bis(dimethylamino)trimethylsilane (BDMADMS) both increased the μ_e of the devices after initial exposure. However, the tris(dimethylamino)trimethylsilane (TDMAMS) and cyclic aminosilane (CAS) both led to decreased μ_e after initial exposure. All of the trimethylsilanes retained μ_e values in air that were higher than the control, however DMATMS exhibited the smallest overall change in μ_e from inert atmosphere to air. Increasing the relative nitrogen content of the silane worsened its ability to retain the μ_e in air. All vapour treatments resulted in an increased V_T under inert conditions compared to the untreated film of approximately 5 to 10 V. After air exposure, regardless of the vapour the devices were exposed to, the V_T of all devices were in the range of 30 to 35 V. While there is some evidence that aminosilanes may improve device stability with DMATMS retaining higher mobility in air, the small impact on V_T in air was less promising.

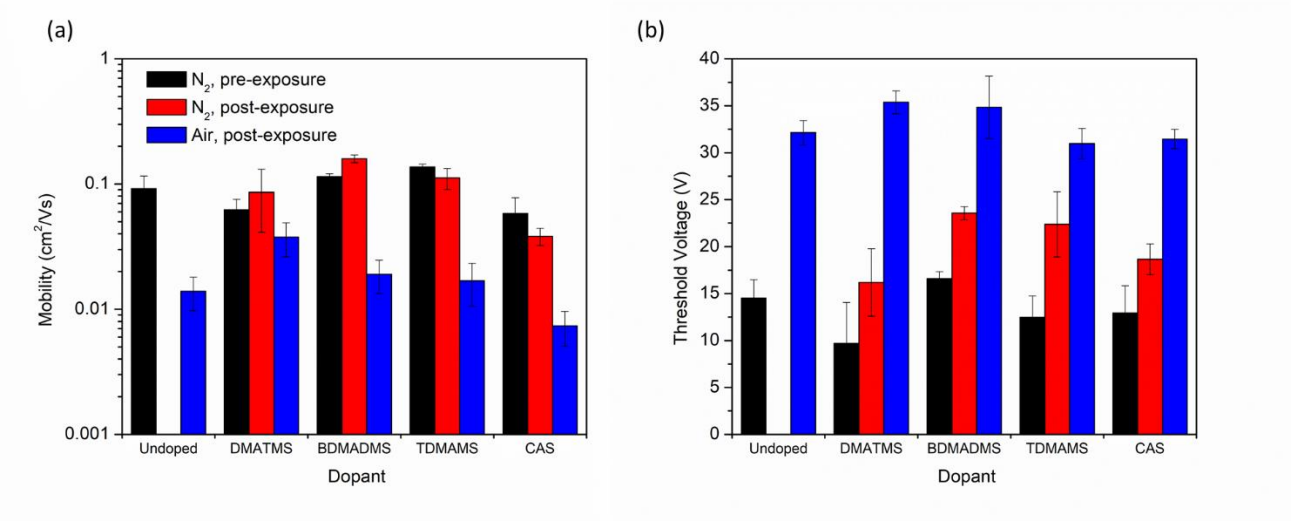

Figure 3.3. (a) saturation electron mobility and (b) threshold voltage of devices before and after vapour exposure to aminosilane vapours under inert conditions, and subsequent changes in performance after exposure to air.

As the amine group is likely to be the main source of n-doping in these devices[7], it was therefore of interest to study exposure of the devices, primary, secondary, and tertiary amines to determine if this impacted the n-doping effect (**Figure 3.4**). Therefore, the addition of aniline, N-methylaniline, and N,N-dimethylaniline to the OTFTs were all characterized. All three had little impact on μ_e under inert conditions, and all three resulted in higher μ_e in air compared to the control. However, only the primary amine, aniline, led to a lower V_T than the control. Devices that had been exposed to methyl- or dimethylaniline displayed greater V_T compared to the control. Increasing V_T was observed with increasing methylation of the aniline. Similarly, the tertiary amine triethylamine also resulted in a V_T nearly triple that of the control (**Figure 3.4**). This reduced performance by tertiary amines may explain why the performance of aminosilanes decreased with increasing nitrogen content, as all amines present in the molecules were tertiary amines. Pyridine displayed the greatest overall μ_e retention in air and also displayed a V_T comparable to the control. Pyridine and aniline both have lower pK_a and ionization potential than alkyl amines[14]. The lower ionization potential may enable the pyridine and aniline to more readily contribute an n-type doping effect, but the trend is not consistent throughout all the additives suggesting there are likely multiple factors at play such as diffusion and molecular geometry. To confirm that the effects observed in this study were due to interactions between the additives and the semiconductor, rather

than an impact on the film morphology, GIWAXS scattering patterns were obtained (**Figure 3.7**). No differences in peak locations or evolution of new peaks were observed in the in-plane scattering (**Figure 3.8**), suggesting that additive exposure did not result in changes in the packing mode of the thin film.

The silane with no amine group, phenyltrimethoxysilane, was used to determine the impact of the presence of the silane group in the additives. The use of phenyltrimethoxysilane reduced the μ_e and increased the V_T in nitrogen, but did not impact the device performance in air compared to the control. Silanes are known to be p-type dopants,[11] which is consistent with the observed decrease in device performance under N_2 in this work. The effect appears reduced in air, indicating either that there are additional interactions between the phenyltrimethoxysilane, oxygen and moisture, or simply that the air exposure has a much more pronounced effect on the P(NDI2OD-T2) device performance compared to the addition of phenyltrimethoxysilane.

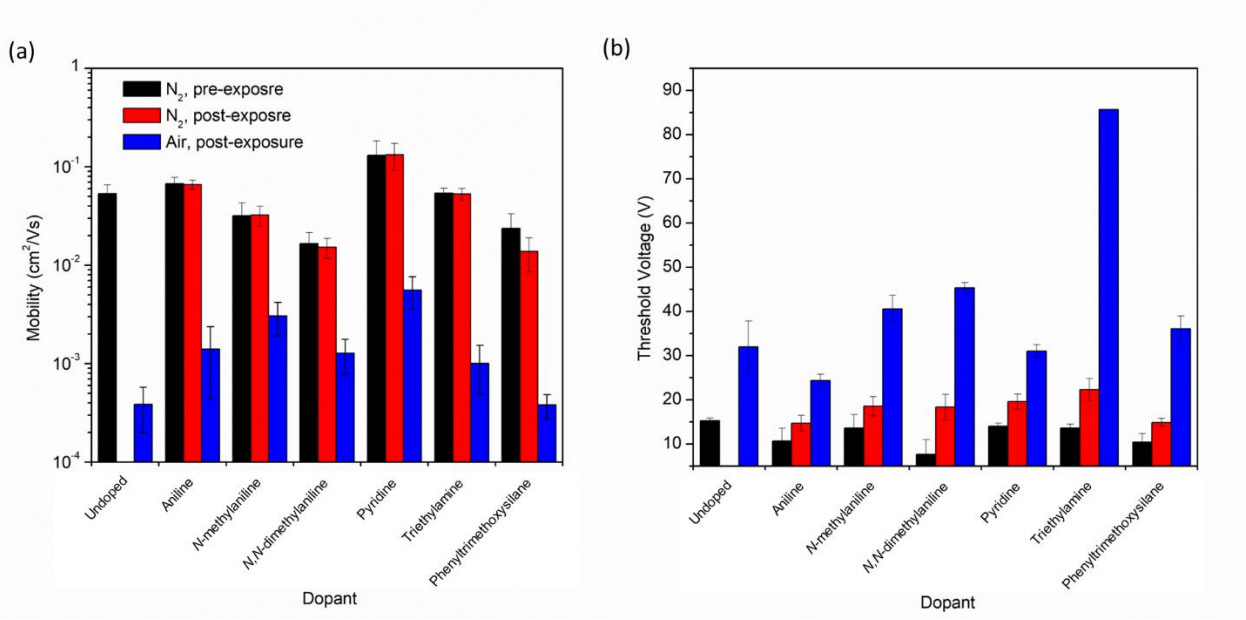

Figure 3.4. (a) electron mobility and (b) Threshold voltage of devices before and after vapour exposure to amine vapours under inert conditions, and subsequent changes in performance after exposure to air.

The transfer curves (**Figure 3.5**) of the conditions giving rise to the best performance and stability expand on the previous results from **Figure 3.4**. Aniline (**Figure 3.5b**) and pyridine (**Figure 3.5c**) both result in an increased V_T after exposure of the device to the vapour, with aniline exhibiting a smaller shift than pyridine. The on-current reached in nitrogen by the films exposed to vapour in both cases is largely unchanged, as a result of the low change in relative μ_e to the raw P(NDI2OD-T2) film. Both treated films exhibit an increased hysteresis, with aniline resulting in a hysteresis of approximately 5 V and pyridine resulting in hysteresis of about 1 V. In air, both treated films see less shift in V_T compared to an untreated sample (**Figure 3.5a**), which contributes to the lower on-current observed in the untreated sample compared to the treated samples. All films display similar hysteresis when exposed to air.

Subsequently, devices were tested after 1 week of exposure to ambient air (**Figure 3.9**). Out of 40 devices for each condition, none exhibited functionality after a week of exposure to air, indicating the volatile additives have likely evaporated from the film as expected. This further highlights the importance of developing non-volatile additives for enhancement of device stability. While these devices were not stable after an extended timeframe, these results identify pyridine and aniline as ideal candidates for ideal moieties to include in the design of a non-volatile additive such as a macromolecule.

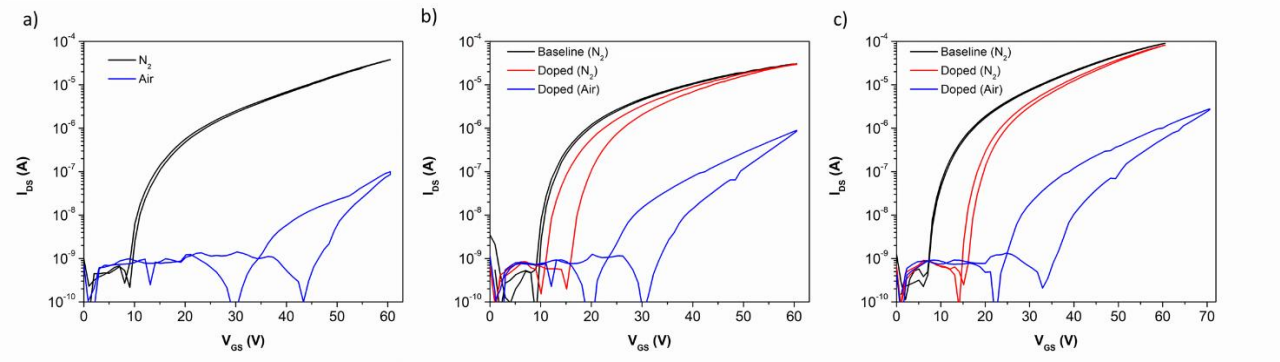

Figure 3.5. Transfer curves of (a) undoped P(NDI2OD-T2) as a baseline, (b) aniline-doped P(NDI2OD-T2), and (c) pyridine-doped P(NDI2OD-T2) in an N_2 glovebox (black, red) and air (blue). V_{DS} = 50 V.

Finally, to further understand the impact of aniline and pyridine on stability of P(NDI2OD-T2) through changes the material's reduction and oxidation behaviour, cyclic voltammetry was performed. The voltammogram is presented in **Figure 3.6**, where neat P(NDI2OD-T2) is used as the baseline. Films treated with aniline and pyridine exhibit clear differences in redox activity compared to the baseline. When exposed to aniline, an increase of peak separation (ΔE_p) for both redox couples was observed. $\Delta E_{p,1}$ and $\Delta E_{p,2}$ for the baseline were both 0.23 V, while they increased to 0.44 V and 0.38 V respectively when exposed to aniline. This increased ΔE_p indicates slower transfer of electrons, which may be due to stabilization caused by the presence of aniline. A negative shift of the half-wave potential ($E_{1/2}$) for redox couple 1 and a positive shift in $E_{1/2}$ for redox couple 2. $E_{1/2,1}$ shifted from -1.30 V at the baseline to -1.33 V when exposed to aniline, while $E_{1/2,2}$ shifted from -0.97 V to -0.92 V. This shift in $E_{1/2}$ may indicate a difference in redox reactions with oxygen and water present in air, therefore impacting the stability of the devices. When the films were exposed to pyridine, a loss of all redox couples was observed. This may indicate that the pyridine is preventing the transfer of electrons from the films to their environment. Thus, the observed increase in stability of the OTFTs may be due to this change in redox behaviour.

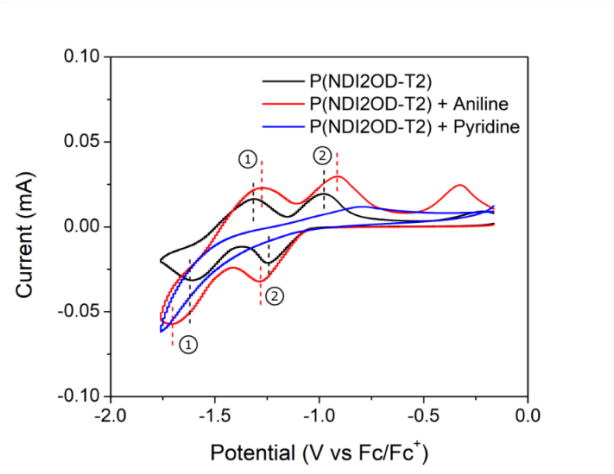

Figure 3.6. Cyclic voltammogram of neat P(NDI2OD-T2) (black line), and films that have been treated with aniline (red line) or pyridine (blue line). Redox couples (1) and (2) are indicated on the voltammogram for clarity.

3.4 Conclusion

Small molecule nitrogen-containing additives such as aniline and pyridine enhanced the stability of P(NDI2OD-T2)-based OTFT devices without degradation of device performance under inert conditions. It appears that increasing the substitution of the amine typically resulted in worse device performance by increasing the V_T. However, the use of aromatic nitrogen, such as pyridine, led to a less significant difference compared to the primary amines such as aniline. While previous studies indicated some aminosilane additives could enhance the performance of n-type devices, it was found that of the subset of materials used here, only marginal increases in μ_e were observed. While this increased μ_e was retained somewhat in air, increasing the nitrogen content of the silane resulted in the performance in air reverting to behaviour similar to the baseline. The most promising additives from the present study were aniline and pyridine, and these functionalities can be used in the design of further stability enhancing additives.

3.5 Experimental

Device Fabrication

Devices were prepared with batches of 20 transistors on a single substrate, and substrates prepared in duplicate for a total of 40 individual transistors for each condition. 15 mm x 20 mm Si substrates with thermally grown SiO_2 dielectric (220 µm thick) were cleaned sequentially in soapy water, water, acetone, then methanol by sonicating in each solvent for 5 minutes. The substrates were then treated in a Harrick PDC-32G Plasma Cleaner for 10 minutes. After plasma cleaning, substrates were rinsed with water and then isopropyl alcohol, dried by blowing N_2 over the substrate, then placed in a solution of 1% (v/v) octyltrichlorosilane (OTS) in toluene for 24 hours. After OTS treatment, the substrates were dried in a vacuum oven at 70 °C for 1 hour. Solutions of P(NDI2OD-T2) were prepared by heating and stirring a 10 mg/mL solution in 1,2-dichlorobenzene on a 50 °C hotplate for 20 minutes, then filtering through a 20 µm PTFE filter. These solutions were spin-coated onto the substrates at 4000 rpm for 60 seconds. Films were annealed at 150 °C for 1 hour in a vacuum oven. Gold contact electrodes with chromium interlayers were deposited by physical vapour deposition with a shadow mask for patterning. 10 nm of chromium was deposited at a rate of 0.5 Å/s, then 50 nm of gold was deposited at a rate of 1 Å/s. The dimensions of the channel were L = 30 µm and W = 1000 µm.

Vapour Exposure Procedure

Following fabrication, devices were characterized under inert conditions in a N_2 glovebox prior to vapour exposure. Inside the glovebox, an open 1 dram vial was placed inside a 20 mL scintillation vial. 20 μL of the desired solvent was pipetted into the 1 dram vial, then the device to be exposed was also placed inside the scintillation vial. The scintillation vial was capped tightly, and the devices were exposed to the vapours of the solvent for 30 minutes. The devices were then re-characterized under inert conditions before moving the samples into air to be subsequently characterized.

Transistor Characterization

Transistors were characterized with source-drain voltage (V_{DS}) of 50 V, while the gate-source voltage (V_{GS}) was varied from 0 to 60 V and the current measured using a Keithley 2614B source meter. Transistors were characterized in a nitrogen glovebox before and after exposure to the additives. Finally, the transistors were removed from the glovebox and tested again under ambient conditions, where RH was < 10% for all experiments. Saturation region characteristics were extracted as previously reported.[13]

Cyclic Voltammetry

Slides of approximately 1 cm x 1.5 cm were cut from ITO-coated glass, then coated with P(NDI2OD-T2) following the spin-coating conditions indicated in the *Device Fabrication* section. These films were annealed at 150 °C under vacuum for 1 hour. Films exposed to aniline and pyridine were immersed into each solvent for 10 seconds then allowed to dry under ambient conditions for 10 minutes. Voltammograms were obtained using 0.1 M tetrabutylammonium perchlorate dissolved in acetonitrile as the electrolyte. Platinum wires were used for the counter and reference electrode, while the P(NDI2OD-T2)-coated ITO was used as the working electrode. A ferrocene standard reference was also measured, with the same solvent and electrolyte system, and a platinum wire for the working electrode. All voltammograms were normalized to the ferrocene standard.

3.6 Acknowledgements

We thank Natural Sciences and Engineering Research Council of Canada (NSERC, RGPIN-2015-509 03987 to B.H.L) and NSERC CGS-D (S.B). The research was undertaken, in part, thanks to funding from the Canada Research Chair program (B.H.L.).

3.7 References

(1) Po, R.; Bianchi, G.; Carbonera, C.; Pellegrino, A. "All That Glisters Is Not Gold": An Analysis of the Synthetic Complexity of Efficient Polymer Donors for Polymer Solar Cells. *Macromolecules* 2015, *48*, 453–461.

(2) Moser, M.; Wadsworth, A.; Gasparini, N.; McCulloch, I.; Moser, M.; Wadsworth, A.; McCulloch, I.; Gasparini, N. Challenges to the Success of Commercial Organic Photovoltaic Products. *Adv. Energy Mater.* 2021, *11*, 2100056.

(3) Lüssem, B.; Keum, C.-M.; Kasemann, D.; Naab, B.; Bao, Z.; Leo, K. Doped Organic Transistors. *Chem. Rev.* 2016, *116*, 13714–13751.

(4) Salzmann, I.; Heimel, G.; Oehzelt, M.; Winkler, S.; Koch, N. Molecular Electrical Doping of Organic Semiconductors: Fundamental Mechanisms and Emerging Dopant Design Rules. *Acc. Chem. Res.* 2016, *49*, 370–378.

(5) Zhang, F.; Dai, X.; Zhu, W.; Chung, H.; Diao, Y. Large Modulation of Charge Carrier Mobility in Doped Nanoporous Organic Transistors. *Adv. Mater.* 2017, *29*, 1700411.

(6) Chou, W. Y.; Cheng, H. L. An Orientation-Controlled Pentacene Film Aligned by Photoaligned Polyimide for Organic Thin-Film Transistor Applications. *Adv. Funct. Mater.* 2004, *14*, 811–815.

(7) He, Y.; Quinn, J. T. E.; Lee, S.; Wang, G. Y.; Li, X.; Wang, J.; Li, Y. An Aromatic Amine-Containing Polymer as an Additive to Ambipolar Polymer Semiconductor Realizing Unipolar n-Type Charge Transport. *Org. Electron.* 2017, *49*, 406–414.

(8) Nikolka, M.; Nasrallah, I.; Rose, B.; Ravva, M. K.; Broch, K.; Sadhanala, A.; Harkin, D.; Charmet, J.; Hurhangee, M.; Brown, A.; et al. High Operational and Environmental Stability of High-Mobility Conjugated Polymer Field-Effect Transistors through the Use of Molecular Additives. *Nat. Mater.* 2017, *16*, 356–362.

(9) Shin, N.; Zessin, J.; Lee, M. H.; Hambsch, M.; Mannsfeld, S. C. B. Enhancement of N-Type Organic Field-Effect Transistor Performances through Surface Doping with Aminosilanes. *Adv. Funct. Mater.* 2018, *28*, 1802265.

(10) Sun, B.; Hong, W.; Thibau, E. S.; Aziz, H.; Lu, Z.-H.; Li, Y. Polyethylenimine (PEI) As an

Effective Dopant To Conveniently Convert Ambipolar and p-Type Polymers into Unipolar n-Type Polymers. *ACS Appl. Mater. Interfaces* 2015, *7*, 18662–18671.

(11) Calhoun, M. F.; Sanchez, J.; Olaya, D.; Gershenson, M. E.; Podzorov, V. Electronic Functionalization of the Surface of Organic Semiconductors with Self-Assembled Monolayers. *Nat. Mater.* 2008, *7*, 84–89.

(12) Dallaire, N. J.; Brixi, S.; Claus, M.; Blawid, S.; Lessard, B. H. Benchmarking Contact Quality in N-Type Organic Thin Film Transistors through an Improved Virtual-Source Emission-Diffusion Model. *Appl. Phys. Rev.* 2022, *9*, 011418.

(13) Brixi, S.; Melville, O. A.; Mirka, B.; He, Y.; Hendsbee, A. D.; Meng, H.; Li, Y.; Lessard, B. H. Air and Temperature Sensitivity of N-Type Polymer Materials to Meet and Exceed the Standard of N2200. *Sci. Rep.* 2020, *10*, 4014.

(14) Jakubiak, J.; Allonas, X.; Fouassier, J. P.; Sionkowska, A.; Andrzejewska, E.; Linden, L. Å.; Rabek, J. F. Camphorquinone–Amines Photoinitating Systems for the Initiation of Free Radical Polymerization. *Polymer.* 2003, *44*, 5219–5226.

3.8 Supplementary Figures

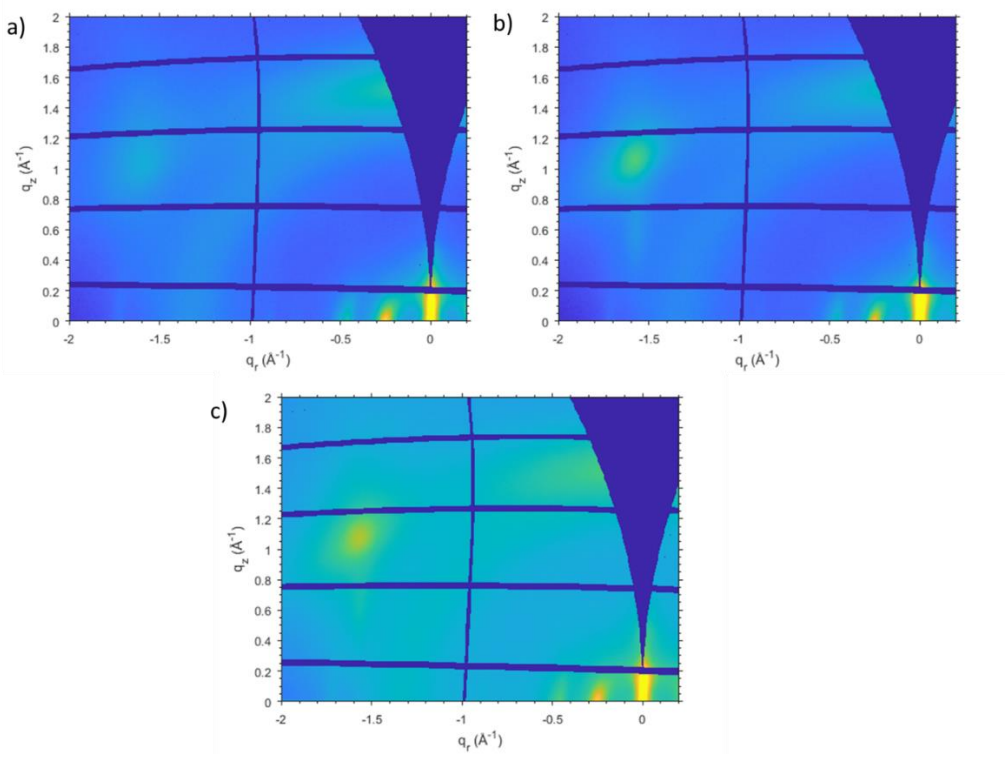

Figure 3.7. GIWAXS scattering patterns of P(NDI2OD-T2). (a) Baseline, (b) Aniline-exposed, (c) Pyridine-exposed

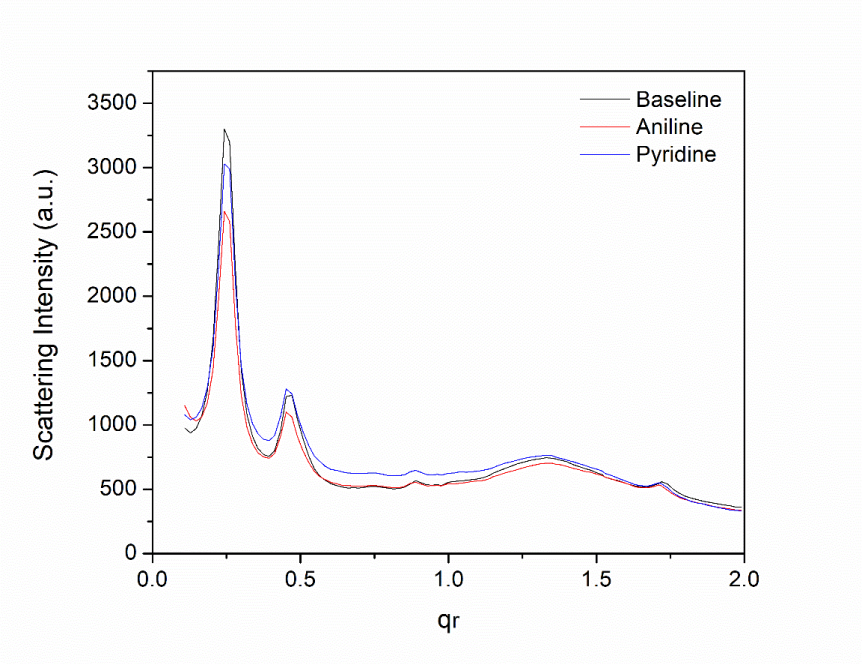

Figure 3.8. Linecuts of GIWAXS in-plane scattering between $0.01 \leq q_z \leq 0.2$.

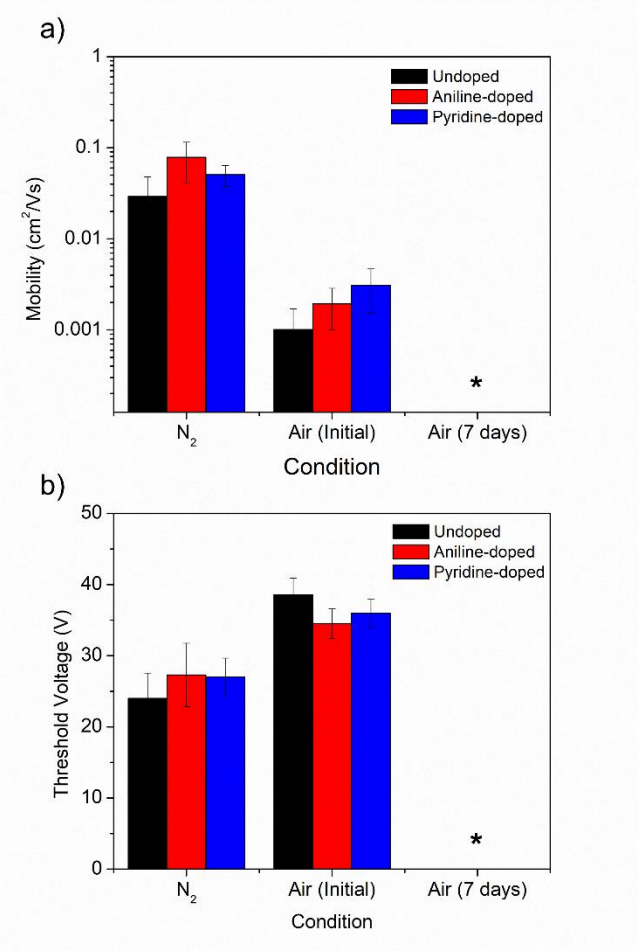

Figure 3.9. Stability of P(NDI2OD-T2) devices over one week. a) Device electron mobility. b) Device threshold voltage.

4. Poly(2-vinylpyridine) as an additive for enhancing n-type organic thin-film transistor stability

Context and Significance of Work

In the previous chapter I determined the ideal candidate moieties for stabilizing n-type transistor; pyridine was identified as one of the most promising additives. Therefore, in this chapter we set out to employ a pyridine functional polymer as an additive. Incorporating the pyridine moiety into a polymer, in this case poly(2-vinylpyridine) (P2VP), would enable us to overcome the major limitation of the previous study: volatile solvents cannot provide longer-term stabilization to the OTFTs. The fact that the polymeric P2VP additive displayed similar stability enhancements to those of the original solvent pyridine additive, and also displayed a longer-term stability (because P2VP is not volatile), gives credibility to using this methodology for studying additives in OTFTs in the future.

Contributions of Authors

I designed the study, completed all device work and the cyclic voltammetry, performed all device and GIWAXS data analysis, and wrote the manuscript. The P2VP synthesis and GIWAXS acquisitions were performed by Benjamin King, who wrote the corresponding experimental sections. Halynne Lamontagne and Chloé Dindault performed the STXM with the help of Sufal Swaraj the beamline scientist, and they provided the data analysis and written experimental. All co-authors contributed to the editing of the manuscript.

This work is published in Advanced Electronic Materials: Brixi, S.; Dindault, C.; King, B.; Lamontagne, H. R.; Shuhendler, A. J.; Swaraj, S.; Lessard, B. H. Poly(2-vinylpyridine) as an Additive for Enhancing N-Type Organic Thin-Film Transistor Stability doi:10.1002/aelm.202300660

4.1 Abstract

N-type organic semiconductors are particularly susceptible to degradation by ambient air. One such solution to this issue is to include additives in the inks these semiconductors would be cast from that would enhance device stability after film deposition. This method would reduce the number of processing steps needed to fabricate devices compared to other stabilization methods, such as encapsulation. In this study, we report the stabilization of n-type performance of the semiconductor poly{[N,N'-bis(2-octyldodecyl)-naphthalene-1,4,5,8-bis(dicarboximide)-2,6-diyl]-alt-5,5'-(2,29-bisthiophene)} (P(NDI2OD-T2)) when it is blended with an increasing proportion by weight of poly(2-vinylpyridine) (P2VP). The simple synthesis of P2VP also makes it an ideal candidate material for large-scale applications. Concentrations as low as 0.1% P2VP incorporated into the P(NDI2OD-T2) blends provided an immediate stabilization effect, and at 10% and 50%, longer-term stability after one week was observed.

4.2 Introduction

Organic thin-film transistors (OTFTs) are electrical switches incorporating organic semiconductors with applications in wearable technology, flexible electronics, and medical devices.[1–3] While this technology is promising, widespread adoption requires further improvements on the stability and performance of these devices.[4,5] Electron-transporting materials (n-type) are particularly susceptible to unstable performance due to their typically lower-lying LUMO (lowest unoccupied molecular orbital) level where electron transport occurs being close to the redox potentials of oxygen and water, present in ambient air.[6] While developing higher-performing and more stable n-type materials has been the focus of significant research in recent years,[7–9] materials that are currently commercially available and viable for production at scale are still in need of improvement for device applications. While the design and scale-up of new materials is an important pursuit, fabricating air-stable devices with existing materials through simple doping/blending can accelerate commercialization of OTFT based applications.

Device encapsulation can enable air stable device operation[10,11], but can be challenging due to the choice of solvent for effective orthogonal processing. As the field moves towards designing semiconductors with solubility in more environmentally-neutral solvents, fewer choices become available to enable orthogonal processing without dissolving or damaging the semiconductor during deposition of an encapsulant. Additionally, encapsulation is not perfect, and air or moisture diffusion can occur through the encapsulation layer over time. Therefore, it is essential to develop new strategies for improved air stability either to replace or to complement encapsulation.

Dopants and additives have been studied for enhancing both stability and performance of OTFTs.[12,13] DMBI (4-(1,3-dimethyl-2,3-dihydro-1H-benzoimidazol-2-yl)phenyl)dimethyl-amine), a popular n-type additive, does not hinder device stability while enhancing performance.[14,15] However, its synthesis is complex which can lead to increased costs. Recently, aromatic amines have shown to lend improvements to both stability and performance of n-type OTFTs.[16] We demonstrated that the addition of amine solvents such as pyridine can lead to enhanced stability of n-type OTFTs.[17] However, this improved stability was determined to be short lived, likely due to the volatility of the solvent escaping the semiconductor layer over time. Therefore, in this study we aim to maximize the stability through the use of non-volatile pyridine functional polymers. Poly(2-vinylpyridine) (P2VP) is an ideal candidate as a non-volatile pyridine-

based additive as it contains only the pyridine functional group attached to the polymer backbone, to ensure minimize any impact on performance caused by other functional groups, and to avoid bulky side chains that may interrupt packing of the semiconductor. We synthesized P2VP and blended it with n-type polymer poly{[N,N'-bis(2-octyldodecyl)-naphthalene-1,4,5,8-bis(dicarboximide)-2,6-diyl]-alt-5,5'-(2,29-bisthiophene)} (P(NDI2OD-T2)) in various ratios. We found that the air stability of the OTFTs could be improved without P2VP disrupting the stacking of the P(NDI2OD-T2) chains resulting in minimal drop in device performance.

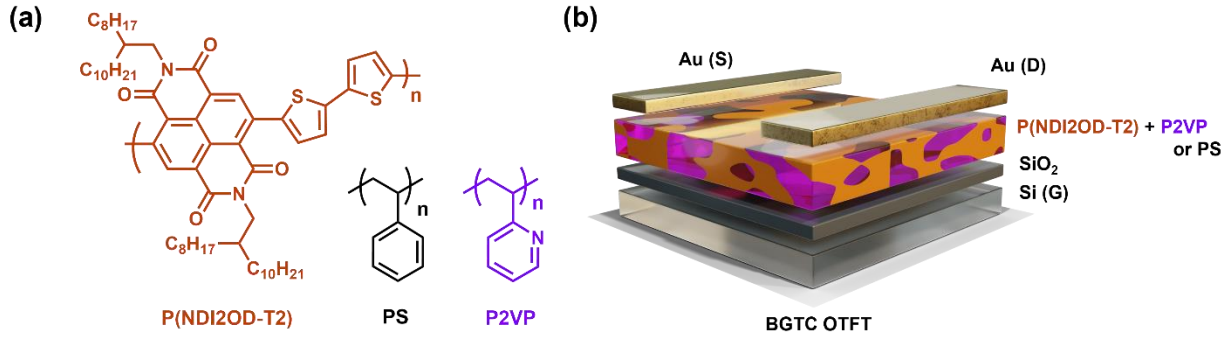

Figure 4.1. (a) Structure of P(NDI2OD-T2), poly(styrene) (PS) and poly(2-viniylpyridine) (P2VP) and (b) Bottom gate top contact (BGTC) organic thin film transistor (OTFT) configuration. Different ratios of P2VP and PS are blended with P(NDI2OD-T2) as the active semiconductor layer.

4.3 Discussion

Bottom gate top contact (BGTC) OTFTs were fabricated using films of P(NDI2OD-T2) blended with varying ratios of poly(2-vinylpyridine) (P2VP) on silicon wafers with SiO_2 as the gate dielectric (**Figure 4.1**). Blends of 0.1, 1, 5, 10, and 50 wt% of P2VP in P(NDI2OD-T2) were compared to a baseline of pure P(NDI2OD-T2). The devices were fabricated and annealed in glovebox prior to electrical characterization. These OTFTs were first characterized in an inert environment, then in air after 30 minutes of air exposure. The devices were then left in air for 7 days and characterized again to assess the effect of P2VP on the device stability. **Figure 4.2** reports the electron mobility (μ_e) and threshold voltage (V_T) for the corresponding OTFTs, and the characteristic transfer curves can be found in the supporting information (**Figure 4.8**). As shown in **Figure 4.2**, when the lowest concentration studied, 0.1 wt% P2VP, is added to P(NDI2OD-T2), an initial drop in μ_e was observed compared to pure P(NDI2OD-T2) when characterized under

inert atmosphere. Increasing the amount of P2VP resulted in further drop in μ_e in an inert environment, but the V_T also decreased with increase in P2VP loading, dropping to approximately 0 V with the addition of ≥ 5 wt% P2VP was included in the blends. The drop in mobility is likely due to incorporation of a non-conducting element in the semiconductor layer, while the drop in V_T could be a result of a doping effect from the P2VP.[13,18,19] When characterizing in air, the presence of as little as 0.1 wt% of P2VP resulted in a greater μ_e and reduced V_T in air compared to the baseline devices characterized in inert atmosphere. OTFT devices with 10 wt% and 50 wt% P2VP were the only conditions which displayed any electrical performance in air after 7 days, suggesting the addition of P2VP improved the device stability.

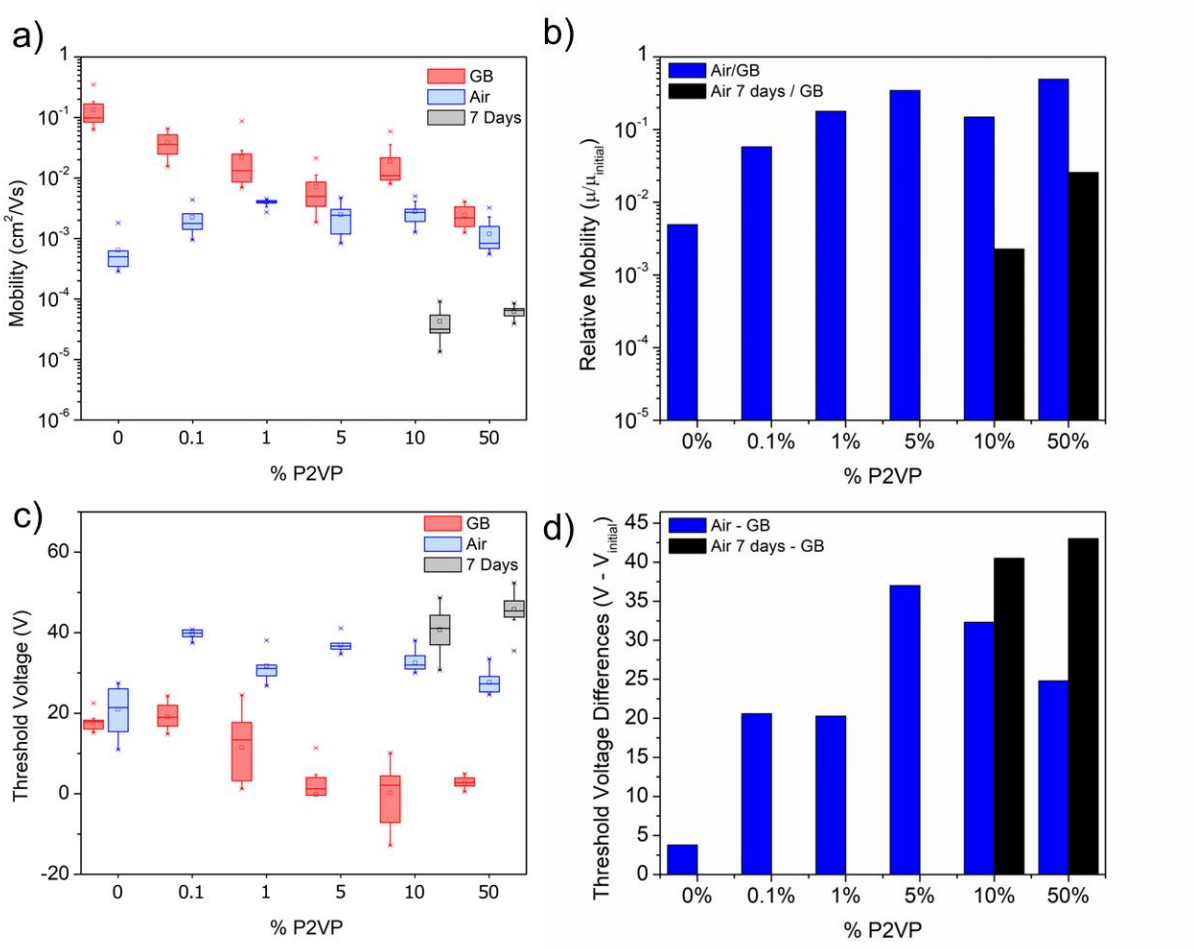

Figure 4.2. Effect of blending P2VP with P(NDI2OD-T2) on (a) mobility of the devices in a glovebox, (b) relative retention of mobility of air-exposed devices compared to performance in the glovebox, (c) threshold voltage of the devices in a glovebox, (d) relative change of threshold voltage of air-exposed devices compared to performance in the glovebox. Statistical analysis in the box plots is derived from 35-40 individual OTFTs.

To correlate the device performance with the morphology of films of blended P(NDI2OD-T2) and P2VP, we characterized the films by scanning transmission X-ray microscopy (STXM) and grazing-incidence wide-angle X-ray scattering (GIWAXS). STXM is a synchrotron-based X-ray transmission microscopy technique which can provide high detail compositional maps, including differentiation between atoms of small atomic cross-section like nitrogen and carbon.[20–22] Unlike AFM, this technique provides domain composition through the entire film, not just surface, providing a more representative understanding of the blend. STXM maps (**Figure 4.3**) of our

blends show the distribution of P(NDI2OD-T2) and P2VP, with black pixels indicating pure P(NDI2OD-T2) domains, white pixels indicating pure P2VP domains and gray pixels representing a blend. While P2VP and P(NDI2OD-T2) are well dispersed throughout the whole volume of each film, some degree of phase separation occurred between P(NDI2OD-T2) and P2VP, as evidenced by the variation in composition through the film. Hildebrand solubility parameters for all three polymers are relatively close in value, being 18.7 $MPa^{1/2}$, 21.3 $MPa^{1/2}$, 20.5 $MPa^{1/2}$ for PS[23], P2VP[24], and P(NDI2OD-T2)[25] respectively. This suggests that the polymers should all have some miscibility, leading to the observed mixing of the polymer phases.[26]

With the addition of 0.1% P2VP (**Figure 4.3a**), the majority of the film is pure P(NDI2OD-T2). Films with 10% P2VP (**Figure 4.3b**) showed a greater degree of phase separation, with some regions having 80% P(NDI2OD-T) (20% P2VP), further suggesting the P2VP had become more concentrated in those regions. Both films with addition of 0.1 wt% and 10 wt% P2VP were characterized by having pure P(NDI2OD-T2) domains intermixed with blended domains of P2VP and P(NDI2OD-T2). However, for the sample of 50 wt% P2VP (**Figure 4.3c**) there were no pure P(NDI2OD-T2) domains, as the P2VP permeated the entire film. With 50 wt% P2VP, some regions showed as little as 28% P(NDI2OD-T2), with regions having a maximum of 89% P(NDI2OD-T2), again indicating significant phase separation from P2VP. An additional version of this figure with an adjusted scale is included for enhance visual fidelity in the Supplementary Information (**Figure 4.9**). Increasing P2VP concentration in the blends also increased the observed sizes of P2VP-rich domains. These results indicate that at low P2VP content, there are still pure P(NDI2OD-T2) domains which participate in the charge transport similar to a pure P(NDI2OD-T2) film, which is why only a small drop in μ_e was observed (**Figure 4.2**). As the P2VP content is increased to 50 wt% there are no pure P(NDI2OD-T2) domains that span the entire film thickness, and therefore the charge transport through the film is significantly affected, as evident by the drop in μ_e compared to the pure P(NDI2OD-T2) film in inert atmosphere (**Figure 4.2**). Among all the samples, no regions of pure P2VP were observed, suggesting P2VP is partially miscible in the P(NDI2OD-T2) domains which is likely favourable for increasing the interactions between the two polymers and favourable for increased device stability.

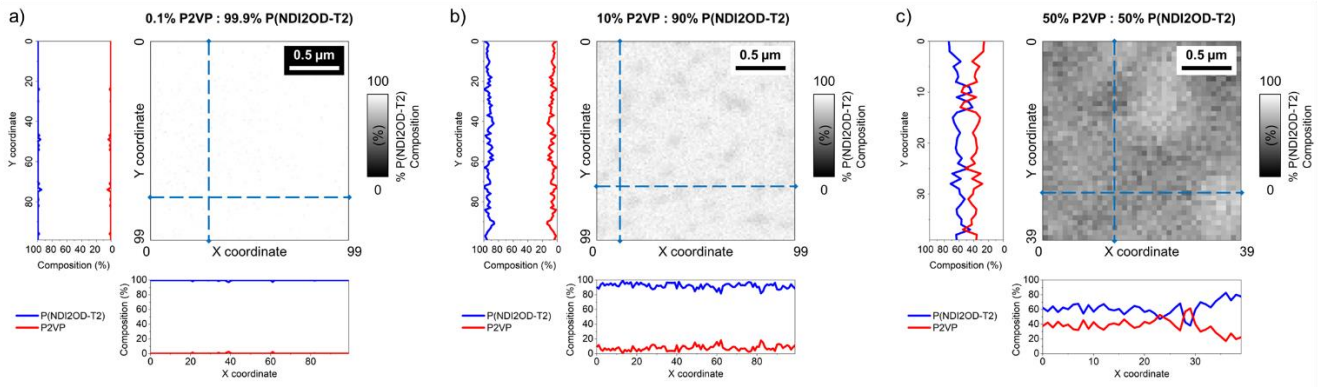

Figure 4.3. STXM composition maps of P(NDI2OD-T2) in blends with (a) 0.1 wt% P2VP, (b) 10 wt% P2VP, and (c) 50 wt% P2VP.

GIWAXS can provide information related to the crystalline regions of the film, which are directly related to the charge transport characteristics of the film. The results from the GIWAXS analysis are shown in **Figure 4.4**. At all P2VP loadings we observe the characteristic semi-crystalline P(NDI2OD-T2) peaks.[27] This indicates that even at 50 wt% P2VP, the regions of film with a high concentration of P(NDI2OD-T2) will likely still exhibit similar packing as the neat films. We do observe a drop in P(NDI2OD-T2) GIWAXS peak intensity with the addition of 50 wt% P2VP which suggests that while the P(NDI2OD-T2) packing is similar, there is less of it, which is consistent with a film that has half the P(NDI2OD-T2) content. Therefore, the addition of P2VP does not appear to interrupt the packing of P(NDI2OD-T2), suggesting charge transport is similar through the P(NDI2OD-T2) domains and that the drop in OTFT performance is likely due to the reduction in P(NDI2OD-T2) domain size (or quantities) with the addition of P2VP. Overall, STXM and GIWAXS results indicate that P2VP appears to confer better long-term stability to the device when it is more dispersed into the film and does not impact the packing of P(NDI2OD-T2) to achieve this.

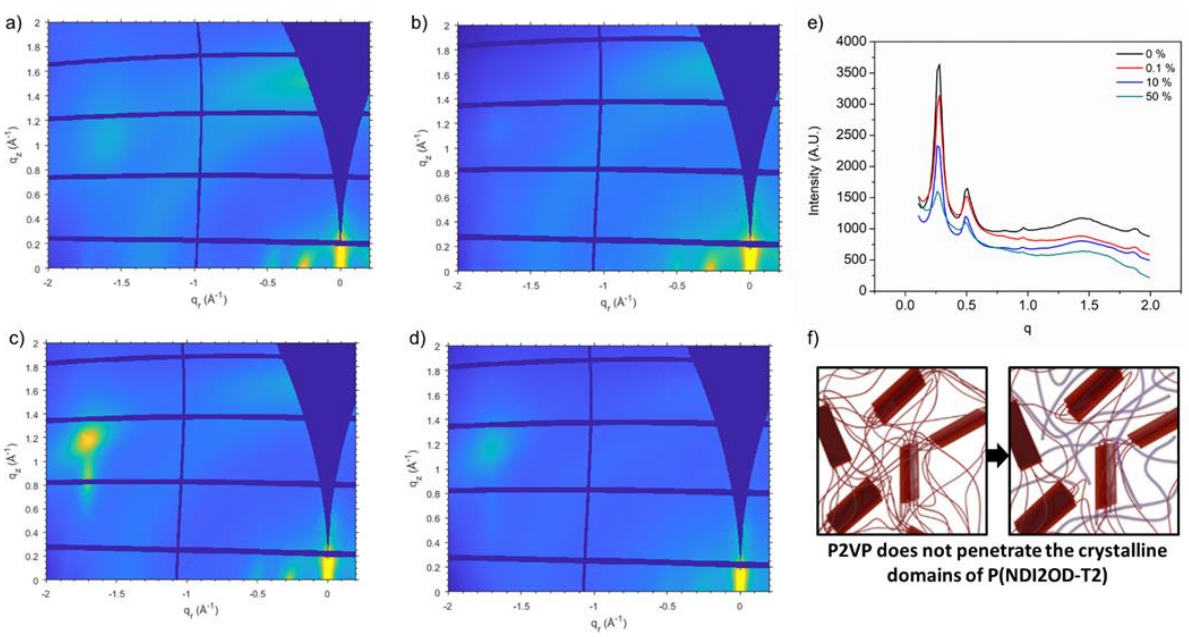

Figure 4.4. GIWAXS scattering patterns of P(NDI2OD-T2) blends (a) neat P(NDI2OD-T2), (b) 0.1 wt% P2VP, (c) 10 wt% P2VP, (d) 50 wt% P2VP, (e) linecuts of these patterns along q, and (f) rendered representation of polymer network, with red regions representing P(NDI2OD-T2) crystalline and amorphous regions, and purple regions representing P2VP.

Recently we reported the screening of different solvents additives and their effect on increasing the air stability of P(NDI2OD-T2) based OTFTs.[17] We found that pyridine was effective at increasing the n-type stability by increasing the resistance of the polymer to oxygen degradation. In this previous study we demonstrated that the improved stability was not a result of a change in morphology but rather a result of the presence of the appropriate pyridine functional group. In the present study, we wanted to confirm that the increased stability comes from the pyridine functional group and not change in morphology, aligning with the results of the previous study. Therefore, we fabricated a series of OTFT devices using blends of P(NDI2OD-T2) with poly(styrene) (PS), which were prepared and characterized under the same conditions. As PS has a similar structure to P2VP without the nitrogen atom present, this makes it possible to determine whether the amine is contributing to the observed stabilizing effect. **Figure 4.5** presents the results obtained with the P(NDI2OD-T2) / PS blends. The presence of PS does not have the same initial impact on performance as P2VP. Only a small initial decrease in μ_e was observed. In fact, the presence of 10 wt% and 50 wt% PS resulted in an increase in μ_e while the devices were in air. However, this does not confer a long-term stabilizing effect. After 7 days, none of the devices displayed functionality

in air regardless of PS content. The initial increase in μ_e with the addition of 10-50 wt% of PS is temporary. This indicates that the amine indeed has a stabilizing effect on these devices. This initial increase in performance in air observed from 10 wt% and 50 wt% PS blends may be due to an initial reduction of air and/or moisture diffusion into the devices due to the PS on the device surface. Similar to the addition of P2VP, the presence of PS was also found not to impact the packing of P(NDI2OD-T2) in the thin films by GIWAXS analysis (**Figure 4.10**). Furthermore, no significant change in V_T was observed for the OTFTs with PS blending suggesting the effects are not influencing the charge injection and contact resistance of the OTFTs, and do not interact with P(NDI2OD-T2) in the same way as P2VP which resulted in a decreased V_T.

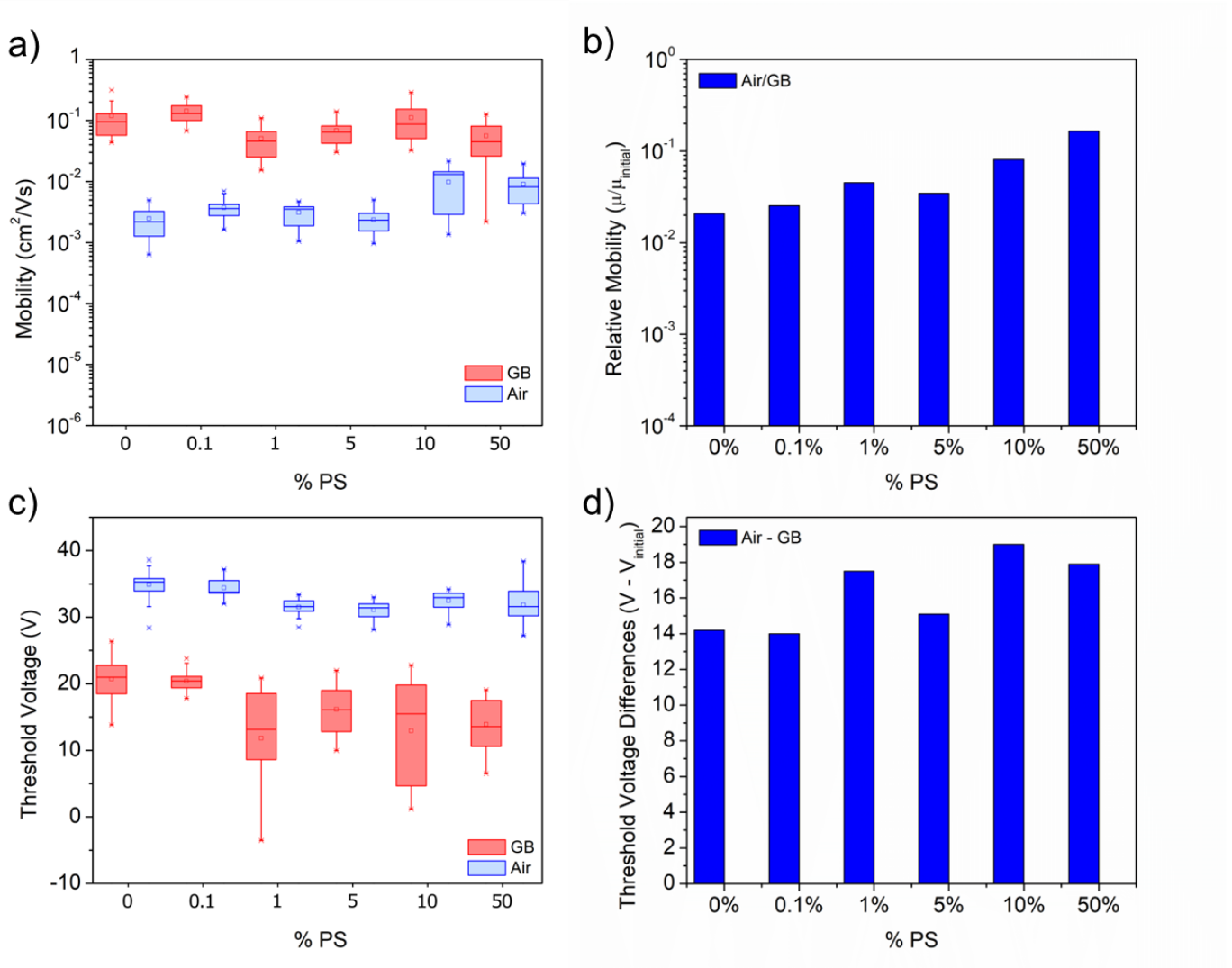

Figure 4.5. Effect of blending PS with P(NDI2OD-T2) on (a) mobility of the devices in a glovebox, (b) relative retention of mobility of air-exposed devices compared to performance in the glovebox, (c) threshold voltage of the devices in a glovebox, (d) relative change of threshold voltage of air-exposed devices compared to performance in the glovebox. Statistical analysis in the box plots is derived from 35-40 individual OTFTs.

While the high percentages of PS did provide some stabilizing effect on the short-term, the presence of P2VP provided greater stabilization of performance over time. Comparing the performance difference between devices characterized in the glovebox to the initial air exposure, the P(NDI2OD-T2) + 50wt% P2VP devices retained 49.5% of their μ_e while the P(NDI2OD-T2) + 50 wt% PS devices only retained 16.5% of their μ_e (**Figure 4.6**). Again, no device performance was observed when using PS after 7 days.

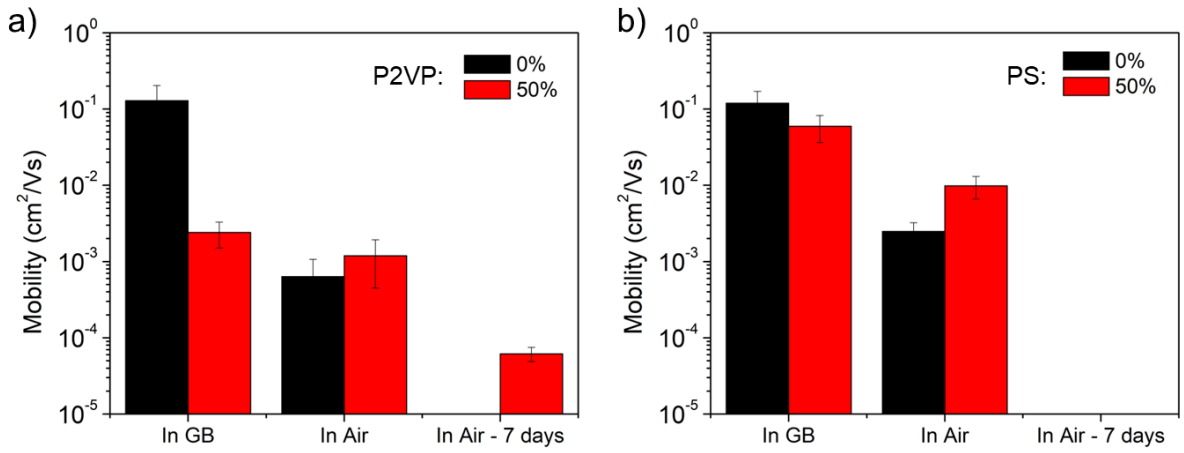

Figure 4.6. Comparison of device stabilization by (a) P2VP and (b) PS. Error bars represent the standard deviation of 35-40 individual OTFTs.

Comparing the results from P2VP in the present study to our previous results from the screening that identified pyridine as a potential stabilizing moiety (**Table 4.1**) shows that μ_e remains in the same order of magnitude, and V_T is comparable as well.

Table 4.1. Comparison of stabilization by pyridine vapour exposure[17] and P2VP blending.

	Pyridine[17]	P2VP (50%)
μ_e in air (cm^2/Vs)	5.6 x 10^{-3}	1.2 x 10^{-3}
μ_e retention (inert to air)	4.2 %	49.6 %
V_T in air (V)	31.0	27.6
V_T shift (inert to air) (V)	17.0 V	24.8 V
Performance after 7 days?	No	Yes

Cyclic voltammetry (CV) was performed on blended films of P(NDI2OD-T2) and P2VP (**Figure 4.7**). With the inclusion of P2VP, the oxidation peaks disappear when 0.1 wt% of P2VP is introduced into the film. As the percent of P2VP increases, the reduction peaks also disappear, until there are no visible redox events occurring. At 5 wt% P2VP and above, there are no visible redox peaks remaining. In addition to this, when the voltammograms are run for multiple cycles, increasing the amount of P2VP decreases peak spreading and shifting in the voltammograms in subsequent cycles (**Figure 4.11**). This decrease in the magnitude of changes observed in CV measurements may also indicate stabilization towards these redox reactions, as there is greater

reversibility. In our previous work,[17] it was found that exposing P(NDI2OD-T2) films to pyridine also resulted in a loss of visible redox peaks in this range. Therefore, these results are consistent with the previous observations with pyridine suggesting the P2VP is improving device stability through the reduction of P(NDI2OD-T2) oxygen oxidation.

Taken with the results from the STXM in **Figure 4.3**, it appears that the morphologies that enhance contact with P2VP and P(NDI2OD-T2) led to greater long-term stability. If P2VP is acting as a stabilizing element by preventing these redox events, it may need to be in contact with P(NDI2OD-T2) to provide longer term stability. Future studies that focus on enhancing the contact between P2VP and P(NDI2OD-T2) would be valuable to determine the extent of this effect, and to optimize the stabilization of the devices.

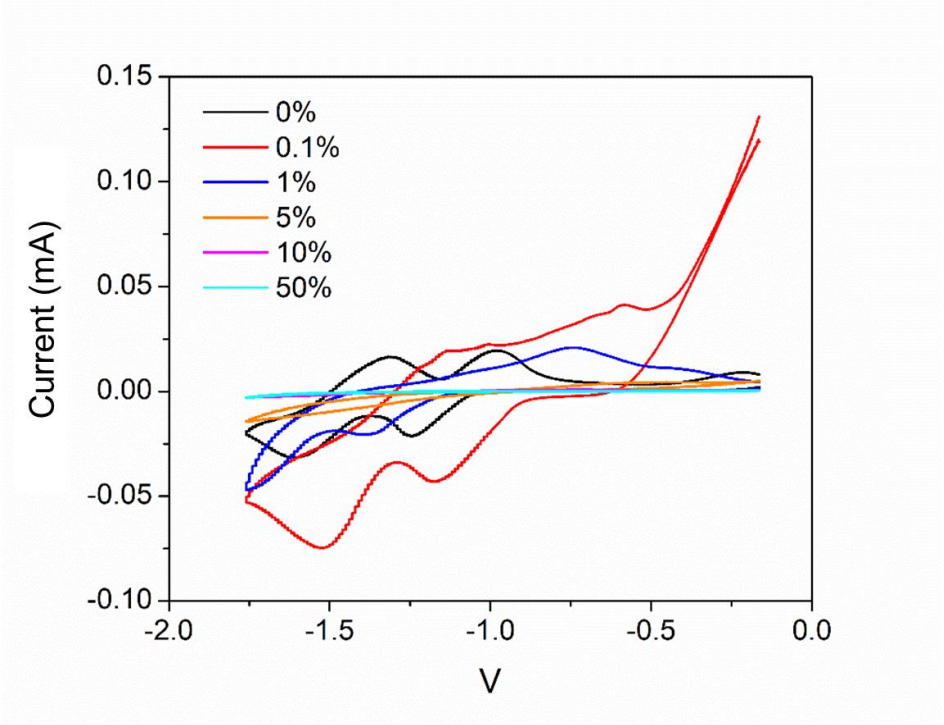

Figure 4.7. Cyclic voltammetry of P2VP / P(NDI2OD-T2) blends vs Fc/Fc^+ with 0.1 M tetrabutylammonium perchlorate dissolved in acetonitrile as the electrolyte.

4.4 Conclusion

Incorporating as little as 0.1% P2VP blended with P(NDI2OD-T2) provided stabilization when exposed to air. However, at least 10% P2VP was required for long-term stability over 7 days. In order to confirm the impact was due to the pyridine moiety of P2VP, devices were also fabricated with PS and these devices did not exhibit improved stability. Cyclic voltammetry indicates P2VP may prevent damaging redox reactions with air or water from occurring. The morphology of the blends may explain why long-term stability is observed in blends with higher ratios of P2VP. In these higher-ratio blends, there is sufficient P2VP present to have few to no regions with only P(NDI2OD-T2), thus ensuring contact with the stabilizing effects from P2VP.

4.5 Experimental

Polymer Synthesis

Poly(2-vinylpyridine) (P2VP, 97%, Sigma Aldrich) was synthesized by Nitroxide Mediated Polymerization (NMP) employing a process similar to literature procedures.[28] First, the initiator NHS-BlocBuilder (NHS-BB) was synthesized by coupling of BlocBuilder-MA (Arkema) and N-hydroxysuccinimide (Oakwood, 98%) following literature procedures.[29] The homopolymerization of 2VP was performed in a 50-mL three-neck round bottom glass flask fitted with a condenser and a magnetic stir bar. Two of the necks in the flask were sealed with rubber septa while the centre neck was connected to the condenser and was capped with a septum pierced with a needle to serve as a vent for the system. The NHS-BlocBuilder (0.030g, 0.065 mmol) was dissolved in 2VP monomer (3.2 g, $M_{n,\ Target}$ = 49.3 kg·mol^{-1}). The solution was then bubbled with nitrogen gas for 30 minutes at room temperature to remove oxygen and then heated to 120 °C using a heating mantle with a heat controller while maintaining the nitrogen purge. The start of the reaction was taken at the start of the reaction (t = 0 min). The solution was allowed to react for 60 minutes before the reaction was stopped by cooling the solution to room temperature. The polymer product was precipitated in hexanes, filtered using filter paper and allowed to dry under vacuum overnight. The purified polymer has number-average molecular weight (M_n = 25.000 kg·mol^{-1}) and dispersity (Đ) = 1.3. M_n and Đ were determined by size exclusion chromatography performed on a Malvern Omnisec equipped with Omnisec Resolve pump and autosampler (CHR7100) with two T6000M columns and Omnisec Reveal differential refractive index (CHR6000), diode-array-based UV-Vis

spectrometer, and Viscotek SEC-MALS 20 multi-angle light scattering detectors. THF (HPLC, Caledon Laboratory Chemicals) was used as the eluent at 30 °C with a flow rate of 1 $mL \cdot min^{-1}$.

Device Preparation

Substrate Preparation

Si/SiO_2 substrates (Ossila, SiO_2 thickness 300 nm) were cleaned by successive 5-minute sonication steps while submerged in water, acetone, and methanol. Substrates were dried with a flow of nitrogen, then plasma treated for 10 minutes. Immediately following sonication, substrates were rinsed with water, then isopropyl alcohol, then dried again with a nitrogen flow. The substrates were then immersed in a solution of 1% (v/v) octyltricholorosilane (TCI Chemicals, OTS) in toluene (Sigma Aldrich) and heated at 70°C for 16 hours. Following OTS treatment, the substrates were rinsed with toluene to remove excess solution, then dried in a vacuum oven for 1 hour at 70°C.

Semiconductor and Electrode Deposition

Solutions of P(NDIOD-T2) (1-Material) blended with P2VP or PS were prepared as follows. P(NDI2OD-T2) was dissolved in 1,2-dichlorobenzene (Sigma Aldrich) at 10 mg/mL by stirring on a hotplate at 50°C for 1 hour. P2VP (or PS) solutions were separately prepared at 10 mg/mL in 1,2-dichlorobenzene by the same method. These solutions were then mixed together to create the appropriate percentages of P2VP (or PS) by mass: 0% (no P2VP or PS), 0.1%, 1%, 5%, and 50%, such that the total concentration of all polymer in solution was 10 mg/mL. For example, the 50% sample contained a concentration of 5 mg/mL P2VP (or PS) and 5 mg/mL P(NDI2OD-T2). These solutions were cast by spin coating with 80 µL of solution at 2000 rpm. The films were annealed at 150°C for one hour under vacuum.

Electrodes were deposited by physical vapour deposition through shadow masks. 10 nm of chromium was deposited at a rate of 0.5 Å/s, then gold was deposited at a rate of 1 Å/s. Electrodes had the following dimensions: 30 µm channel length, 1000 µm channel width. 20 individual transistor devices were prepared per substrate, and two substrates were prepared per condition. Devices were stored in a dry glovebox for a maximum of 1 day prior to electrical characterization.

Electrical Characterization

Devices were characterized first in a dry nitrogen glovebox. A Keithley 2614B sourcemeter was used to vary the gate-source voltage (V_{gs}) from 0-60 V and the source-drain voltage (V_{ds}) from 0-60 V to generate output curves, and V_{gs} from 0-60 V while holding V_{ds} at 50 V to generate transfer curves. Devices were then removed from the glovebox and characterized after 30 minutes of air exposure, with the characterization apparatus also exposed to air. After 7 days leaving the devices in ambient conditions, the devices were characterized again in air.

Scanning Transmission X-ray Microscopy (STXM)

Substrate Preparation

Silicon nitride windows (SiN) with a 50 nm thickness on a Si frame were purchased from NORCADA. The SiN membranes were treated for 15 minutes with oxygen plasma to clean them. SiN membranes were spin-coated with films as previously described in Device Preparation.

Imaging and Analysis

STXM measurements were performed on the HERMES beamline at the SOLEIL synchrotron. A 25 nm Fresnel Zone Plate was used to focus the monochromatized X-ray beam on the sample, and transmitted X-rays were collected using a PMT. The microscope chamber was maintained under a vacuum of 10^{-4} mbar during all measurements. High resolution image stacks composed of 24 images (2 x 2 μm, 20 nm step size, 3 ms dwell time) at the carbon K-edge were obtained, in an energy range of [284.5-288] eV. The beam was maintained at linear horizontal polarization for all measurements.

The composition maps of P2VP:P(NDI2OD-T2) blends (Figure 3) were drawn from thickness values obtained from singular value decomposition (SVD) of energy stacks at the carbon K edge. Reference spectra were scaled down to an elemental thickness of 1 nm using simulated OD spectra (simulations parameters: P2VP monomer of chemical formula C_7H_7N with a density of 0.977 g/cm^3 and P(NDI2OD-T2) monomer of chemical formula $C_{62}H_{88}N_2O_4S_2$ with a density of 1 g/cm^3). These 1 nm experimental OD spectra of pure materials were used to fit the energy stacks of the different blends following the SVD linear regression (blend spectrum = a * 1 nm P2VP spectrum + b * 1 nm P(NDI2OD-T2) spectrum) to yield thickness maps of both components in

each blend (a and b in the above formula). The composition maps shown in Figures 4.3 and 4.1 are obtained from the thickness maps as follows: % of P(NDI2OD-T2) = thickness of P(NDI2OD-T2) / (thickness of P2VP + thickness of P(NDI2OD-T2)).

The beamline energy was calibrated on a polystyrene film, and data was processed using aXis2000 (available at http://unicorn.chemistry.mcmaster.ca/aXis2000.html).[30]

Grazing Incidence Wide-Angle X-Ray Scattering (GIWAXS)

GIWAXS measurements were performed at the SIRIUS beamline at the SOLEIL Synchrotron in Saint-Aubin, France.[31] The samples were placed in a chamber that was flushed with helium gas to reduce air scattering. The sample-to-detector distance was calculated to be 339 mm and the X-ray energy was 10 keV. The detector was placed at an angle of 8.9°. Grazing incidence patterns were taken at $\alpha = 0.1°$ with 10 images taken at an exposure time of 10 s each. The final spectra are the sum of 10 images. The GIWAXS data were calibrated against a silver behenate (AgBe) standard and analyzed using the GIXSGUI software package.[32]

4.6 References

(1) Rogers, J. A.; Bao, Z.; Baldwin, K.; Dodabalapur, A.; Crone, B.; Raju, V. R.; Kuck, V.; Katz, H.; Amundson, K.; Ewing, J.; et al. Paper-like Electronic Displays: Large-Area Rubber-Stamped Plastic Sheets of Electronics and Microencapsulated Electrophoretic Inks. *Proc. Natl. Acad. Sci.* 2001, *98*, 4835–4840.

(2) Klauk, H. Organic Thin-Film Transistors. *Chem. Soc. Rev.* 2010, *39*, 2643–2666.

(3) Katz, H. E.; Lovinger, A. J.; Johnson, J.; Kloc, C.; Siegrist, T.; Li, W.; Lin, Y. Y.; Dodabalapur, A. A Soluble and Air-Stable Organic Semiconductor with High Electron Mobility. *Nature* 2000, *404*, 478–481.

(4) Brabec, C.; Egelhaaf, H.-J.; Salvador, M. The Path to Ubiquitous Organic Electronics Hinges on Its Stability. *J. Mater. Res.* 2018, *33*, 1839–1840.

(5) Lamport, Z. A.; Haneef, H. F.; Anand, S.; Waldrip, M.; Jurchescu, O. D. Tutorial: Organic Field-Effect Transistors: Materials, Structure and Operation. *J. Appl. Phys.* 2018, *124*, 71101.

(6) Griggs, S.; Marks, A.; Bristow, H.; McCulloch, I. N-Type Organic Semiconducting Polymers: Stability Limitations, Design Considerations and Applications. *J. Mater. Chem. C* 2021, *9*, 8099–8128.

(7) Anthony, J. E.; Facchetti, A.; Heeney, M.; Marder, S. R.; Zhan, X. N-Type Organic Semiconductors in Organic Electronics. *Adv. Mater.* 2010, *22*, 3876–3892.

(8) Sui, Y.; Deng, Y.; Du, T.; Shi, Y.; Geng, Y. Design Strategies of N-Type Conjugated Polymers for Organic Thin-Film Transistors. *Mater. Chem. Front.* 2019, *3*, 1932–1951.

(9) Quinn, J. T. E.; Zhu, J.; Li, X.; Wang, J.; Li, Y. Recent Progress in the Development of N-Type Organic Semiconductors for Organic Field Effect Transistors. *J. Mater. Chem. C* 2017, *5*, 8654–8681.

(10) Arias, A. C.; Endicott, F.; Street, R. A. Surface-Induced Self-Encapsulation of Polymer Thin-Film Transistors. *Adv. Mater.* 2006, *18*, 2900–2904.

(11) Rapisarda, M.; Simeone, D.; Fortunato, G.; Valletta, A.; Mariucci, L. Pentacene Thin Film

Transistors with (Polytetrafluoroethylene) PTFE-like Encapsulation Layer. *Org. Electron.* 2011, *12*, 119–124.

(12) Bin, Z.; Liu, Z.; Qiu, Y.; Duan, L. Efficient N-Dopants and Their Roles in Organic Electronics. *Adv. Opt. Mater.* 2018, *6*, 1800536.

(13) Scaccabarozzi, A. D.; Basu, A.; Aniés, F.; Liu, J.; Zapata-Arteaga, O.; Warren, R.; Firdaus, Y.; Nugraha, M. I.; Lin, Y.; Campoy-Quiles, M.; et al. Doping Approaches for Organic Semiconductors. *Chem. Rev.* 2022, *122*, 4420–4492.

(14) Wei, P.; Oh, J. H.; Dong, G.; Bao, Z. Use of a 1 H -Benzoimidazole Derivative as an n -Type Dopant and to Enable Air-Stable Solution-Processed n -Channel Organic Thin-Film Transistors. *J. Am. Chem. Soc.* 2010, *132*, 8852–8853.

(15) Naab, B. D.; Zhang, S.; Vandewal, K.; Salleo, A.; Barlow, S.; Marder, S. R.; Bao, Z. Effective Solution- and Vacuum-Processed n-Doping by Dimers of Benzimidazoline Radicals. *Adv. Mater.* 2014, *26*, 4268–4272.

(16) He, Y.; Quinn, J. T. E.; Lee, S.; Wang, G. Y.; Li, X.; Wang, J.; Li, Y. An Aromatic Amine-Containing Polymer as an Additive to Ambipolar Polymer Semiconductor Realizing Unipolar n-Type Charge Transport. *Org. Electron.* 2017, *49*, 406–414.

(17) Brixi, S.; Lamontagne, H. R.; King, B.; Shuhendler, A. J.; Lessard, B. H. Exposure to Solvent Vapours for Enhanced N-Type OTFT Stability. *Mater. Adv.* 2023, ASAP.

(18) Lüssem, B.; Keum, C.-M.; Kasemann, D.; Naab, B.; Bao, Z.; Leo, K. Doped Organic Transistors. *Chem. Rev.* 2016, *116*, 13714–13751.

(19) Paterson, A. F.; Singh, S.; Fallon, K. J.; Hodsden, T.; Han, Y.; Schroeder, B. C.; Bronstein, H.; Heeney, M.; McCulloch, I.; Anthopoulos, T. D.; et al. Recent Progress in High-Mobility Organic Transistors: A Reality Check. *Adv. Mater.* 2018, *30*, 1801079.

(20) Grant, T. M.; Dindault, C.; Rice, N. A.; Swaraj, S.; Lessard, B. H. Synthetically Facile Organic Solar Cells with >4% Efficiency Using P3HT and a Silicon Phthalocyanine Non-Fullerene Acceptor. *Mater. Adv.* 2021, *2*, 2594–2599.

(21) Meier, R.; Schindler, M.; Müller-Buschbaum, P.; Watts, B. Residual Solvent Content in

Conducting Polymer-Blend Films Mapped with Scanning Transmission x-Ray Microscopy. *Phys. Rev. B - Condens. Matter Mater. Phys.* 2011, *84*, 174205.

(22) McNeill, C. R.; Greenham, N. C. Conjugated-Polymer Blends for Optoelectronics. *Adv. Mater.* 2009, *21*, 3840–3850.

(23) Hughes, L. J.; Britt, G. E. Compatibility Studies on Polyacrylate and Polymethacrylate Systems. *J. Appl. Polym. Sci.* 1961, *5*, 337–348.

(24) Shizuo, A.; Hiroatsu, M.; Yoshio, T.; Hiromu, M. Studies of Poly-2-Vinylpyridine. II. Solubilities in Various Solvents. *Bull. Chem. Soc. Jpn.* 1966, *39*, 434–439.

(25) Pavlopoulou, E.; Kim, C. S.; Lee, S. S.; Chen, Z.; Facchetti, A.; Toney, M. F.; Loo, Y. L. Tuning the Morphology of All-Polymer OPVS through Altering Polymer-Solvent Interactions. *Chem. Mater.* 2014, *26*, 5020–5027.

(26) Barton, A. F. M. Polymer Solutions. In *CRC Handbook of Solubility Parameters and Other Cohesion Parameters*; CRC Press: New York, 1991.

(27) Simatos, D.; Spalek, L. J.; Kraft, U.; Nikolka, M.; Jiao, X.; McNeill, C. R.; Venkateshvaran, D.; Sirringhaus, H. The Effect of the Dielectric End Groups on the Positive Bias Stress Stability of N2200 Organic Field Effect Transistors. *APL Mater.* 2021, *9*, 41113.

(28) Zhang, C.; Maric, M. PH- and Temperature-Sensitive Statistical Copolymers Poly[2-(Dimethylamino)Ethyl Methacrylate-Stat-2-Vinylpyridine] with Functional Succinimidyl-Ester Chain Ends Synthesized by Nitroxide-Mediated Polymerization. *J. Polym. Sci. Part A Polym. Chem.* 2012, *50*, 4341–4357.

(29) Vinas, J.; Chagneux, N.; Gigmes, D.; Trimaille, T.; Favier, A.; Bertin, D. SG1-Based Alkoxyamine Bearing a N-Succinimidyl Ester: A Versatile Tool for Advanced Polymer Synthesis. *Polymer.* 2008, *49*, 3639–3647.

(30) Hitchcock, A. P. Analysis of X-Ray Images and Spectra (AXis2000): A Toolkit for the Analysis of X-Ray Spectromicroscopy Data. *J. Electron Spectros. Relat. Phenomena* 2023, *266*, 147360.

(31) Fontaine, P.; Ciatto, G.; Aubert, N.; Goldmann, M. Soft Interfaces and Resonant Investigation on Undulator Source: A Surface X-Ray Scattering Beamline to Study Organic Molecular Films at the SOLEIL Synchrotron. *Sci. Adv. Mater.* 2014, *6*, 2312–2316.

(32) Jiang, Z. GIXSGUI: A MATLAB Toolbox for Grazing-Incidence X-Ray Scattering Data Visualization and Reduction, and Indexing of Buried Three-Dimensional Periodic Nanostructured Films. *J. Appl. Crystallogr.* 2015, *48*, 917–926.

4.7 Supplementary Information

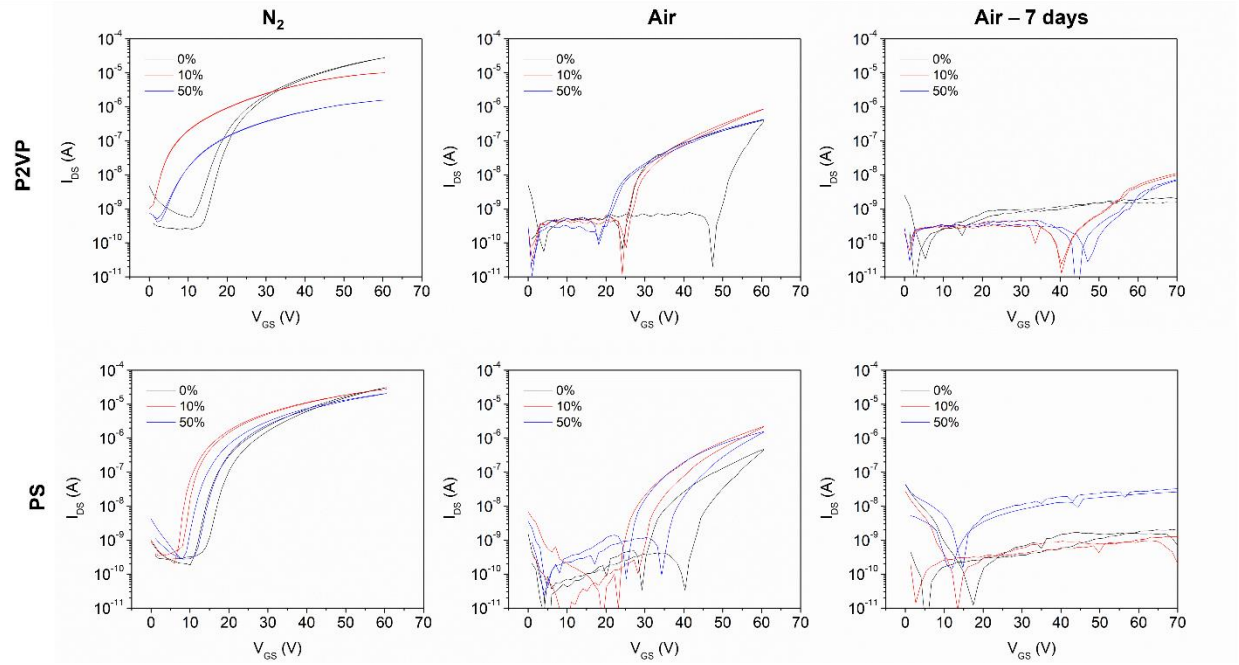

Figure 4.8. Example transfer curves.

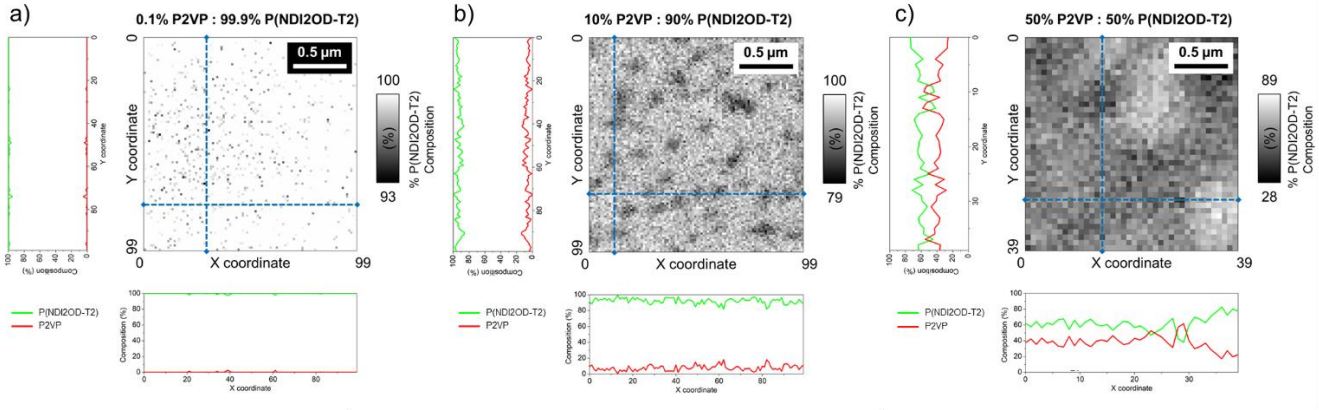

Figure 4.9. STXM maps as shown in Figure 3, with colour scales from maximum to minimum observed % P(NDI2OD-T2) for enhanced visual clarity.

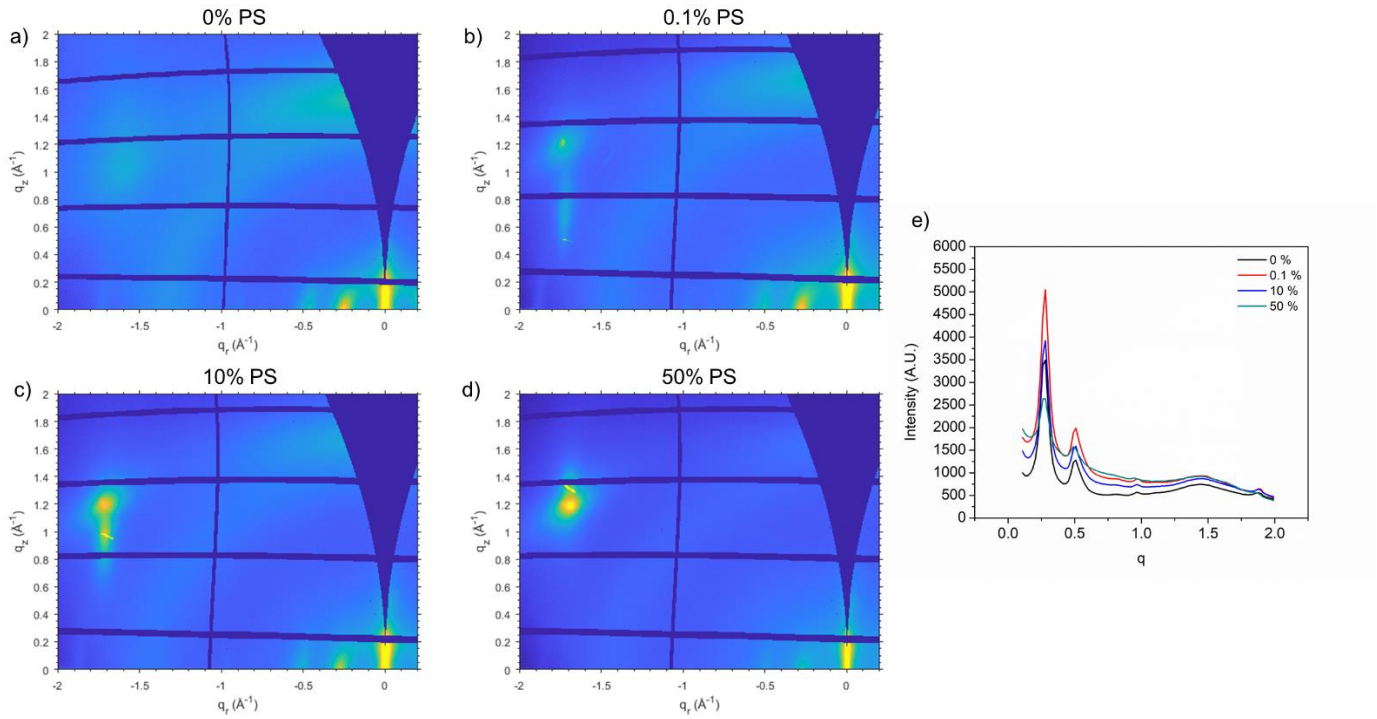

Figure 4.10. GIWAXS of P(NDI2OD-T2) blended with PS. a) 0% PS, b) 0.1% PS, c) 10% PS, d) 50% PS, e) Linecuts of (a)-(d).

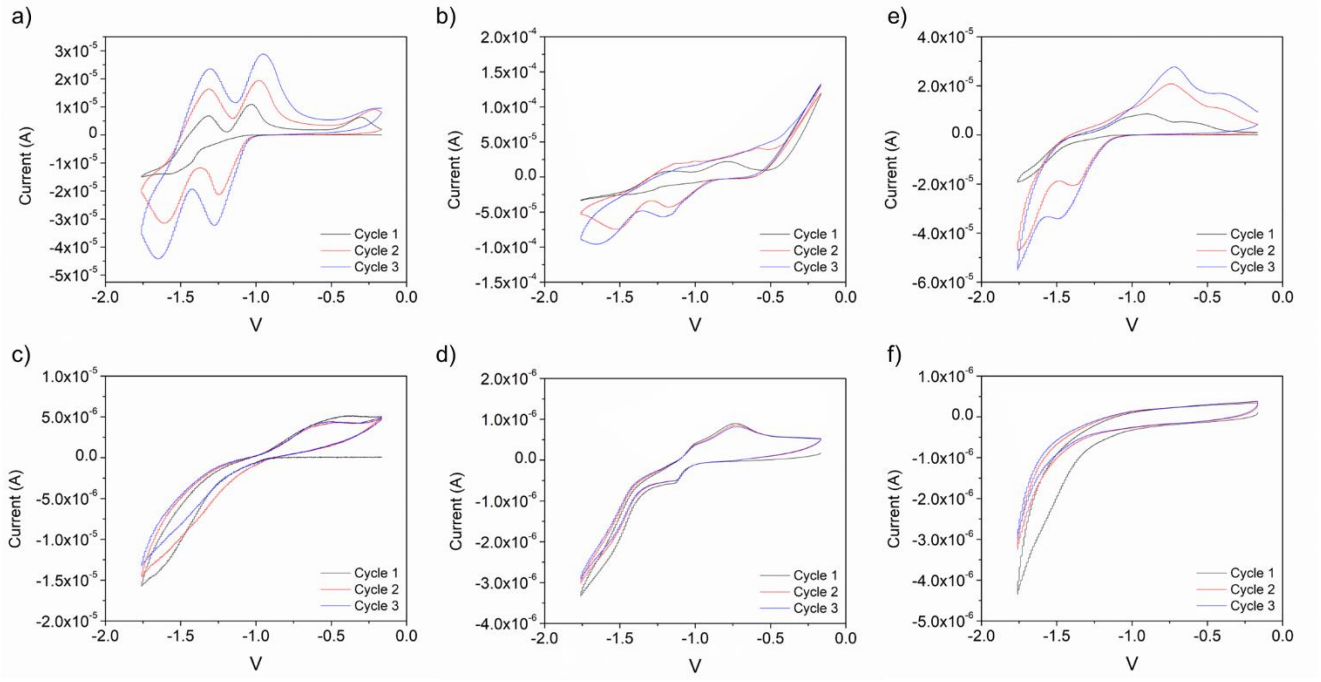

Figure 4.11. Cyclic voltammetry of each blend composition with 3 cycles for each condition. (a) 0% P2VP, (b) 0.1% P2VP, (c) 1% P2VP, (d) 5% P2VP, (e) 10% P2VP, (f) 50% P2VP

5. Poly(ionic liquid) gating materials for high performance organic thin-film transistors: the role of block copolymer self-assembly at the semiconductor interface

Context and Significance of Work

While the majority of the work presented in the previous thesis chapters examined the stability of OTFTs, it is important to recognize some of the requirements necessary for proliferation of this technology: low-power and flexible systems are most likely to see realistic use of OTFTs. Using inflexible SiO_2 dielectrics, while practical from a modelling perspective, will not be transferrable to applications for wearable or flexible devices. Additionally, high threshold voltages were observed in the previous devices, which would make low-power applications impossible. Therefore, the design of polymeric dielectric or gating materials makes it possible to fabricate both flexible and low-power devices. This chapter demonstrates that through the design of polymeric ionic liquids, we achieved the fabrication of OTFTs that could be operated using the same voltage output as an AA battery. Previous group members had developed the chemistry to synthesize these novel polymer dielectrics and I strove to develop an understanding of the mechanisms by which this device performance was possible, to enable further development of these promising dielectrics.

Contributions of Authors

This chapter contains work from the following publications:

1. *Peltekoff, A. J.;* ***Brixi, S.;*** *Niskanen, J.; Lessard, B. H.; Ionic Liquid Containing Block Copolymer Dielectrics: Designing for High-Frequency Capacitance, Low-Voltage Operation, and Fast Switching Speeds. doi:10.1021/jacsau.1c00133 (Found in Section 5.2)*

2. ***Brixi, S.;*** *Radford. C.; Tousignant, M.; Peltekoff, A. J.; Manion, J. G.; Kelly, T.; Lessard, B. H.* Poly(ionic liquid) gating materials for high performance organic thin-film transistors: the role of block copolymer self-assembly at the semiconductor interface. doi:10.1021/acsami.2c07912 (Found in Section 5.3 onward)*

I fabricated and characterized the transistor performance as well as compiled all data for the proof-of-concept devices in the JACS Au publication and contributed to editing of the manuscript. The remaining sections of this first publication involved in the synthesis I did not contribute to and therefore were not included in this chapter. For the work published in ACS AMI, I designed the study, fabricated and characterized the transistors, and prepared samples for GISAXS and AFM. Chase Radford conducted GISAXS experiments with analysis and assisted in writing the manuscript. Mathieu Tousignant conducted AFM imaging and assisted in revising the manuscript. Alexander Peltekoff synthesized the polymers. Joseph Manion developed 3D renderings and assisted in revising of the manuscript.

5.1 Abstract

The widespread realization of wearable electronics requires printable active materials capable of operating at low voltages. Polymerized ionic liquid (PIL) block copolymers exhibit thickness independent double-layer capacitance that makes them a promising gating medium for the development of organic thin-film transistors (OTFTs) with low operating voltages and high switching speed. PIL block copolymer structure and self-assembly can influence ion conductivity and resulting OTFT performance. In OTFTs self-assembly of the PIL gate on the semiconducting polymer may differ from bulk self-assembly, which would directly influence electrical double layer formation. To this end, we used poly{[N,N′-bis(2-octyldodecyl)-naphthalene-1,4,5,8-bis(dicarboximide)-2,6-diyl]-alt-5,5′-(2,2′-bithiophene)} (P(NDI2OD-T2)) as a model semiconductor for our OTFTs, on which our PILs exhibited self-assembly. In this study we explore this critical interface by grazing-incidence small angle X-ray scattering (GISAXS) and atomic force microscopy (AFM) of P(NDI2OD-T2) and a series of poly(styrene)-*b*-poly(1-(4-vinylbenzyl)-3-butylimidazolium-random-poly(ethylene glycol) methyl ether methacrylate) (poly(S)-*b*-poly(VBBI$^+$[X]-r-PEGMA)) block copolymers, with varying PEGMA/VBBI$^+$ ratios and three different mobile anions (where X = TFSI$^-$, PF_6^- or BF_4^-). We investigate the thin film self-assembly of block copolymers as a function of device performance. Overall, a mixed orientation at the interface leads to improved device performance while predominantly hexagonal packing leads to non-functional devices, regardless of the anion present. These PIL gated OTFTs were characterized with a threshold voltage below 1 V, making understanding of their structure-property relationships crucial to enable the further development of high-performance gating materials.

5.2 Introduction

Organic electronics have the potential for low-cost manufacturing through low temperature printing techniques. From wearable electronics[1] to low-cost point of care sensors[2,3], organic thin film transistors (OTFTs) are integral to the function of these devices. Electrolyte gated organic transistors (EGOT) are emerging as a fascinating platform for biological sensing in aqueous medium[4]. However, some applications require solid state gating material and operation with high switching speeds such as memory devices and logic-based circuits. Electrolyte gated transistors suffer from slow switching speeds due to the electrochemical doping and un-doping of the semiconductor layer.

To ensure devices can be applied in a wide variety of applications, low-voltage operation is necessary. Common commercial batteries supply a nominal voltage from 1 – 3 V, therefore it is necessary to design OTFTs that operate within or below this range. The gate dielectric is key to enabling low-voltage operation of OTFTs, as polarization of the gating material leads to generation of charge carriers in the semiconductor layer through the field-effect phenomenon. Polymerized ionic liquids (PILs) are a promising class of materials for this application due to their ability to form an electrical double-layer (EDL) when an electric field is applied[5–7]. A mobile anion diffuses through the polymer matrix in response to an electric field, while the charged polymer backbone remains stationary. This leads to higher capacitance than can be obtained by traditional dielectric materials, which in turn leads to improved OTFT performance and low turn-on voltage[8,9]. In addition, the capacitance of the EDL is independent of thickness, which makes the use of PILs especially interesting for fully printed devices, as minor thickness variations will not impact device performance.

However, PILs suffer from poor mechanical stability due to their low glass transition temperature (T_g)[10,11]. This can be improved through the use of block copolymers with a highly conductive PIL block, and another block of a high-T_g, mechanically strong material[9,12,13]. To achieve this, we developed a library of 27 block copolymers with a poly(styrene)-*b*-poly(1-(4-vinylbenzyl)-3-butylimidazolium-random-poly(ethylene glycol) methyl ether methacrylate) (poly(S)-*b*-poly(VBBI$^+$ [X]-r-PEGMA)) structure[9]. In our initial study, proof-of-concept OTFT devices were developed with three of the most promising candidate materials, and bulk film investigation techniques were applied to obtain an initial understanding of the self-assembly of

these block copolymers. The desired low-voltage operation with mechanically stable films was achieved, but it was not possible to fully develop structure-property relationships for these materials. Due to the critical interactions of the semiconductor-dielectric interface, thin-film techniques should be applied to complement the bulk film techniques to improve our understanding of the true thin-film properties in devices. This interface is crucial to operation of the device by enabling accumulation of charge carriers in the semiconductor, therefore it is essential to understand how the thin-film morphology impacts the device performance[14]. Techniques such as grazing incidence small angle X-ray scattering (GISAXS) have been proven to be ideal for characterizing the morphology of self-assembled block copolymer thin films.[15,16]

This study incorporates 12 candidate materials from our library into top gate top contact OTFTs with a poly{[N,N′-bis(2-octyldodecyl)-naphthalene-1,4,5,8-bis(dicarboximide)-2,6-diyl]-alt-5,5′-(2,2′-bithiophene)} (P(NDI2OD-T2)) semiconductor layer, and examines the thin-film morphology of these films through GISAXS and atomic force microscopy (AFM) (**Figure 1**). Through comparison of the mobile anion and the $VBBI^+$/PEGMA ratio, structure-property relationships are developed, informing the design of future styrene-*b*-($VBBI^+$/PEGMA) polymers for applications in OTFTs. Nine of these gating materials have not previously been reported in OTFT devices.

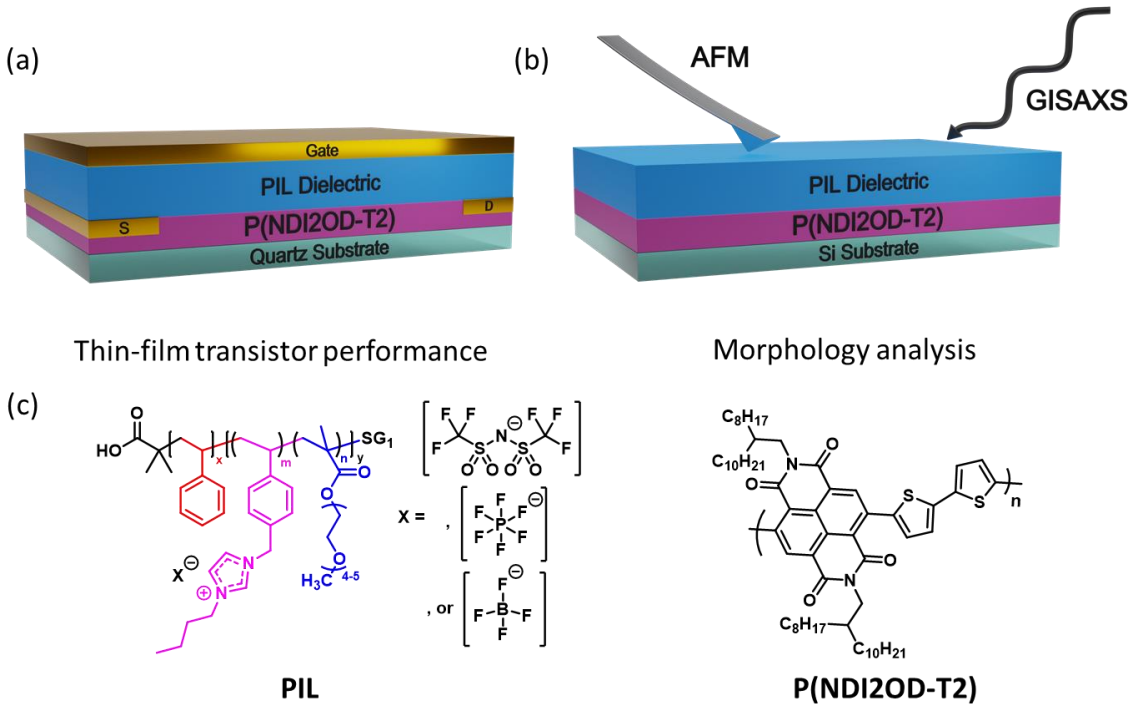

Figure 5.1. a) Schematic of a P(NDI2OD-T2) OTFT. b) Thin-film characterization of PILs performed through GISAXS and AFM. c) Structure of styrene-*b*-(VBBI$^+$/PEGMA) polymers and P(NDI2OD-T2).

5.3 Proof-of-Concept Devices

We synthesized a library of 27 well-defined, poly(styrene)-*b*-poly(1-(4-vinylbenzyl)-3-butylimidazolium-random-poly(ethylene glycol) methyl ether methacrylate) (poly(S)-*b*-poly(VBBI$^+$[X$^-$]-*r*-PEGMA)) block copolymers, with varying PEGMA/VBBI$^+$ ratios and three different mobile anions (where X = TFSI$^-$ (bis(trifluoromethanesulfonyl)imide), PF_6^- or BF_4^-), to be incorporated as a gating layer in organic thin film transistors (OTFTs). A selection of 12 materials from this library (4 PEGMA/VBBI$^+$ ratios, each paired with the three anions), having the highest electrical double-layer (EDL) capacitance and conductivity were identified to be ideal candidates for OTFT fabrication[9]. These compounds and their properties are summarized in **Table 5.1**.

Table 5.1. Physical properties of poly(S)-*b*-poly(VBBI$^+$ [X$^-$]-*r*-PEGMA) block copolymers (X = TFSI, BF_4^-, or PF_6^-).

Polymer ID [a]	Anion	σ (S cm^{-2})	$\bar{M}_n$ [b] $[kg\ mol^{-1}]$	Đ $[\bar{M}_w/\bar{M}_n]$	F_{STY} [c]	F_{CMS} [c]	F_{PEGMA} [c]	$R_{CMS/PEGMA}$ [d]
S-*b*-(V25-*r*-P75)	$TFSI^-$	3.6×10^{-8}	28.0	1.07	0.95	0.02	0.03	0.64
	BF_4^-	-						
	PF_6^-	-						
S-*b*-(V50-*r*-P50)	$TFSI^-$	3.4×10^{-7}	35.9	1.23	0.67	0.18	0.15	1.27
	BF_4^-	7.9×10^{-8}						
	PF_6^-	4.1×10^{-9}						
S-*b*-(V75-*r*-P25)	$TFSI^-$	1.7×10^{-7}	31.4	1.12	0.74	0.20	0.06	3.17
	BF_4^-	1.2×10^{-8}						
	PF_6^-	5.8×10^{-11}						
S-*b*-(V100-*r*-P0)	$TFSI^-$	1.4×10^{-9}	39.6	1.17	0.70	0.30	-	-
	BF_4^-	4.6×10^{-9}						
	PF_6^-	7.4×10^{-11}						

[a] We define the polymer names as S-*b*-(VX-*r*-PY) where X/Y = the target ratio of chloromethylstyrene (CMS) (converted to VBBI$^+$ after initial polymerization) versus poly(ethylene glycol) methyl ether methacrylate (PEGMA) used in the synthesis of the pre-polymer. The polymer synthesis and characterization data in this table are initially reported in Peltekoff et al.[9]

[b] The molecular weight of the polystyrene block is identical for all polymers, at 22.5 kg mol^{-1}.

[c] Molar composition of monomer unit determined by ^{1}H NMR. STY = styrene, CMS = chloromethyl styrene, PEGMA = poly(ethylyene glycol) methyl ether methacrylate.

[d] Ratio of CMS to PEGMA on a molar basis in the second block.

While analysis of bulk films confirmed self-assembly of the PILs on glass,[9] this could not verify that the PILs would behave as predicted when incorporated into a device with different interfaces, film thicknesses, and components. Therefore, a proof-of-concept set of devices was fabricated using the most conductive PILs.

The transfer characteristics for the OTFTs were obtained by sweeping the gate voltage (V_{GS}) at a sweep rate of approximately 250 mV/s to ensure EDL formation whilst holding the V_{SD} constant at 1 V. All materials displayed hysteresis which is commonly observed in electrolyte dielectrics as a consequence of the relatively slow movement of ions and moisture.[17–19] As can be observed from the transfer curves (**Figure 5.2**), devices fabricated from S-*b*-(V50-*r*-P50) with $TFSI^-$ and BF_4^- anions exhibited on-currents in the same order of magnitude, whereas those with the PF_6^- anion were smaller by an order of magnitude. The threshold voltage (V_T) of $TFSI^-$ and PF_6^- ranged between 1 and 2 V whereas BF_4^- devices consistently turned on below 1 V. These V_T are exceptional when compared to BGBC devices made using the same P(NDI2OD-T2) on SiO_2 in air (V_T = 33.9 V).[20]

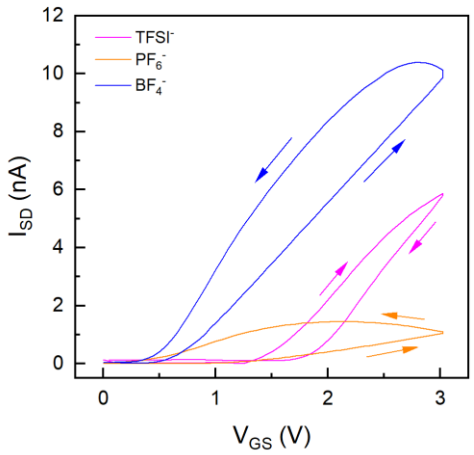

Figure 5.2. Representative transfer characteristics in the linear regime (V_{DS} = 1 V) of poly(S)-*b*-poly(VBBI$^+$[X]-*r*-PEGMA) (where [X] = BF_4^-, PF_6^-, or $TFSI^-$) OTFTs with Polymer ID S-*b*-(V50-*r*-P50).

With these results, it was clear that these PILs could successfully be incorporated into OTFTs. The low V_T was highly promising, but further understanding of the self-assembly of the PIL on the semiconductor was needed in order to develop the relationship between the polymer structure and device performance.

5.4 Analysis of Film Morphology

These polymerized ionic liquid (PIL) block copolymers were cast in thin films and used to fabricate OTFTs with the semiconductor poly{[N,N′-bis(2-octyldodecyl)-naphthalene-1,4,5,8-bis(dicarboximide)-2,6-diyl]-alt-5,5′-(2,2′-bithiophene)} (P(NDI2OD-T2)) in a top gate top

contact (TGTC) device configuration. It is well known that when developing thin film electronics, it is critical to understand the effects of orthogonal processing, where the morphology and surface chemistry of the initial layer dictate the self-assembly or crystallinity of the subsequent layer. Therefore, it is likely that the block copolymer self-assembly will differ depending on the PIL composition and its interaction with the semiconductor layer. In this study we deposited the 12 candidate poly(S)-*b*-poly(VBBI$^+$[X$^-$]-*r*-PEGMA) polymers onto identical P(NDI2OD-T2) layers and studied the block copolymer self-assembly as a function of PIL composition. The thin film morphologies of the poly(S)-*b*-poly(VBBI$^+$[X$^-$]-*r*-PEGMA) were characterized under similar conditions to their integration into P(NDI2OD-T2)-based OTFTs, enabling the development of structure-property relationships between PIL block copolymer self-assembly and OTFT performance.

Block copolymers, such as these PILs, will self assemble into microdomains which are thermodynamically favourable, based on the block length, the miscibility parameters, and the surface chemistry[21–24]. As OTFTs are devices with numerous interfaces, and the interactions at these interfaces strongly impact the performance of the devices[25], it was crucial to study the morphology of these thin films with the same interfacial interactions that would appear in the TGTC devices.

Therefore, P(NDI2OD-T2) films were cast on plasma-treated Si substrates and annealed, then candidate PILs were cast on the P(NDI2OD-T2) films and annealed. Grazing-incidence small angle X-ray scattering was used to elucidate this microphase self-assembly of the PIL films on P(NDI2OD-T2).[15]

GISAXS scattering patterns were analyzed by taking linecuts of the Yoneda peak along q_r. Expected q-spacing of typical block-copolymer self assembly phases (lamellae, cylinders, and bicontinuous gyroid) were plotted along the linecuts to indicate where peaks should appear and highlight the observed correlations between scattering and morphology. Due to weak ordering, many of the features are broad and appear as a shoulder of the strongest peak. The presented analysis is for the most likely modes of packing based on these observed peaks.

Atomic force microscopy was used to image the surface morphology of the PIL to compare to the thin film bulk morphologies identified by the GISAXS analysis. Bruker ScanAsyst PeakForce Tapping was used to study the surface morphology of the PILs.

Figure 5.3 summarizes the results of GISAXS and AFM analyses of S-*b*-(V100-*r*-P0) (**Figure 5.3a,e,i**), S-*b*-(V75-*r*-P25) (**Figure 5.3b,f,j**), S-*b*-(V50-*r*-P50) (**Figure 5.3c,g,k**), and S-*b*-(V25-*r*-P75) (**Figure 5.3d,h,l**) with the $TFSI^-$ anion bound to the cationic backbone. Idealized representations of the probable packing modes are indicated in the overlaid renderings of **Figure 5.3e-l**, where the most strongly identified morphologies are depicted. Due to the weak order of the films, these depictions are intended to enhance comparison of the differing morphologies, rather than present an exact representation of the films. With the $TFSI^-$ anion, GISAXS linecuts along q_r (**Figures 5.3e-g,i-k**) indicate these PILs exhibit a preference towards lamellar packing (LAM). Symbols used on linecuts represent the expected q-spacing of lamellar (red squares), cylinder (green inverted triangles), and bicontinuous gyroidal (blue triangles) phases. Where shoulders and peaks appear and line up with the indicated symbols, the film morphology therefore displays more characteristics of that packing mode. There is an increase in hexagonal cylinders (HEX) becoming present when PEGMA loading was increased to 50% with S-*b*-(V50-*r*-P50). Increasing the PEGMA loading further to 75% in S-*b*-(V25-*r*-P75) (**Figure 5.3l**) leads to a primarily HEX packing motif. The AFM reflects these changes with longer features visible in samples S-*b*-(V100-*r*-P0) (**Figure 5.3a**) and S-*b*-(V25-*r*-P75) (**Figure 5.3b**), while smaller circular features begin to appear in S-*b*-(V50-*r*-P50) (**Figure 5.3c**). GISAXS scattering patterns for the Si substrate and the substrate with P(NDI2OD-T2) only were also obtained and are presented in **Figure 5.8** of the Supplementary Information.

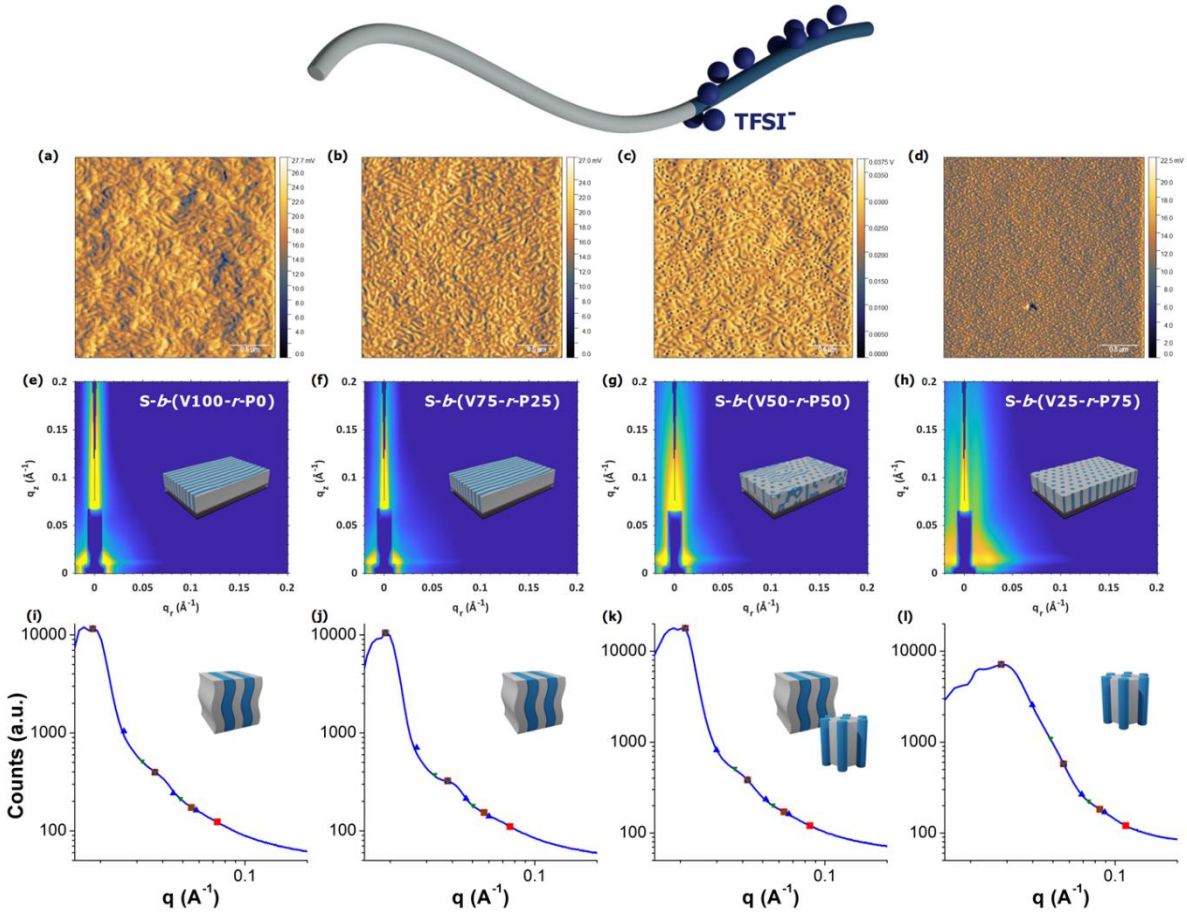

Figure 5.3. (a-d) Atomic force microscopy InPhase images, (e-h) grazing incidence small angle X-ray scattering diffraction patterns with overlaid depiction of the probable combination of packing modes, and (i-l) line cut for thin films of poly(S)-*b*-poly(VBBI$^+$ [TFSI$^-$]-*r*-PEGMA) block copolymers, with varying PEGMA/VBBI$^+$ ratios: S-*b*-(V100-*r*-P0) (a), e) and i)), S-*b*-(V75-*r*-P25) (b), f) and j)), S-*b*-(V50-*r*-P50) (c), g) and k)), and S-*b*-(V25-*r*-P75) (d), h) and l)) with the TFSI$^-$ counterion. Red squares = LAM, Blue triangles = BCG, Green inverted triangles = HEX. Top is a graphical representation of the block copolymer with TFSI$^-$ counterion bound to the charged VBBI$^+$ backbone.

In **Figure 5.4**, the morphologies observed when the anion is substituted for BF_4^- are presented. The BF_4^- counterion confers a preference for the bicontinuous gyroid (BCG) packing mode, as observed in **Figures 5.4e-g** and **5.4i-k**. Increasing PEGMA loading of the block increases the preference towards the HEX morphology. With the BF_4^- counterion, it appears a HEX packing mode begins to exhibit a small population at 25 mol% PEGMA loading (**Figure 5.4b, 5.4f and 5.4j**). AFM of the surfaces of these films shows strong ordering, especially for S-*b*-(V75-*r*-P25) (**Figure 5.4b)** and S-*b*-(V50-*r*-P50) (**Figure 5.4c**). Similar structures were observed by TEM of

the bulk phase of these same polymers[9]. S-*b*-(V25-*r*-P75), with 75% PEGMA loading, shows fewer surface features than those with lower PEGMA loading (**Figure 5.4d**).

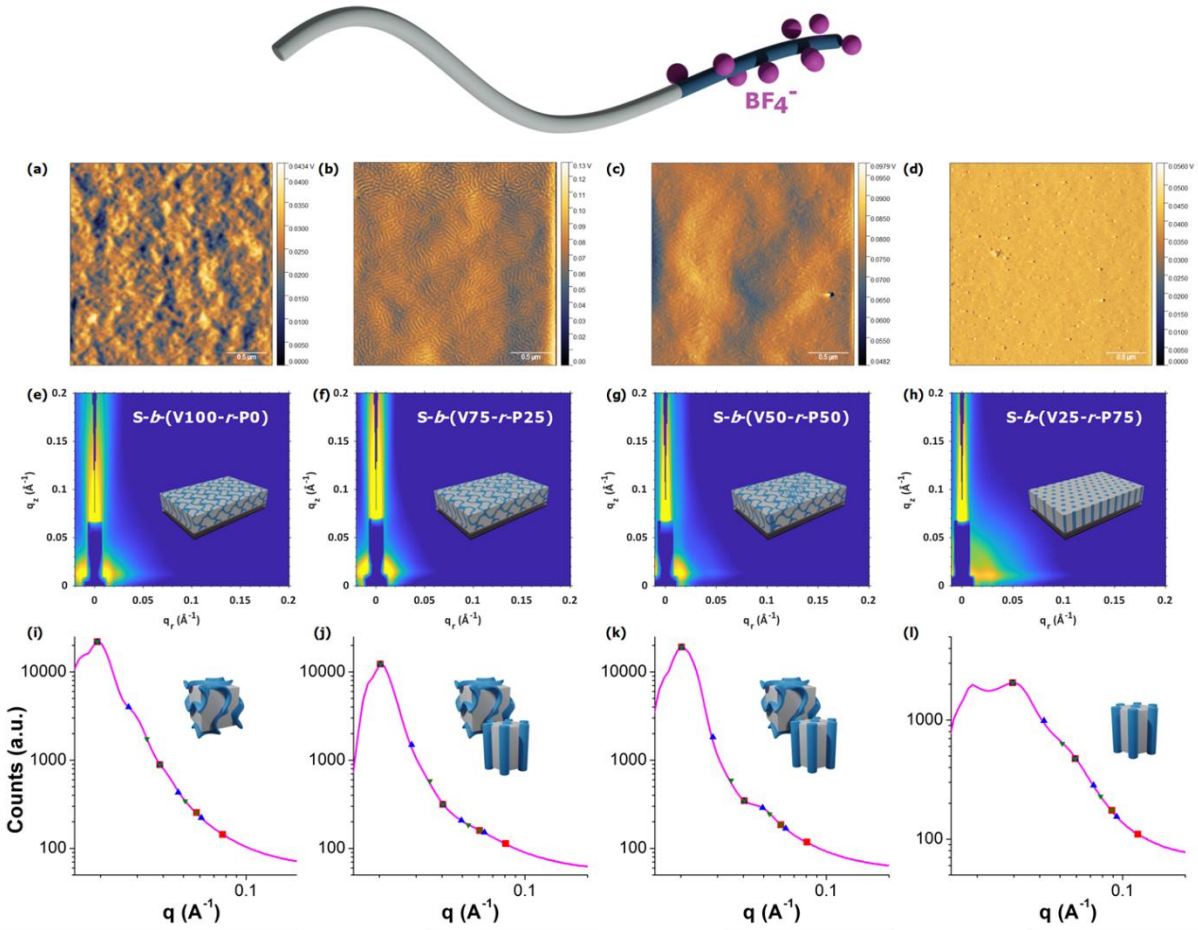

Figure 5.4. (a-d Atomic force microscopy InPhase images, (e-h) grazing incidence small angle X-ray scattering diffraction patterns with overlaid depiction of the probable combination of packing modes, and (i-l) line cuts for thin films of poly(S)-*b*-poly(VBBI$^+$[BF_4^-]-*r*-PEGMA) block copolymers, with varying PEGMA/VBBI$^+$ ratios: S-*b*-(V100-*r*-P0) (a), e) and i)), S-*b*-(V75-*r*-P25) (b), f) and j)), S-*b*-(V50-*r*-P50) (c), g) and k)), and S-*b*-(V25-*r*-P75) (d), h) and l)) with the BF_4^- counterion. Red squares = LAM, Blue triangles = BCG, Green inverted triangles = HEX. Top is a graphical representation of the block copolymer with BF_4^- counterion bound to the charged VBBI$^+$ backbone.

Figure 5.5 summarizes the morphology analysis of these PILs having the PF_6^- anion present when deposited on P(NDI2OD-T2). GISAXS spectra (**Figures 5.5e-g**) and their linecuts (**Figures 5.5i-k**) of PEGMA loadings below 75% indicate LAM being preferred and HEX appearing at 50% PEGMA loading (**Figure 5.5k**). However, when PEGMA is not present in the second block, the PIL with PF_6^- does not exhibit any preference for a specific packing mode, and only displays weak

long-range ordering (**Figures 5.5e,i**). As with the other counterions, S-*b*-(V25-*r*-P75) with 75% PEGMA loading has a relatively flat surface with a strong preference for cylindrical packing. Relatively amorphous surface features are observed by AFM with S-*b*-(V100-*r*-P0) (**Figure 5.5a**) and S-*b*-(V75-*r*-P25) (**Figure 5.5b**), as reflected by the relatively weak ordering observed (**Figures 5.5i,j**) from GISAXS.

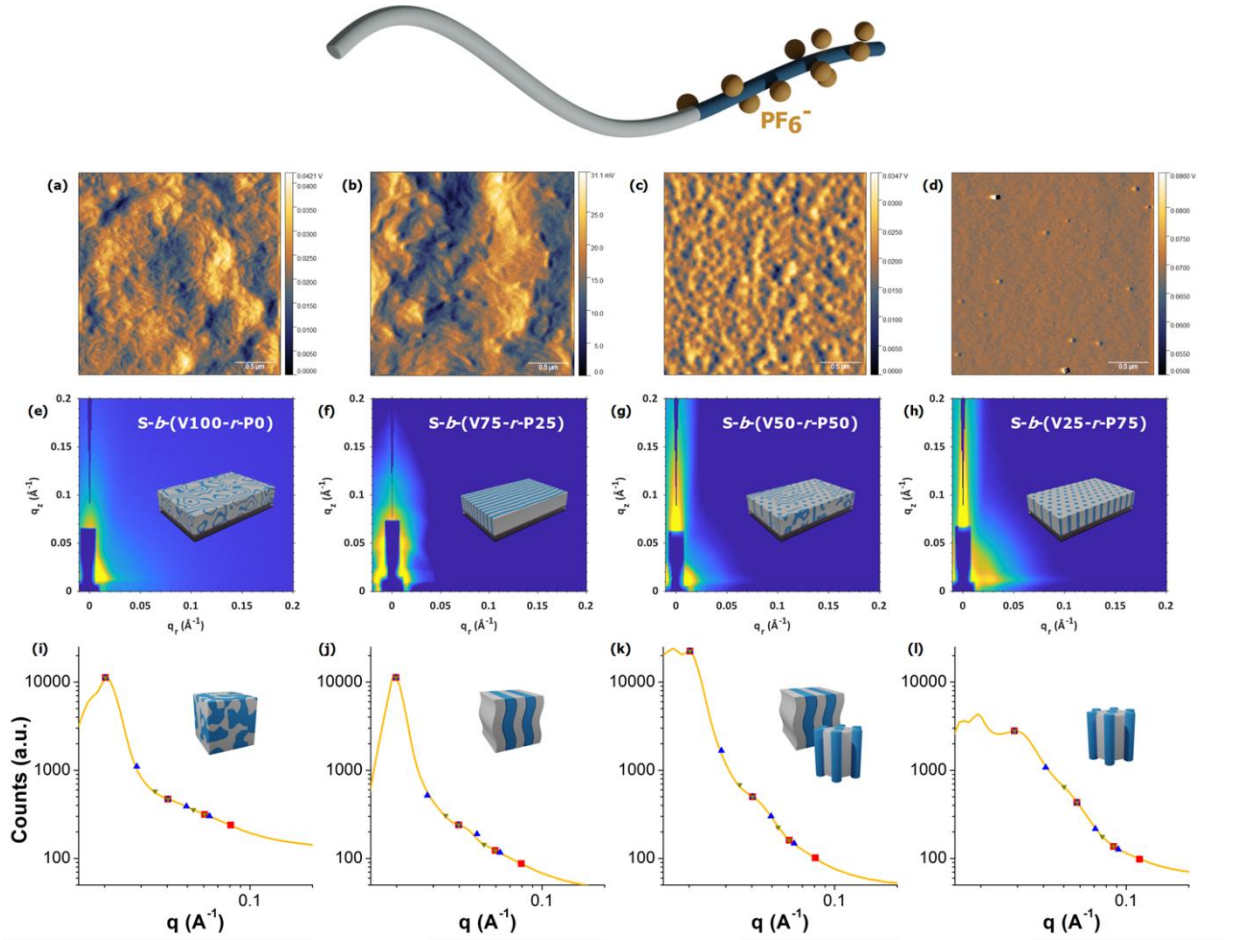

Figure 5.5. (a-d) Atomic force microscopy images, (e-h) grazing-incidence small angle X-ray scattering spectra with overlaid depiction of the probable combination of packing modes, and (i-l) line cuts for thin films of poly(S)-*b*-poly(VBBI$^+$[PF_6^-]-*r*-PEGMA) block copolymers, with varying PEGMA/VBBI$^+$ ratios: S-*b*-(V100-*r*-P0) (a), e) and i)), S-*b*-(V75-*r*-P25) (b), f) and j)), S-*b*-(V50-*r*-P50) (c), g) and k)), and S-*b*-(V25-*r*-P75) (d), h) and l)) with the PF_6^- counterion. Red squares = LAM, Blue triangles = BCG, Green inverted triangles = HEX. Top is a graphical representation of the block copolymer with PF_6^-. counterion bound to the charged VBBI$^+$ backbone.

Overall, polymer samples showed weak order with a tendency towards mixed morphology, typically with a preference for one morphology over the others. The depictions of the thin-films presented in **Figures 5.3-5.5(e-h)** represent an idealized visualization of packing modes, but the disorder in packing and experimental constraints limit the certainty of absolute orientation analysis. Surface morphology measured by AFM typically displayed features indicative of the strongest ordering observed in the GISAXS diffraction patterns. The low degree of order observed may be due in part to the polymer architecture; block copolymers with pure well-defined blocks (i.e., A-*b*-B), tend to self assemble with a higher degree of order compared to block copolymers having a greater degree of random monomer distribution (i.e. A-*ran*-B)[26–28]. This is likely to apply to the case where the overall polymer architecture is a block copolymer, but one block has a random monomer distribution while the other is pure (i.e. A-*b*-(B-*ran*-C)), which is the case for the poly(S)-*b*-poly(VBBI$^+$[X$^-$]-*r*-PEGMA) polymers in the present study. This random distribution in the second block characteristic of the PILs in this study could contribute to the observed weaker order. However, with the observation that even the S-*b*-(V100-*r*-P0) polymer displays weak order, this cannot fully account for this observation. The PILs themselves are cast on top of a semicrystalline polymer, which itself is somewhat disordered. Some of the weak ordering of the films may stem from this surface interaction. Additionally, it has been noted that specifically with PIL block copolymers the relative concentration of the ionic liquid block can influence disorder[29], and that relative salt concentration can impact the morphology and lead to phase preferences, which may also impact the relative disorder of the polymers with competing preferences for phases[30].

The identity of the counterion impacts the morphology of the films, as observed by the differing morphologies observed from TFSI$^-$, BF_4^-, and PF_6^- in **Figures 5.3**, **5.4**, and **5.5**, respectively. TFSI$^-$ and PF_6^- tended to display more similar packing modes, with a preference for a mixture of LAM and HEX. However, irrespective of the anion, S-*b*-(V25-*r*-P75) always exhibited a strong preference for the HEX packing motif over any others (**Figures 5.3l, 5.4l, 5.5l**) and a relatively uniform surface with fewer features by AFM compared to the other PEGMA/VBBI$^+$ ratios (**Figures 5.3d, 5.4d, 5.5d**). Although the weak ordering and broad features of the GISAXS patterns make it difficult to definitively assign orientational preferences in the films, the GISAXS patterns of the S-*b*-(V25-*r*-P75) samples are consistent with a predominantly

vertical arrangement of the hexagonal cylinders with respect to the substrate (**Figures 5.3h, 5.4h, 5.5h**), leading to poor device performance (see following section).

An analysis of the AFM images was carried out using the power spectral density function (PSDF). The radial PSD was calculated for each image, and a Lorentz correction applied by multiplying by q^2. This enabled the identification of common domain sizes at the film surface through identification of the maximum of the peak appearing in each PSDF curve (**Figure 5.6**). Lorentzian functions were fitted to the PSDF curves to emphasize the existing trends, and the q value of the maximum of each peak was taken to be the dominant feature size for that sample. Lorentzian functions could not be fitted to S-*b*-(V25-*r*-P75) for the BF_4^- (**Figure 5.6b**) and PF_6^- (**Figure 5.6c**) anion. For these samples, the maximum of the strongest feature was taken to be the q value of the dominant domain to provide an approximation most prominent domain size.

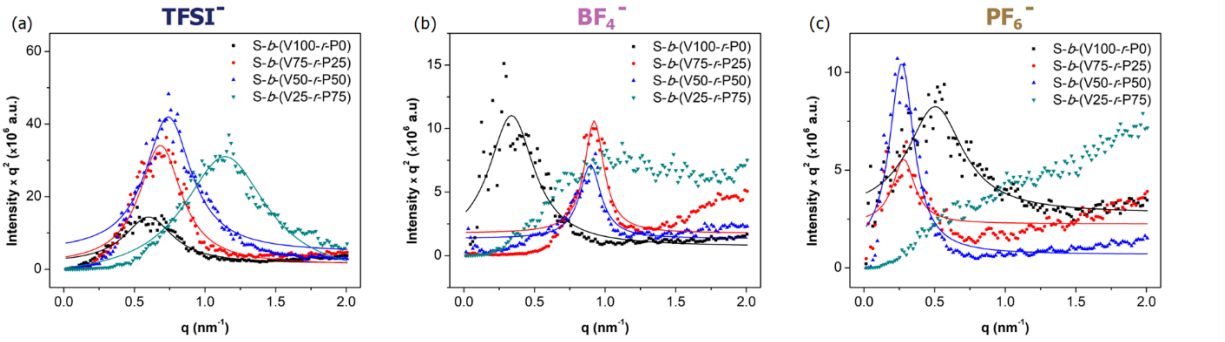

Figure 5.6. Power spectral density function (PSDF) of (a) (poly(S)-*b*-poly(VBBI$^+$[TFSI$^-$]-*r*-PEGMA)), (b) (poly(S)-*b*-poly(VBBI$^+$[BF_4^-]-*r*-PEGMA)), and (c) (poly(S)-*b*-poly(VBBI$^+$[PF_6^-]-*r*-PEGMA)). Normalized intensity is presented.

In general, the PSDF in **Figure 5.6** displays a narrower dispersity of domain sizes for the samples that displayed the highest degree of order in GISAXS. Particularly, S-*b*-(V25-*r*-P75) with all anions had the broadest distribution, indicating that the cylindrical features are likely sparsely distributed across the surface, or that the AFM could not sufficiently resolve the cylindrical features.

Additionally, domain size tended to decrease with decreasing molecular weight of the polymer. The domain sizes and full width at half-maximum (FWHM, representing the relative dispersity of domain sizes) are presented in **Table 5.2**.

Table 5.2. Domain size and peak width determined from PSDF analysis.

Polymer ID	Anion	Domain Size (nm)	FWHM [a] (nm^{-1})
S-*b*-(V25-*r*-P75)	$TFSI^-$	5.5	0.72
	BF_4^-	5.6	[b]
	PF_6^-	9.5	[b]
S-*b*-(V50-*r*-P50)	$TFSI^-$	8.4	0.40
	BF_4^-	7.0	0.18
	PF_6^-	23.4	0.21
S-*b*-(V75-*r*-P25)	$TFSI^-$	9.2	0.36
	BF_4^-	6.8	0.17
	PF_6^-	22.3	0.19
S-*b*-(V100-*r*-P0)	$TFSI^-$	10.5	0.2
	BF_4^-	18.6	0.39
	PF_6^-	12.5	0.48

[a] Full width at half-maximum, presented in terms of q from **Figure 5.6**.

[b] FWHM could not be calculated for these peaks due to weak order in the AFM.

The sizes of observed features by AFM are similar in scale to those observed by TEM in our previous work[9], suggesting that self-assembly in the bulk leads to similar feature sizes to when assembled on a surface. However, the morphologies observed by TEM and SAXS in the bulk from our previous work do not entirely reflect the morphologies observed by GISAXS and AFM of the thin films in the current study, highlighting the necessity of using thin-film characterization techniques in order to understand these nanometer-scale systems. At this scale, surface interactions are likely playing a significant role in the morphology of the final thin films.

5.5 Device Performance

Top gate top contact, organic thin-film transistors were fabricated using the poly(S)-*b*-poly(VBBI$^+$[X$^-$]-*r*-PEGMA) polymers as a gating material deposited on top of the P(NDI2OD-T2) semiconducting layer. The transfer curves can be found in **Figure 5.7a,b,c** for $TFSI^-$, BF_4^-, and PF_6^-, respectively. The resulting electron mobility (μ_e) and threshold voltage values are compared in **Figure 5.7d-f**. Representative output curves can be found in **Figure 5.9** and the thickness of the PIL layers can be found in **Table 5.3** of the ESI. Mobilities were found to range from 0.4 x 10^{-3} to 8 x 10^{-3} $cm^2V^{-1}s^{-1}$.

P(NDI2OD-T2) has previously been reported to display V_T of 5 to 35 V with conventional organic dielectric materials such as poly(methyl methacrylate) and poly(styrene)[31]. Such devices were operated at source-drain voltages (V_{SD}) of 60 V, with gate-voltage (V_{GS}) ranges from 0 to 60 V. Similarly high voltages and operating ranges were required for P(NDI2OD-T2) on SiO_2 dielectrics[32], including our previous studies with he material on SiO_2[20,33]. These PILs enable significantly lower operating voltages compared to these previous studies, with V_{SD} of 1 or 2 V, and V_{GS} sweeps from 0 to 3 V, and V_T from 1.5 V and approaching 0 V. In our previous works developing PIL gating materials using a poly(methyl methacrylate)-b- $VBBI^+[TFSI^-]$ copolymer, we found the best-performing block copolymers achieved a V_T of 4 V, thus our new material design has improved on the potential for low-voltage operation[8]. Choi, *et al* reported a triblock PIL in OTFTs that also used P(NDI2OD-T2) as the n-type semiconductor, and similarly achieved a mobility of 8 x 10^{-3} $cm^2V^{-1}s^{-1}$ with threshold voltages ranging from 0 to 1 V [6]. The low-voltage performance is even comparable to ion gel gating materials in all-organic[34], or inorganic semiconductor[35] based electrolyte-gated transistors, which achieved sub 1 V threshold voltage operation.

Increasing the PEGMA loading increased the device mobility for $TFSI^-$ and BF_4^- (**Figures 5.7d and e**, respectively), following our previous findings that increasing PEGMA loading led to increased conductivity of the PILs[9]. The higher conductivity of the PIL enables greater charge separation due to the improved transport of the mobile anion through the polymer matrix, thus leading to greater generation of charge carriers in the organic semiconductor which is observed as a higher mobility in the OTFTs. However, the highest mobility was obtained with S-*b*-(V75-*r*-P25) for PF_6^-. It may be that despite the increased ionic conductivity of S-*b*-(V50-*r*-P50), the relatively high preference for HEX packing observed by GISAXS and AFM leads to poor performance. Additionally, the combination of BCG and HEX morphologies led to the higher performance overall of S-*b*-(V50-*r*-P50) with the BF_4^- counterion. This mixed type of morphology may lead to enhanced pathways for the counterions to diffuse within the dielectric for proper EDL formation, and improved surface interactions for charge induction leading to improved mobility in the P(NDI2OD-T2).

These results indicate HEX morphology leads to a lack of ability for the PIL film to act as a capacitor, meaning it is ineffective as a gating material. In our previous work, we noted that metal-

insulator-metal capacitors did not exhibit a measurable capacitance at 75% PEGMA loadings. From the results of this work, this indicates that the network for ion transport in the PIL is not effectively conducting the anions away from the semiconductor. Due to the weak order of the films, the orientation of the hexagonally packed cylinders (ie. primarily horizontally or vertically aligned) is not known, but either orientation could explain the poor performance. If the cylinders were to be aligned horizontally to the substrate, the anion simply cannot be transported toward the gate, and therefore the intended function of the PIL gate does not occur. If the cylinders were to be aligned vertically, there would be localized spots at the surface where the anions may migrate from the polymer backbone. In fact, the domain side observed in the PSDF analysis was smallest for the S-*b*-(V25-*r*-P75) polymers, all under 10 nm. With a channel length of 30 μm in the OTFTs, it appears such small domains cannot bridge the gap between electrodes to induce a conducting channel.

The electron mobility of S-*b*-(V50-*r*-P50) with the BF_4^- counterion is the highest among all samples, at 8 x 10^{-3} $cm^2V^{-1}s^{-1}$. All other materials, regardless of anion or composition tended to only approach 10^{-3} $cm^2V^{-1}s^{-1}$, except for S-*b*-(V50-*r*-P50)with the TFSI- counterion, which displayed the section highest mobility of 3 x 10^{-3} $cm^2V^{-1}s^{-1}$. A decrease in V_T was observed as PEGMA loading increased for polymers with $TFSI^-$ and PF_6^- counterions, while a larger variability in the V_T values for those with the BF_4^- anion makes determination of a trend less clear. It should be noted that all devices were operated at 1 V_{SD}, except for S-*b*-(V100-*r*-P0) with the BF_4^- anion, as it did not turn on at 1 V. Device data was obtained at 2 V_{SD} for S-*b*-(V100-*r*-P0) with the BF_4^- anion to demonstrate the device was still functional, unlike the S-*b*-(V25-*r*-P75) polymers.

Devices fabricated with S-*b*-(V25-*r*-P75) as the gating material exhibited no field effect under the applied voltages used regardless of counterions. Devices typically failed after increasing V_{GS} past 5 V, and S-*b*-(V25-*r*-P75) did not show any indication of field effect before a device failure (short-circuit) was observed. From this devices data, the HEX morphology appears to lead to poor capacitance. This is consistent with the observed inability to form an EDL in metal-insulator-metal capacitors from these materials in our previous report[9].

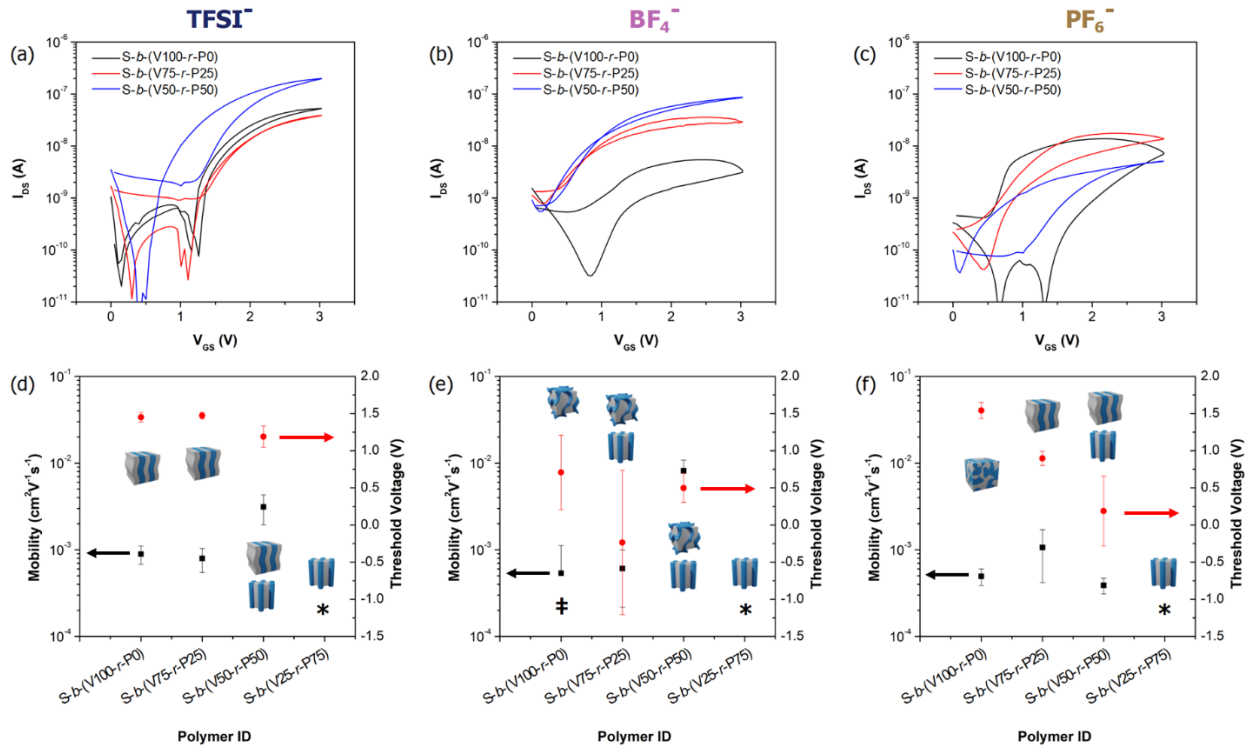

Figure 5.7. (a-c) Representative transfer curves, and (d-f) average mobility (black) and threshold voltage (red) for OTFT devices fabricated with P(NDI2OD-T2) and thin films of S-*b*-(V100-*r*-P0), S-*b*-(V75-*r*-P25), S-*b*-(V50-*r*-P50), and S-*b*-(V25-*r*-P75) having $TFSI^-$, BF_4^-, or PF_6^- anions. Values presented are the average of 4 measurements each from 5 devices, with error bars representing the standard deviation. The performance was taken as the average across all measurements and devices for a particular polymer. Each device was operated at 1 V_{SD}. ‡Device data for S-*b*-(V100-*r*-P0) with BF_4^- had to be obtained with 2 V_{SD}, as the devices did not function at the lower voltage. *Devices did not function, and parameters could not be calculated.

While the ordering of the films is weak, the differences in the GISAXS scattering patterns and AFM show differences in the preferred film morphology where order exists. Overall, films that displayed mixed morphologies of the poly(S)-*b*-poly(VBBI$^+$[X$^-$]-*r*-PEGMA) block copolymers tended to have higher OTFT performance. Increasing the PEGMA loading to a moderate level tended to improve device performance, but at high PEGMA loadings (75%), a strong preference for the HEX packing mode inhibits the formation of the EDL. This study demonstrates the importance of PIL block copolymer self-assembly at the semiconductor interface and how it needs to be optimized for the specific PIL structure to enable high performance OTFTs with low V_T and high switching speeds.

5.6 Conclusion

OTFTs were successfully fabricated using a library of 12 poly(S)-*b*-poly(VBBI$^+$[X$^-$]-*r*-PEGMA) block copolymers, having 4 VBBI$^+$/PEGMA ratios, each paired with 3 different anions. A combination of morphology analysis and device performance assessment has indicated that devices having PIL films that displayed some degree of order and also a mixed morphology typically gave the highest performance. Mobilities up to 8 x 10^{-3} $cm^2V^{-1}s^{-1}$ and threshold voltages below 1 V were recorded with these materials. S-*b*-(V50-*r*-P50) paired with the BF_4^- anion remains the highest-performing dielectric from this library so far. Increasing the ratio of PEGMA in the second block of the PILs tends to improve device performance, which is consistent with previous findings that the higher ratio leads to enhanced conductivity of the polymer. However, increasing the PEGMA loading also led to increased presence of hexagonally packed cylindrical morphology. When the PEGMA loading is too high (75%), an electrical double-layer cannot be formed due to a strong preference for cylinders, and the transistors do not function. This is a promising outlook for the design of this class of PILs, where an ideal performance as a gating material can be achieved with a moderate ratio of PEGMA in the second block, leading to low-voltage operation.

5.7 Experimental

Materials

P(NDI2OD-T2) was obtained from 1-Material, all solvents were obtained from Sigma Aldrich, and gold was obtained from Angstrom Engineering. Materials were used as received. Polymerized ionic liquids were synthesized as previously reported[9].

Grazing-incidence small-angle X-ray scattering (GISAXS)

Films for GISAXS experiments were prepared by first cleaning Si substrates in subsequent sonication baths of water, acetone, and methanol for 5 minutes each, followed by a 10 minute plasma treatment which would generate a thin layer of oxide on the surface of the Si. P(NDI2OD-T2) (10 mg/mL in 1,2-dichlorobenzene) was then spin-coated onto the substrates at 2000 rpm for 60 seconds. The P(NDI2OD-T2) films were annealed in a vacuum oven for 1 hour at 100 °C prior to deposition of the PILs. PILs (60 mg/mL in 2-butanone) were deposited by spin coating at 2000 rpm for 60 seconds. The film was annealed at 130 °C for 1 hour under vacuum, and then a second spin-coating step under the same conditions was repeated. The films were then annealed again at 130 °C for 1 hour.

GISAXS experiments were performed at the Canadian Light Source (CLS) using the Brockhouse X-ray diffraction sector – low energy wiggler (BXDS-WLE) beamline. A photon energy of 15.1 keV was selected using a Si(111) monochromator. The beam size was defined by slits having a 0.2 mm vertical gap and a 0.3 mm horizontal gap, and the angle of incidence was set to 0.01°. GISAXS patterns were collected with a Rayonix MX300 CCD detector (73.242 μm pixel size; 30 cm diameter), which was placed 2506 mm from the sample center. The GISAXS data were calibrated against a silver behenate standard and analyzed using the GIXSGUI software package[36]. Both polarization and solid-angle corrections were applied. The Yoneda peak was used for linecuts, wherein the cut was taken at approximately q = 0.012 $Å^{-1}$ for each sample.

Transistor fabrication and characterization

Transistors were fabricated on quartz substrates, which were cleaned by sonication bath in water, then acetone, then methanol. These substrates were then plasma treated for 10 minutes to remove any residual organic residues. The semiconductor layer was deposited by spin coating P(NDI2OD-T2) with a concentration of 10 mg/mL in 1,2-dichlorobenzene at 2000 rpm for 60 s. This layer was then annealed at 100 °C for 1 hour. Following this, source-drain electrodes were deposited using channel masks to obtain 30 μm length channels, with 1000 μm width. Gold was deposited at a rate of 1 Å/s by physical vapour deposition to a thickness of 50 nm. The (poly(S)-*b*-poly(VBBI$^+$[X$^-$]-*r*-PEGMA) block copolymers were dissolved in 2-butanone to obtain a concentration of 60 mg/mL, then spin coated onto the P(NDI2OD-T2) surfaces at 2000 rpm. These films were annealed at 130 °C, then the PILs were spin coated again under the same conditions to minimize the formation of pinholes in the gating material. The films were then annealed again at 130 °C. The gate electrodes were deposited by physical vapour deposition using a shadow mask. Gold was again deposited at a rate of 1 Å/s until a thickness of 50 nm was reached.

Device characterization

Transistor devices were characterized on a custom probe station, oesProbe A10000-P290 (Element Instrumentation Inc. & Kreus Design) and a Keithley 2614B source meter. All measurements were obtained in air. Output curves were obtained by sweeping the source-drain voltage (V_{SD}) from 0 to 2 V, while holding the gate-source voltage (V_{GS}) constant in steps of 0.75 V from 0 to 3 V and measuring the resultant source-drain current (I_{SD}). Transfer curves were obtained by maintaining a constant V_{SD} of 1 V, with the exception of S-*b*-(V100-*r*-P0) with the BF_4^- anion which had to be

obtained at 2 V. The V_{GS} was swept from 0 to 3 V at a rate of 50 mV every 80 ms, or 0.625 V/s, with a full forward and backward sweep being performed in 9.6 s, resulting in a frequency of approximately 0.1 Hz. The measurements were performed at this frequency to ensure EDL formation could occur in all the materials, based on the frequencies of EDL formation observed in our previous work[9].

Atomic force microscopy (AFM)

2.5 μm x 2.5 μm AFM images were obtained using a Bruker Dimension Icon AFM, with ScanAsyst-Air probes in PeakForce Tapping mode to generate InPhase images using a scan rate 0.85 Hz with varied gain of 0.93 and a peak force of 0.192 V. Basic image processing (flattening, removal of errant scan lines) as well as removal of periodic noise via 2D FFT filtering was performed in Gwyddion.

Power spectral density functions (PSDF) were calculated in Gwyddion. The output intensity W_r, was adjusted by multiplying by q^2. PSDF curves were fitted with a Lorentzian function using Origin's curve-fitting feature. Domain sizes were calculated as $n = 2\pi/q$, where q was taken to be the peak of the Lorentzian function. The full width at half-maximum was taken directly from the output of the Lorentzian function in Origin.

5.8 Acknowledgements

Technical support from CLS staff Dr. Chang-Yong Kim and Dr. Adam Leontowich is gratefully acknowledged. We also thank the Centre for Research in Photonics at the University of Ottawa (CRPuO) for access to the AFM.

5.9 References

(1) Ling, H.; Liu, S.; Zheng, Z.; Yan, F. Organic Flexible Electronics. *Small Methods* 2018, *2*, 1800070.

(2) Wang, N.; Yang, A.; Fu, Y.; Li, Y.; Yan, F. Functionalized Organic Thin Film Transistors for Biosensing. *Acc. Chem. Res.* 2019, *52*, 277–287.

(3) Sun, Q.; Qian, B.; Uto, K.; Chen, J.; Liu, X.; Minari, T. Functional Biomaterials towards Flexible Electronics and Sensors. *Biosens. Bioelectron.* 2018, *119*, 237–251.

(4) Wang, G. Y.; Lian, K.; Chu, T. Y. Electrolyte-Gated Field Effect Transistors in Biological Sensing: A Survey of Electrolytes. *IEEE J. Electron Devices Soc.* 2021, *9*, 939–950.

(5) Fujimoto, T.; Awaga, K. Electric-Double-Layer Field-Effect Transistors with Ionic Liquids. *Phys. Chem. Chem. Phys.* 2013, *15*, 8983–9006.

(6) Choi, J. H.; Xie, W.; Gu, Y.; Frisbie, C. D.; Lodge, T. P. Single Ion Conducting, Polymerized Ionic Liquid Triblock Copolymer Films: High Capacitance Electrolyte Gates for N-Type Transistors. *ACS Appl. Mater. Interfaces* 2015, *7*, 7294–7302.

(7) Chen, S.; Frenzel, F.; Cui, B.; Gao, F.; Campanella, A.; Funtan, A.; Kremer, F.; Parkin, S. S. P.; Binder, W. H. Gating Effects of Conductive Polymeric Ionic Liquids. *J. Mater. Chem. C* 2018, *6*, 8242–8250.

(8) Peltekoff, A. J.; Hiller, V. E.; Lopinski, G. P.; Melville, O. A.; Lessard, B. H. Unipolar Polymerized Ionic Liquid Copolymers as High-Capacitance Electrolyte Gates for n-Type Transistors. *ACS Appl. Polym. Mater.* 2019, *1*, 3210–3221.

(9) Peltekoff, A. J.; Brixi, S.; Niskanen, J.; Lessard, B. H. Ionic Liquid Containing Block Copolymer Dielectrics: Designing for High-Frequency Capacitance, Low-Voltage Operation, and Fast Switching Speeds. *JACS Au* 2021, *1*, 1044–1056.

(10) Snyder, J. F.; Carter, R. H.; Wetzel, E. D. Electrochemical and Mechanical Behavior in Mechanically Robust Solid Polymer Electrolytes for Use in Multifunctional Structural Batteries. *Chem. Mater.* 2007, *19*, 3793–3801.

(11) Yuan, J.; Mecerreyes, D.; Antonietti, M. Poly(Ionic Liquid)s: An Update. *Prog. Polym.*

Sci. 2013, *38*, 1009–1036.

(12) Singh, M.; Odusanya, O.; Wilmes, G. M.; Eitouni, H. B.; Gomez, E. D.; Patel, A. J.; Chen, V. L.; Park, M. J.; Fragouli, P.; Iatrou, H.; et al. Effect of Molecular Weight on the Mechanical and Electrical Properties of Block Copolymer Electrolytes. *Macromolecules* 2007, *40*, 4578–4585.

(13) Gomez, E. D.; Panday, A.; Feng, E. H.; Chen, V.; Stone, G. M.; Minor, A. M.; Kisielowski, C.; Downing, K. H.; Borodin, O.; Smith, G. D.; et al. Effect of Ion Distribution on Conductivity of Block Copolymer Electrolytes. *Nano Lett.* 2009, *9*, 1212–1216.

(14) Sun, X.; Di, C. an; Liu, Y. Engineering of the Dielectric–Semiconductor Interface in Organic Field-Effect Transistors. *J. Mater. Chem.* 2010, *20*, 2599–2611.

(15) Müller-Buschbaum, P. GISAXS and GISANS as Metrology Technique for Understanding the 3D Morphology of Block Copolymer Thin Films. *Eur. Polym. J.* 2016, *81*, 470–493.

(16) Smilgies, D. M. GISAXS: A Versatile Tool to Assess Structure and Self-Assembly Kinetics in Block Copolymer Thin Films. *J. Polym. Sci.* 2022, *60*, 1023–1041.

(17) Kim, S. H.; Nam, S.; Jang, J.; Hong, K.; Yang, C.; Chung, D. S.; Park, C. E.; Choi, W. S. Effect of the Hydrophobicity and Thickness of Polymer Gate Dielectrics on the Hysteresis Behavior of Pentacene-Based Field-Effect Transistors. *J. Appl. Phys.* 2009, *105*.

(18) Gu, G.; Kane, M. G. Moisture Induced Electron Traps and Hysteresis in Pentacene-Based Organic Thin-Film Transistors. *Appl. Phys. Lett.* 2008, *92*.

(19) Noh, Y. H.; Young Park, S.; Seo, S. M.; Lee, H. H. Root Cause of Hysteresis in Organic Thin Film Transistor with Polymer Dielectric. *Org. Electron.* 2006, *7*, 271–275.

(20) Brixi, S.; Melville, O. A.; Mirka, B.; He, Y.; Hendsbee, A. D.; Meng, H.; Li, Y.; Lessard, B. H. Air and Temperature Sensitivity of N-Type Polymer Materials to Meet and Exceed the Standard of N2200. *Sci. Rep.* 2020, *10*, 4014.

(21) Kim, H. C.; Park, S. M.; Hinsberg, W. D.; Division, I. R. Block Copolymer Based Nanostructures: Materials, Processes, and Applications to Electronics. *Chem. Rev.* 2009,

110, 146–177.

(22) Darling, S. B. Directing the Self-Assembly of Block Copolymers. *Prog. Polym. Sci.* 2007, *32*, 1152–1204.

(23) Farrell, R. A.; Fitzgerald, T. G.; Borah, D.; Holmes, J. D.; Morris, M. A. Chemical Interactions and Their Role in the Microphase Separation of Block Copolymer Thin Films. *Int. J. Mol. Sci. 2009, Vol. 10, Pages 3671-3712* 2009, *10*, 3671–3712.

(24) Cummins, C.; Lundy, R.; Walsh, J. J.; Ponsinet, V.; Fleury, G.; Morris, M. A. Enabling Future Nanomanufacturing through Block Copolymer Self-Assembly: A Review. *Nano Today* 2020, *35*, 100936.

(25) Klauk, H. Organic Thin-Film Transistors. *Chem. Soc. Rev.* 2010, *39*, 2643–2666.

(26) Palermo, E. F.; McNeil, A. J. Impact of Copolymer Sequence on Solid-State Properties for Random, Gradient and Block Copolymers Containing Thiophene and Selenophene. *Macromolecules* 2012, *45*, 5948–5955.

(27) Koo, K.; Ahn, H.; Kim, S. W.; Ryu, D. Y.; Russell, T. P. Directed Self-Assembly of Block Copolymers in the Extreme: Guiding Microdomains from the Small to the Large. *Soft Matter* 2013, *9*, 9059–9071.

(28) Mai, Y.; Eisenberg, A. Self-Assembly of Block Copolymers. *Chem. Soc. Rev.* 2012, *41*, 5969–5985.

(29) Harris, M. A.; Heres, M. F.; Coote, J.; Wenda, A.; Strehmel, V.; Stein, G. E.; Sangoro, J. Ion Transport and Interfacial Dynamics in Disordered Block Copolymers of Ammonium-Based Polymerized Ionic Liquids. *Macromolecules* 2018, *51*, 3477–3486.

(30) Nakamura, I.; Balsara, N. P.; Wang, Z. G. First-Order Disordered-to-Lamellar Phase Transition in Lithium Salt-Doped Block Copolymers. *ACS Macro Lett.* 2013, *2*, 478–481.

(31) Yan, H.; Chen, Z.; Zheng, Y.; Newman, C.; Quinn, J. R.; Dötz, F.; Kastler, M.; Facchetti, A. A High-Mobility Electron-Transporting Polymer for Printed Transistors. *Nature* 2009, *457*, 679–686.

(32) Chen, Z.; Zheng, Y.; Yan, H.; Facchetti, A. Naphthalenedicarboximide- vs

Perylenedicarboximide-Based Copolymers. Synthesis and Semiconducting Properties in Bottom-Gate N-Channel Organic Transistors. *J. Am. Chem. Soc.* 2009, *131*, 8–9.

(33) Dallaire, N.; Brixi, S.; Claus, M.; Blawid, S.; Lessard, B. H. Benchmarking Contact Quality in N-Type Organic Thin Film Transistors Through an Improved Virtual-Source Emission-Diffusion Model. *Appl. Phys. Rev.* 2022, *ASAP*.

(34) Nketia-Yawson, B.; Kang, S.-J.; Dansoa Tabi, G.; Perinot, A.; Caironi, M.; Facchetti, A.; Noh, Y.-Y.; Nketia-Yawson, B.; Kang, S.-J.; Tabi, G. D.; et al. Ultrahigh Mobility in Solution-Processed Solid-State Electrolyte-Gated Transistors. *Adv. Mater.* 2017, *29*, 1605685.

(35) Zare Bidoky, F.; Tang, B.; Ma, R.; Jochem, K. S.; Jin Hyun, W.; Song, D.; Koester, S. J.; Lodge, T. P.; Daniel Frisbie, C.; Zare Bidoky, F.; et al. Sub-3 V ZnO Electrolyte-Gated Transistors and Circuits with Screen-Printed and Photo-Crosslinked Ion Gel Gate Dielectrics: New Routes to Improved Performance. *Adv. Funct. Mater.* 2020, *30*, 1902028.

(36) Jiang, Z. GIXSGUI: A MATLAB Toolbox for Grazing-Incidence X-Ray Scattering Data Visualization and Reduction, and Indexing of Buried Three-Dimensional Periodic Nanostructured Films. *J. Appl. Crystallogr.* 2015, *48*, 917–926.

5.10 Supplementary Information

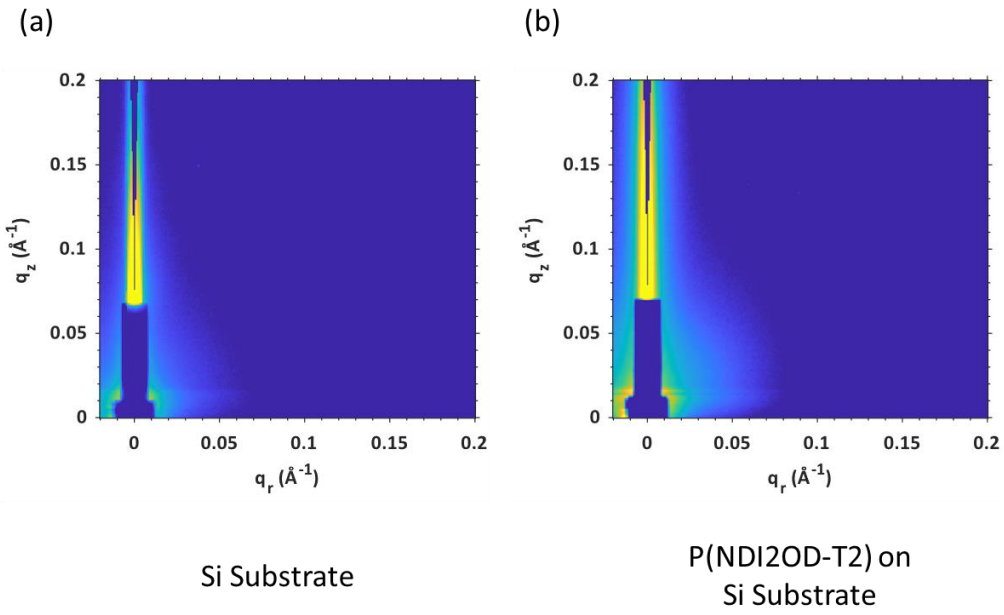

Figure 5.8. GISAXS scattering diffraction patterns for (a) Si substrate with no film, and (b) P(NDI2OD-T2) film on Si substrate.

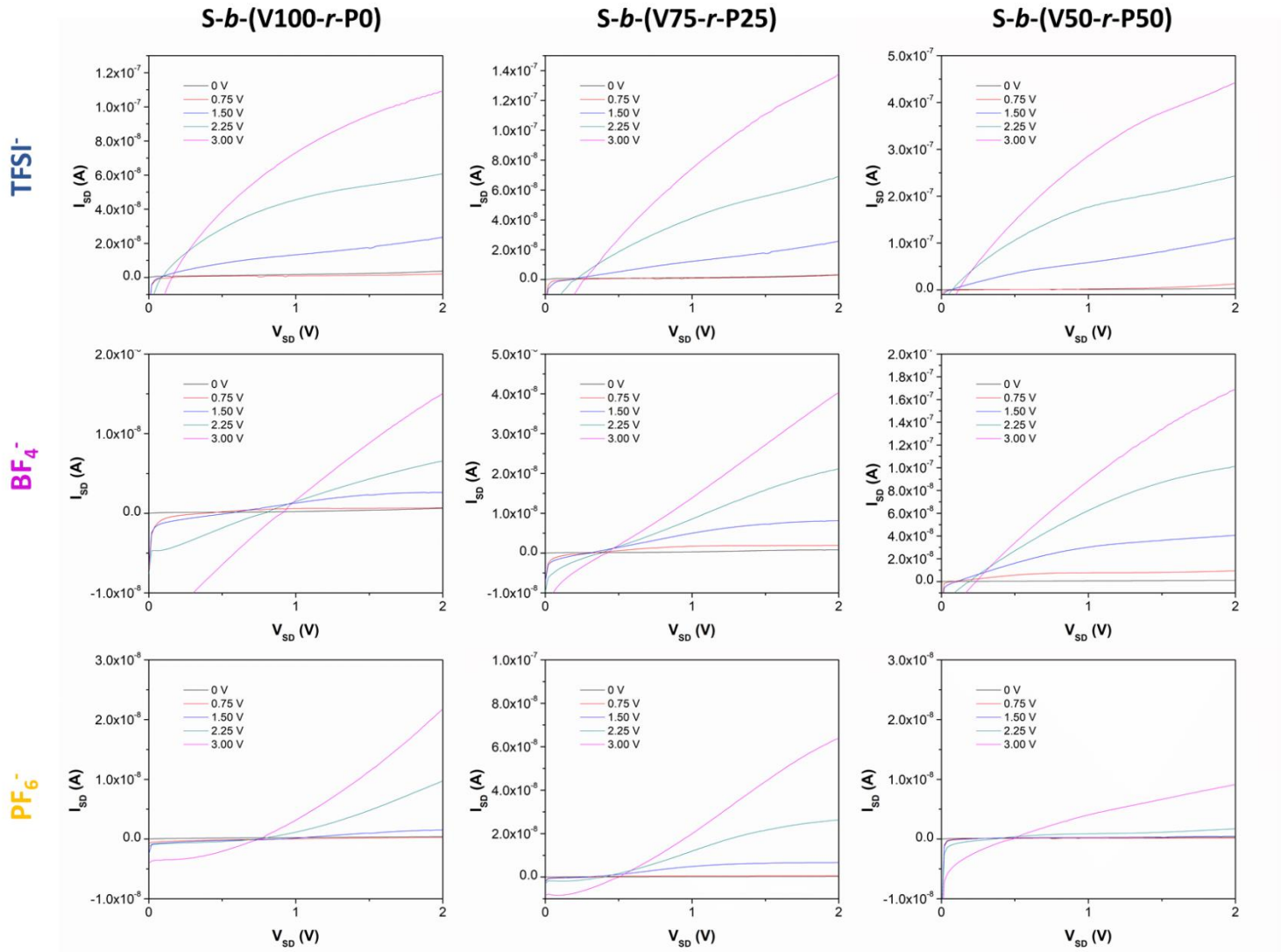

Figure 5.9. Characteristic output curves for devices fabricated with P(NDI2OD-T2) semiconductor and poly(S)-*b*-poly(VBBI^{+}[X^{-}]-*r*-PEGMA) gating material, where [X^{-}] is the anion indicated on the left of the image, and the VBBI^{+}/PEGMA ratio of the polymer is indicated at the top.

Table 5.3. PIL gating layer thickness determined by profilometry. Averages are presented plus/minus the standard deviation of 8 individual measurements.

Polymer ID	Anion	Thickness (nm)
S-*b*-(V25-*r*-P75)	$TFSI^-$	383 ± 48
	BF_4^-	448 ± 54
	PF_6^-	459 ± 105
S-*b*-(V50-*r*-P50)	$TFSI^-$	372 ± 55
	BF_4^-	493 ± 92
	PF_6^-	377 ± 15
S-*b*-(V75-*r*-P25)	$TFSI^-$	347 ± 8
	BF_4^-	658 ± 76
	PF_6^-	417 ± 64
S-*b*-(V100-*r*-P0)	$TFSI^-$	356 ± 19
	BF_4^-	684 ± 64
	PF_6^-	383 ± 57

6. Conclusions and Recommendations

6.1 Overall Conclusions

To push towards commercialization of n-type organic thin-film transistors (OTFTs), these devices must have sufficient stability and performance for their intended applications. This can be achieved by targeting scalable solutions to enhancing stability and developing new materials to improve device performance.

In Chapter 2 of this thesis, it has been shown that using a known relatively air-stable material as a benchmark to compare stability of a variety of materials. In this study, it was demonstrated that despite napthalenediimide-based materials being one of the most promising classes of air-stable materials in literature at the time, there are materials based on other cores that are also worth studying for the goal of synthesizing new air-stable organic semiconductors.

Chapter 3 explores a scalable solution to improving n-type OTFT stability by exposing devices to vapour-phase additives. Aminosilane and amine-based additives were targeted for this study based on promising prior work in literature. A broad scope of additives were studied, making it possible to identify trends on the impacts of functional groups. Increasing the number of alkyl substituents of amines decreased their effectiveness as additives. The most promising additives identified in this study were aniline and pyridine, however they did not confer long-term stabilization due to their volatility.

Chapter 4 builds on the work developed in Chapter 3. Having identified pyridine as a promising moiety for enhancing stability, poly(2-vinylpyridine) (P2VP) was synthesized to overcome the limitation of volatility discovered in the previous study. P2VP was used as an additive in n-type OTFTs and was found to provide a stabilizing effect with as little as 0.1 wt% in the active layer. When 10 wt% of the active layer included P2VP, an increase in long-term stability was evident, and therefore the hypothesis that P2VP would confer stabilizing behaviour based on the previous results from pyridine but overcome the volatility limitation was proven correct. This study has shown that performing simpler screening studies to identify additives to improve OTFTs can be used before synthesizing more complex materials that incorporate those moieties.

The study presented in Chapter 5 looks at improving another essential portion of the structure of an n-type OTFT: the gate dielectric layer. This study examines the effects of the structure of poly(ionic liquids) (PIL) and film morphology of the dielectric on device performance, with the goal of achieving low-voltage operation to enable more practical applications of OTFTs. Polymer structures that exhibited a more mixed type of morphology, likely leaving many pathways for ions to transport through the film, led to the highest-performing devices. Those with the best performance could be turned on at and below 1.5 V, which is equivalent to the voltage supplied by an AA battery.

Taken together, this thesis represents steps forward in improving n-type OTFTs. Scalable methods of enhancing device stability can be combined with other research in the field, such as novel n-type semiconductors with enhanced air-stability, or encapsulation. The work in PILs confirms the continued need to understand the complex relationships between film morphology, polymer structure, and device performance, while also demonstrating n-type OTFTs with high mechanical stability and low operating voltage.

6.2 Recommendations for Future Work

There are a number of avenues that the work in this thesis could be continued and built upon. In Chapter 4, we examined one candidate material, pyridine, from the conclusions of Chapter 3. However, aniline also proves to be a promising avenue to pursue in finding non-volatile additives for stability enhancement. Initial efforts into using aniline-based polymers were hindered by a lack of solubility of the poly(4-aminostyrene) we planned to use in the study. It would be of interest to synthesize a more soluble poly(4-aminostyrene), perhaps a copolymer of poly(styrene) and poly(4-aminostyrene) to enhance solubility in organic solvents. This would open up the study to also investigate polymer composition and any critical threshold of 4-aminostyrene in the polymer backbone for stability enhancement to be observed. This would increase the synthetic complexity of the additive, which may draw this avenue away from the initial goal of low-cost and highly scalable solutions to improving n-type transistors, however, if the synthesis can remain low-cost, this would still fall within the original scope.

Blending polymers with the semiconducting layer is not the only way to incorporate additives into an OTFT. As indicated throughout this thesis, the semiconductor-dielectric interface is an important region for charge transport. It is possible that localizing a stabilizing additive to the

semiconductor-dielectric interface could have a stronger impact on device stabilization than by simple bulk blending. This could be pursued by surface grafting stabilizing molecules or polymers to the dielectric, or incorporating stabilizing moieties into a polymer dielectric. Early results from my colleague Bahar Ronnasi's work has demonstrated potential doping of the semiconductor by contact with doping groups in her novel polymer dielectric, and it is feasible to imagine this could be extended to device stability. Additionally, the contact-semiconductor interface may be worth exploring, as this is the region of charge injection. Our group has significant experience in modifying interlayers between the contact and semiconductor, and an approach similar to contact doping that instead confers stability with the functional groups identified in this thesis could prove to enhance stability. However, this approach may also lead to increased contact resistance if charge transfer becomes inhibited between the contacts and semiconductor.

Encapsulation is a common avenue of improving OTFT stability. The methods of improving stability presented in this thesis are intended to be used in situations where encapsulation is not possible, or in tandem with encapsulation to even further improve stability. A study combining P2VP/organic semiconductor blend in the active layer of an n-type OTFT with encapsulation would prove that these methods work together. The study should include mechanical strain testing as well, as one of the main concerns with encapsulation is mechanical failure of the encapsulant. This would provide the opportunity to demonstrate whether failure of the encapsulant over time due to formation of microfractures and diffusion of air/moisture could be overcome or enhanced with the presence of P2VP.

The main practical challenge encountered with PIL devices was their poor air stability. Devices that were left in air over the course of a day would display low to no performance. It is unclear where the source of this instability is arising from. The device structure left the gating material exposed to air, which could have encouraged absorption of water by the hygroscopic PIL. As water is a major source of instability in OTFTs, this is one likely cause. However, we have not conducted an in-depth analysis of the matter. While there are numerous studies on the stability of ion-conducting polymers for applications such as fuel cells, there are few in the field of organic electronics, and the focus seems to be bias-stress stability. A study into the source of instability in PIL OTFTs would be valuable to the field, identifying all avenues by which performance can be degraded, and studying the mechanisms of degradation.

7. Additional Contributions

Presented in this chapter are additional contributions I have made to publications not included in the body of this thesis. The publication in Section 7.1 was among our group's foundational work on device stability, which enabled us to develop a better understanding of our equipment's capabilities and how to approach studying air and temperature stability. This work ultimately informed how I moved forward with my future device studies, presented in this thesis. Sections 7.2 – 7.5 are national and international collaborations, applying our expertise in device fabrication, testing, characterization, and stability to study materials developed for OTFTs. The work in Section 7.6 takes advantage of lessons learned during unpublished optimization experiments for the work presented in Chapter 3, applying new a model developed by the Blawid group to characterize OTFTs and developing a better understanding of contact resistance. This work is another step in our group's continual efforts towards the realistic and accurate reporting of characteristics in devices that are highly non-ideal, yet have often been reported using simplified and idealized models in the field. Finally, Section 7.7 demonstrates the continued efforts to develop new n-type OSCs, contributing towards the development of new high-performing materials.

7.1 The Influence of Oxygen and Temperature on the Performance of PBDB-T and P3HT in Organic Thin Film Transistors

S. Brixi, O. Melville, N. Boileau, B. Lessard

J. Mater. Chem., 6, 11972-11979, May 2018

https://doi.org/10.1039/C8TC00734A

Abstract

Conjugated polymers such as poly(3-hexylthiophene) (P3HT) are commonly used as semiconducting components in organic photovoltaics (OPVs) and organic thin-film transistors (OTFTs). Such devices may be exposed to oxygen or moisture in air and increased temperature during operation, potentially affecting their charge transport properties. Therefore, we produced the first reported examples of OTFTs using PBDB-T, a conjugated push–pull polymer used in high performance OPVs, and assessed their performance compared to P3HT under different environmental conditions. Drop casted and annealed bottom-gate, bottom-contact (BGBC) devices had an average mobility of 0.06 $cm^2 V^{-1} s^{-1}$, an on/off current ratio of 10^4 and a desirable threshold voltage around 0 V. These OTFTs showed distinct responses to characterization at increased temperature in vacuum ($P < 0.1$ Pa) and air, with PBDB-T devices retaining their performance better than P3HT over time. These findings suggest PBDB-T has higher stability to oxidation when exposed to air than P3HT, especially at high temperatures, and therefore represent a more stable alternative for use in OTFTs and OPVs.

Contributions

This publication was completed during my undergraduate thesis under Dr. Lessard. In this study, I contributed to the experimental design with Owen Melville and carried out all OTFT experiments. Owen Melville performed the AFM and Nicholas Boileau performed the UV-vis experiments, and both created the relevant figures for those experiments. I created all figures for the rest of the paper, and wrote the first draft of the manuscript.

7.2 A N-H functionalized perylene diimide chromophore for alcohol processed organic electronics

D. H. Harris, **S. Brixi,** B. Lessard, G. Welch

J. Mater. Chem. C, 8, 9811-9815, July 2020

https://doi.org/10.1039/D0TC02284E

Abstract

The synthesis of a new perylene diimide organic semiconductor via the use of an acid-catalyzed condensation reaction is presented. The strategy involves the incorporation of an N–H moiety into the molecular design which can be polarized to facilitate green solvent processing. Compared to the parent chromophore, onset of optical absorption in solution is redshifted by 180 nm. Utility as an electron transporting semiconductor in organic field effect transistors is demonstrated.

Contributions

I fabricated the transistor devices for this study, performed optimization on the devices, designed and carried out the transistor characterization experiments, wrote the corresponding section in the manuscript, created the relevant figure for this section, and edited the manuscript.

7.3 Conjoint use of Naphthalene Diimide and Fullerene Derivatives to Generate Organic Semiconductors for n-type Organic Thin Film Transistors

S. Birajdar, **S. Brixi,** P. Rao, R. Bhosale, M. Kobaisi, A. Akhil Gupta, B. Lessard, S. Bhosale, S. Bhosale

ChemistryOpen, 10, 1-8, February 2021
https://doi.org/10.1002/open.202000230

Abstract

In this paper, we described the design, synthesis, and characterization of two novel naphthalene diimide (NDI) core-based targets modified with terminal fullerene (C60) yield – so called S4 and S5, in which NDI bearing 1 and 2 molecules of C60, respectively. The absorption, electrochemical and thin-film transistor characteristics of the newly developed targets were investigated in detail. Both S4 and S5 displayed broad absorption in the 450–500 nm region, owing to the effect of conjugation due to fullerene functionalities. The electrochemical measurement suggested that the HOMO and the LUMO energy levels can be altered with the number of C60 units. Both S4 and S5 were employed as organic semiconductor materials in n-channel transistors. The thin film transistor based on S4 exhibited superior electron mobility (μ_e) values ranging from 1.20×10^{-4} to 3.58×10^{-4} cm2 V^{-1} s^{-1} with a current on-off ratio varying from 10^2 to 10^3 in comparison with the performance of S5 based transistor, which exhibited μ_e ranging from 8.33×10^{-5} to 2.03×10^{-4} cm^2 V^{-1} s^{-1} depending on channel lengths.

Contributions

I fabricated the OTFTs, designed and carried out the transistor characterization experiments, wrote the corresponding section in the manuscript, designed the figure and tables for this section, and edited the manuscript.

7.4 The effect of TCNE and TCNQ Acceptor Units on Triphenylamine-Naphthalenediimide Push-Pull Chromophore Properties

S. Rao, **S. Brixi,** D. Shaikh, M. Kobaisi, B. Lessard, S. Bhosale, S. Bhosale

EurJOC, 18, 2615-2624, April 2021

https://doi.org/10.1002/ejoc.202100198

Abstract

Asymmetrical and symmetrical push-pull chromophore-based on triphenylamine (TPA) donors and naphthalenediimide (NDI) acceptors are designed and successfully synthesized via [2+2] cycloaddition-retroelectrocyclization (CA-RE) reaction with well-known electron-accepting tetracyanoethylene (TCNE) and 7,7,8,8, -tetracyanoquinodimethane (TCNQ) groups. The novel series of compounds NDI-TPA-1 to NDI-TPA-6 were characterized to identify the influence of the TCNE and TCNQ π-conjugated linkers on the optical, electrochemical, and electronic properties of these molecules. We found that in dichloromethane the NDI-TPAs 1, 4, 5, and 6 display absorbance peaks at increasing wavelengths 605, 641, 646, and 645 nm, respectively. We demonstrated that through simple chemical modification we could drop the lowest occupied molecular orbital of NDI-TPA-1 to 6. Furthermore, NDI-TPA-1 to 6 were integrated into organic thin-film transistors (OTFTs) via spin-coating technique, and charge transfer properties were investigated. We found that the choice of the functional group led to either p-type, n-type, or ambipolar characteristics.

Contributions

I fabricated the OTFTs, designed and carried out the transistor characterization experiments for both n- and p-type device behaviour, wrote the corresponding section in the manuscript, created the table for this section, and edited the manuscript.

7.5 An air-stable n-type bay-and-headland substituted bis-cyano N-H functionalized perylene diimide for printed electronics

I. Park, **S. Brixi,** M. Martell, M. Ocheje, R. Pettipas, D. Harris, B. Gelfand, S. Rondeau-Gagné, B. Lessard, G. Welch

J. Mater. Chem. C, 9, 13630-13634, September 2021
https://doi.org/10.1039/D1TC03873G

Abstract

The synthesis of a 6,11-bis-cyano N–H functionalized perylene diimide is reported. Electron withdrawing cyano groups were installed to counter the electron donating cyclic amine moiety with retention of functionality. Solution-processed, air-stable organic field-effect transistors are demonstrated using this new material.

Contributions

I fabricated the transistor devices for this study, performed optimization on the devices, designed and carried out the transistor characterization experiments and stability study, wrote the corresponding section in the manuscript, created the relevant figure for this section, and edited the manuscript.

7.6 Benchmarking Contact Quality in N-type Organic Thin Film Transistors Through an Improved Virtual-Source Emission-Diffusion Model

N. Dallaire, **S. Brixi,** M. Claus, S. Blawid, B. Lessard

App. Phys. Rev. 9, 011418, January 2022

https://doi.org/10.1063/5.0078907

Abstract

Due to nonideal behavior, current organic thin film transistor technologies lack the proper models for essential characterization and thus suffer from a poorly estimated parameter extraction critical for circuit design and integration. Organic thin film transistors are often plagued by contact resistance, which is often less problematic in inorganic transistors; consequently, common models used for describing inorganic devices do not properly work with organic thin film transistors. In this work, we fabricate poly{[N,N′-bis(2-octyldodecyl)-naphthalene-1,4,5,8-bis(dicarboximide)-2,6-diyl]-alt-5,5′-(2,2′-bithiophene)} based organic thin film transistors with reduced contact resistance through the introduction of metallic interlayers between the semiconductor and gold contacts. The addition of 10 nm thick manganese interlayer provides optimal organic thin film transistor device performance with the lowest level of contact resistance. Improved organic thin film transistors were characterized using an improved organic virtual-source emission diffusion model, which provides a simple and effective method to extract the critical device parameters. The organic virtual-source emission diffusion model led to nearly perfect prediction using effective gate voltages and a gate dependant contact resistance, providing a significant improvement over common metal–oxide–semiconductor field-effect transistor models such as the Shichman–Hodges model.

Contributions

I provided some guidance for Nicholas Dallaire, fabricated the OTFT devices, contributed to experimental design, assisted in some of the device characterization experiments, and edited the manuscript.

7.7 Synthesis of thieno[3,4-c] pyrrole-4,6-dione-based small molecules for application in organic thin-film transistors

M. Cyr, **S. Brixi,** A. Ganguly, B. Lessard, J. Brusso

Dyes Pigm. 210, 110964, February 2023

https://doi.org/10.1016/j.dyepig.2022.110964

Abstract

The synthesis of two alternating donor-acceptor (D-A) small molecules revolving around thieno[3,4-c]pyrrole-4,6-dione (TPD) as the main acceptor building block is reported herein. The materials are synthesized using a robust Stille coupling to attach the TPD core with thiophene donors on either of its side, and completed with an aldol condensation under mild conditions for the addition of terminal secondary acceptor building blocks, representing a sought out A^2-D-A^1-D-A^2 structure. The two newly synthesized materials are set to be used as organic semiconductors in organic thin-film transistor (OTFT) devices. Comparative optical, computational, and electrochemical studies were carried out on these new materials to investigate their ability to act as potential n-type organic semiconductors. The materials were then incorporated into bottom-gate bottom-contact OTFT devices, and subsequent thin-film engineering studies were done to probe the effects that solvent and post-deposition annealing conditions had on device performance. From these conditions, the rhodanine-derived D-A material exhibited the greatest electron field-effect mobility (0.011 $cm^2\ V^{-1}\ s^{-1}$), and a threshold voltage of 20.1 V under vacuum.

Contributions

I advised Melanie Cyr as she was learning to fabricate and characterize OTFTs, contributed ideas to experimental design, and edited the manuscript.